NORTHWESTERN UNIVERSITY

Near-field Optical Characterization of Mesoscale Structures

A DISSERTATION

SUBMITTED TO THE GRADUATE SCHOOL
IN PARTIAL FULFILLMENT OF THE REQUIREMENTS

for the degree

DOCTOR OF PHILOSOPHY

Field of Chemistry

By

Yelizaveta Babayan

EVANSTON, ILLINOIS

December 2007

ABSTRACT

Near-field Optical Investigations of Mesoscale Structures

Yelizaveta Babayan

The work described in this dissertation focuses on the optical characterization of micron-sized structures with mesoscale (100-1000 nm) features to investigate of the optical analog to the quantum corral. Lithographically patterned arrays of metallic rings and ellipses were used to study how light can be manipulated and confined within these corral structures. Near-field optical results demonstrated that it was possible to confine electromagnetic (EM) waves within the circular corrals were produced, and standing wave patterns similar to those observed in the quantum corrals. We showed that only certain wavelengths of light could be efficiently sustained inside of these structures to produce a bright spot at the center of the corral. Elliptical corrals, with different eccentricities, were further investigated for their ability to tailor the standing waves by varying the polarization of the incident light. The results revealed that ellipses with larger eccentricities had the ability to modulate light at the focal points to produce bright or dark spots depending on the wavelength of the incident light. Lithographic techniques were also used to generate circular structures of CdSe/ZnS quantum dots (QDs). The photoluminescence (PL) properties of these rings of close-packed QDs were measured, and a red-shift, which was attributed to either the change of the dielectric environment around the QDs or to the resonant energy transfer between the QDs, in the emission peak was observed.

The final chapter of this thesis describes a set of experiments that were developed to supplement lecture-only courses on nanotechnology in undergraduate curriculum. The labs were

based on soft lithographic techniques, including replica molding, micro-molding in capillaries, and micro-contact printing and etching. These simple experiments require only readily available and inexpensive materials such as compact discs, glass microscope slides, poly(dimethylsiloxane), and polyurethane.

_____
Professor Teri W. Odom
Research Advisor

ACKNOWLEDGEMENTS

I would like to thank my research advisor, Prof. Teri Odom, for her guidance and support during my graduate studies. I am grateful to her for establishing a collaborative learning environment, in which it has been enjoyable to develop as a scientist. Teri has given me opportunities to be involved in many educational activities, for which I am especially thankful. I believe that it is because of Teri's persistence and dedication that I have become a better scientific writer and speaker.

I would like to thank Prof. George C. Schatz and Prof. Richard P. Van Duyne for serving as committee members, for challenging me, and for providing constructive comments and suggestions during the past five years. Prof. Schatz and Dr. Shuzhou Li have also been collaborators and I am thankful to them for their contributions to this work.

Many personal contributions have made my time at Northwestern a more enriching and enjoyable experience. First, I would like to thank my friends Eric Greyson and Jeremy Barton for their friendship and help during the first couple of years. Eric, Jeremy and I were the first three members of the Odom group and we worked hard together to set up the laboratory. I have also been fortunate to have met a fantastic friend, Warefta Hasan, in graduate school. Warefta made the last three years at Northwestern very memorable. We spent many hours together - working, shopping, exercising, eating, exploring Chicago and the world of cultural arts.

I want to thank many, former and present, colleagues who have helped to create a friendly and productive environment in the group: Jeremy Barton, Hanwei Gao, Eric Greyson, Warefta Hasan, Joel Henzie, Laura Hughes, Doo Young Kim, Jeounghoon Lee, Min Hyung Lee, Tom McDonald, Colleen Nehl, Sekar Perumal, Scott Price, Christopher Stender, Christina

Sweeney, Meenakshi Viswanathan, Liying Wang, Eun-Ah You, and Wei Zhou. Thank you all for providing an excellent place for scientific growth. I would like to offer special thanks to Hanwei Gao for being not only a good friend, but also for being a talented scientist with whom I have had many enjoyable and stimulating scientific discussions. I have been very lucky to have a great friend, Olya Lyandres, outside of the group. I cannot forget to thank Alyson Whitney for being a wonderful roommate during the past four years.

I would like to say thank you to several people who have made my time away from home special. I would like to thank Ira Davtyan and Samvel Mkrtchyan, along with their family, for being great friends. I have spent a lot of time with them during the past five years and will miss them when I move. Thanks are also due to my brother-in-law, Gianluigi Ferrari, and the McFarland family for making my holidays during graduate school special. Gianluigi and my sister Anna visited me several times for 4th of July and Thanksgiving, and I have spent numerous holidays with the McFarlands in Ohio.

One of the best things that happened at Northwestern was meeting Adam McFarland. Adam has been a great support during my graduate studies. I am especially thankful to him for his encouragement and patience. He has been a great help in proof-reading my papers, giving constructive feedback on important presentations, and setting-up the laser for our group. His advice concerning scientific matters has been invaluable.

I am very fortunate and grateful to have an amazing family, who has given me their love and support, without which this work would not have been possible. My sister Anna has been there for me during good times and bad times – always willing to listen to me and provide moral support. I am thankful to her for visiting me often and for always being in good spirits. Her

cheerful outlook on life and continued encouragement have been a great help; she has been my strength throughout the past five years. Special thanks to my little brother Mish for visiting me during his spring breaks and being a catalyst for many new experiences, such as horseback riding and cave exploration. My grandma Zina deserves a special acknowledgement for being the most wonderful grandma. I am forever grateful to her for everything she has done for me throughout my life; there are no words that can fully express my appreciation.

Finally, many special thanks to my wonderful parents for their unconditional love and support. I am eternally grateful and indebted to them for all the sacrifices they have made for me and my siblings to have a better life. I am grateful to them for making a difficult decision to move to US in order to give us good education and future. It is because of them that I was able to go to graduate school and fulfill my dream of getting a doctorate degree in chemistry. Thanks, Mom & Dad!

Graduate school has been a long and winding road and although it has been wonderfully enjoyable I am happy it is coming to an end. As I close this chapter of my life and start a new one, I realize that the most important thing in my life is my family and to them I dedicate this thesis. I am looking forward to moving to Indianapolis and starting a new chapter in my life with Adam.

YB
Evanston, IL
December 2007

In memory of my grandfather Gabrielyan Sergey Misakovich

to my parents, Yelena & Rustam Babayan

my siblings, Anna & Mikhail Babayan

and

my grandma Zinaida Gabrielyan

TABLE OF CONTENTS

LIST OF ILLUSTRATIONS

LIST OF COMMON ABBREVIATIONS

2D – two-dimensional

3D – three-dimensional

AFM – atomic force microscope

APD – avalanche photodiode

CCD – charge coupled device

DF – dark-field

E-beam – electron beam

EBL – electron beam lithography

EW – evanescent wave

EM – electromagnetic

FL – focal length

IPA – isopropyl alcohol

ITO – Indium tin oxide

LN_2 – liquid nitrogen

LSPR – localized surface plasmon resonance

μCP – micro-contact printing

MIBK – methyl isobutyl ketone

MIMIC – micro-contact molding in capillaries

NA – numerical aperture

NC – nanocrystals

NP – nanoparticle

NSOM – near-field scanning optical microscope

PC – photonic crystal

PDMS – polydimethylsiloxane

PMMA – polymethyl methacrylate

PSP – phase-shifting photolithography

PSTM – photon scanning tunneling microscope

PU – polyuretane

QD – quantum dots

RM – replica molding

SAM – self assembled monolayer

SC – spectral coverage

SEM – scanning electron microscope

S/N – signal-to-noise

SP – surface plasmon

SPP – surface plasmon polariton

SPS – single point spectroscopy

SR – spectral resolution

STM – scanning tunneling microscope

TEM – transmission electron microscope

TIR – total internal reflection

UV – ultraviolet

Chapter 1

Introduction

1.1 General Overview

Dielectric waveguides are the key components of modern integrated optics and optical communications. Traditionally, waveguiding has been achieved by dielectric slab waveguides and optical fibers. Current advances in nanofabrication techniques and the means to pattern materials in three dimensions have driven the development of new structures – photonic crystals (PCs)[1-4] – for confining and guiding electromagnetic (EM) fields at near-infrared and visible wavelengths. PCs, which are periodic structures made of alternating layers of different dielectric materials, have attracted attention for their ability to manipulate light in two and three dimensions (3D).[2] These structures can be thought of as optical analogs to semiconductors, because they exhibit photonic band gaps, regions in which some wavelengths of light cannot propagate along certain crystal directions. PCs provide a powerful means to manipulate and control photons in three dimensions (3D). For example, they have been used to localize photons to a specific area at restricted frequencies and to serve as low-loss waveguides to direct the propagation of light along a specific channel, even with a bend. The manipulation of light at the nanoscale (1-100 nm) and mesoscale (100-1000 nm) has become an important problem for progress in areas of photonics, optoelectronics,[5, 6] single-molecule sensing,[7, 8] and new forms of microscopy.[5, 9]

Most dielectric waveguides confine and guide light using reflection of a plane wave from the interfaces that make up the waveguide. For example, dielectric slab waveguides, which consist of a layered structure with the outer layers having lower index of refraction, have been used to guide light in the infrared region in the direction parallel to interfaces of the dielectric layers. A waveguide, composed of polystyrene and tellurium, was shown to exhibit metallic-like

omnidirectional reflectivity in the 10-15 μm range.[10] Unlike metallic structures, which become lossy at high frequencies due to their finite conductivity, dielectric waveguides do not suffer from these limitations and can be used for applications requiring high optical frequencies. These types of optical waveguides have been used in integration circuits, laser diodes, and interferometers.

Optical fibers have been widely studied and have been used for applications in optical telecommunications. These waveguides are composed of a core layer, usually made of silica or chalcogenide glass (used for longer wavelength infrared applications), and a surrounding cladding layer, which has a smaller refractive index than the core. In these fibers, light is confined by total internal reflection, which occurs when the angle of the incident light relative to the propagation direction and the normal to the material interface is grater than the critical angle. One advantage of these dielectric optical fibers over metallic wires is their ability to transmit light over longer distances (over several km) with smaller losses. Progress in the field of PCs led to the development of PC fibers,[11] which guide light by means of diffraction from a periodic structure, rather than total internal reflection. PC fibers can be designed to carry higher powers and represent an improved version of well-established conventional optical fibers.

PCs not only provide a powerful means to manipulate and control photons in three dimensions, but they also allow for complete tunability. Their structures can be manipulated to tailor the band gap to confine light in a desired spectral range. Variation in the properties of these PC structures can be achieved by changing the refractive index contrast between the dielectric layers, the thickness of the alternating dielectric layers, or by introducing defects.[3, 12]

Additionally, a method for manipulating the band gap by applying external magnetic fields has been reported.[13]

Another mechanism for manipulating light involves the use of surface plasmon polaritons (SPPs). Metal-insulator-metal (MIM) or insulator-metal-insulator (IMI) heterostructures are used to create waveguides by coupling the SPPs from the metal/insulator interfaces into the dielectric spacer (for MIMs) or the dielectric cladding (for IMIs). For example, thin metal (Au and Ag) films of finite widths embedded in a dielectric material (SiO_2) have been used as plasmonic waveguides.[14, 15] In this geometry, propagation lengths as long as 13.6 mm in the near-infrared have been achieved. This long range propagation, however, is accomplished at the expense of light confinement in the perpendicular direction.[15] Therefore, these IMI structures are not suitable as subwavelength waveguides. MIM structures, which guide light using refractive index differences between the metal and the dielectric have shown both long-range propagation and confinement of light in lateral dimension.[16] Planar MIM structures composed of $Ag/SiO_2/Ag$ with varying thicknesses (12-250 nm) of SiO_2, have shown that as the thickness of the insulator layer increases, the propagation lengths increase but without compromising the confinement.[16] By altering the thicknesses and the materials of different layers in these types of waveguiding heterostructures, the propagations lengths and degree of light confinement can be controlled.

Although dielectric structures have been used to manipulate light in 2D and 3D, their use for manipulating light on surfaces has been limited. One type of structure that has been created to help understand confinement of light on dielectric surfaces is an optical analog[17-19] of the quantum corral.[20] It has been demonstrated that individual 100-nm Au posts positioned into circular and stadium shaped structures on indium tin oxide (ITO) surface were able to localize

EM waves in the visible range at the surface. The investigation of these structures provides an avenue for further testing of analogous behavior of electrons and photons in confined regions. This idea motivates many of the studies described in this thesis.

1.2 Tools

Structures with well defined nano- and mesoscale features that can tailor light propagation on surfaces are usually made using nanofabrication techniques such as electron-beam lithography (EBL), focused ion beam (FIB) milling, or photolithography. EBL and FIB are powerful direct-write methods that allow the fabrication of features with less than 20 nm resolution. These serial techniques, however, are costly and slow, and therefore impractical for large-scale manufacturing of nanostructures. Despite these drawbacks, EBL and FIB provide flexibility in designing arbitrary patterns. Conventional photolithography, a parallel technique, is used less often because it requires a patterned mask to produce the desired features. The resolution of this technique is limited by the wavelength of light used to expose the photoresist, and typically is about ~400 nm. A form of conventional photolithography called phase-shifting photolithography (PSP), which utilizes a phase-shifting patterned polymeric mask, has been recently developed and can be used to pattern structures with smaller features.

To characterize the optical properties of nanoscale and mesoscale structures several methods including far-field and near field microscopy have been used.[1, 21] While far-field techniques are reliable, they suffer from the drawback of diffraction-limited resolution. Optical characterization using far-field methods is limited to measuring responses at certain locations. Unfortunately, these methods cannot directly observe light propagation on surfaces. Near-field techniques[22] offer a clear advantage to far-field techniques, not only because they can achieve

sub-diffraction limited resolution, but also because they can provide detailed information on light propagation on surfaces. Therefore, near-field scanning optical microscopy (NSOM), is the tool of choice for characterizing light propagation along surfaces.[23] Specifically, photon scanning tunneling microscopy (PSTM), a form of collection mode NSOM, has been essential for imaging wave propagation in plasmonic waveguides.[24]

1.3 Goals and Organization of Thesis

The goals of this thesis are to develop new techniques and tools to fabricate and characterize optical mesoscale structures. Chapter 2 describes the instrumentation for performing near-field microscopy and far-field spectroscopy for single particles. This chapter also introduces lithographic tools for fabricating resist templates with different patterns, which were used for creating structures described in the next two chapters. Chapter 3 discusses the templated, hierarchical assembly of semiconductor CdSe/ZnS quantum dots into patterned arrays. These surface-patterned QDs exhibit photoluminescence spectra that is red-shifted compared to the spectra acquired in solution. This chapter also highlights the improved resolution that was achieved in negative resist using soft lithography. Chapter 4 includes work on light confinement in mesoscale structures, which we refer to as optical corrals, on dielectric surfaces. Near-field optical characterization demonstrating the manipulation of light with corral structures of different sizes and shapes is reported. Finally, using our knowledge of nanofabrication we developed a set of benchtop nanoscale experiments that can be used to introduce high school and college students to concepts of nanofabrication. These experiments, which are based on soft lithographic techniques, are described in Chapter 5.

Chapter 2

Tools for Characterization and Fabrication of Optical Structures

2.1 Introduction

Recent advances in micro- and nanofabrication techniques have made it possible to create nanoscale (1-100 nm) and mesoscale (100-1000 nm) structures that exhibit interesting optical properties on these length scales. For example, the surface plasmon (SP) resonances of noble metal nanoparticles (NPs) and films perforated with nanoholes depend on the size and shape of the nanostructures.[25, 26] Therefore, control over the specific sizes and shapes of material, enables their optical properties (such as absorption and scattering) to be tuned.[27, 28] Several methods for creating small-scale structures have been developed, including chemical synthesis, serial direct writing techniques (e.g. electron beam (e-beam) lithography, focused ion beam milling), and parallel techniques such as photolithography. Synthetic techniques offer the ability to make NPs with various geometries and dimensions; however, they cannot easily create assemblies of these nanostructures on surfaces. Besides tunability by size and shape, the different spacing of particles in an array can be used to control their optical behavior.[29] Lithographic techniques can generate arrays of nanoscale and mesoscale particles as well as perforations in metallic films with defined geometries over different length scales. This ability to organize nanostructures enables detailed studies of the properties of individual structures and the collective properties of their assemblies.

Nanotechnology has been driven by the development of new characterization tools. Specifically, scanning probe instruments such as the atomic force microscope (AFM), the scanning tunneling microscope (STM), and the near-field scanning optical microscope (NSOM) were developed to overcome the diffraction limitations in optical microscopy and to provide a means to study nanoscale optical phenomena. Unlike other scanning probe techniques, NSOM

provides simultaneous topographical and optical information, which allows nano-optical studies of localized emission from nanoparticles and SP propagation on perforated metallic films.[26, 30] The development of NSOM has advanced and expanded applications of optical spectroscopy to the nanometer-scale.

This chapter focuses primarily on the tools used for optical characterization and fabrication of nano- and mesoscale structures. Section 2.2 provides a general overview of NSOM and its different modes of operation, while Section 2.3 describes a set-up that couples an optical microscope with a spectrometer for performing single particle spectroscopy. The last section of this chapter, Section 2.4, provides a review of lithographic methods and provides experimental details for the fabrication of microscale structures with mesoscale features, which can be used to manipulate electromagnetic (EM) waves on surfaces (Chapter 4).

2.2 Overview of Near-field Scanning Optical Microscopy

NSOM allows optical imaging with sub-diffraction resolution. In near-field microscopy, light propagates through a fiber optic tip with a subwavelength size aperture (40-150 nm), which determines the resolution of the image obtained. Although the concept of NSOM was proposed almost 80 years ago, the prototype of the instrument did not appear until the early 1970s. The first experimental demonstration was performed in the microwave region and was able to achieve a spatial resolution of $\lambda/60$.[31] The feasibility of NSOM in the optical regime was demonstrated by Pohl and Lewis.[32, 33]

The essential components of an NSOM system include: a tapered fiber optic probe with sub-wavelength aperture, a scanning stage, and a detection system (Figure 2.1). The most important component is the fiber optic probe because the aperture size, along with the sample-
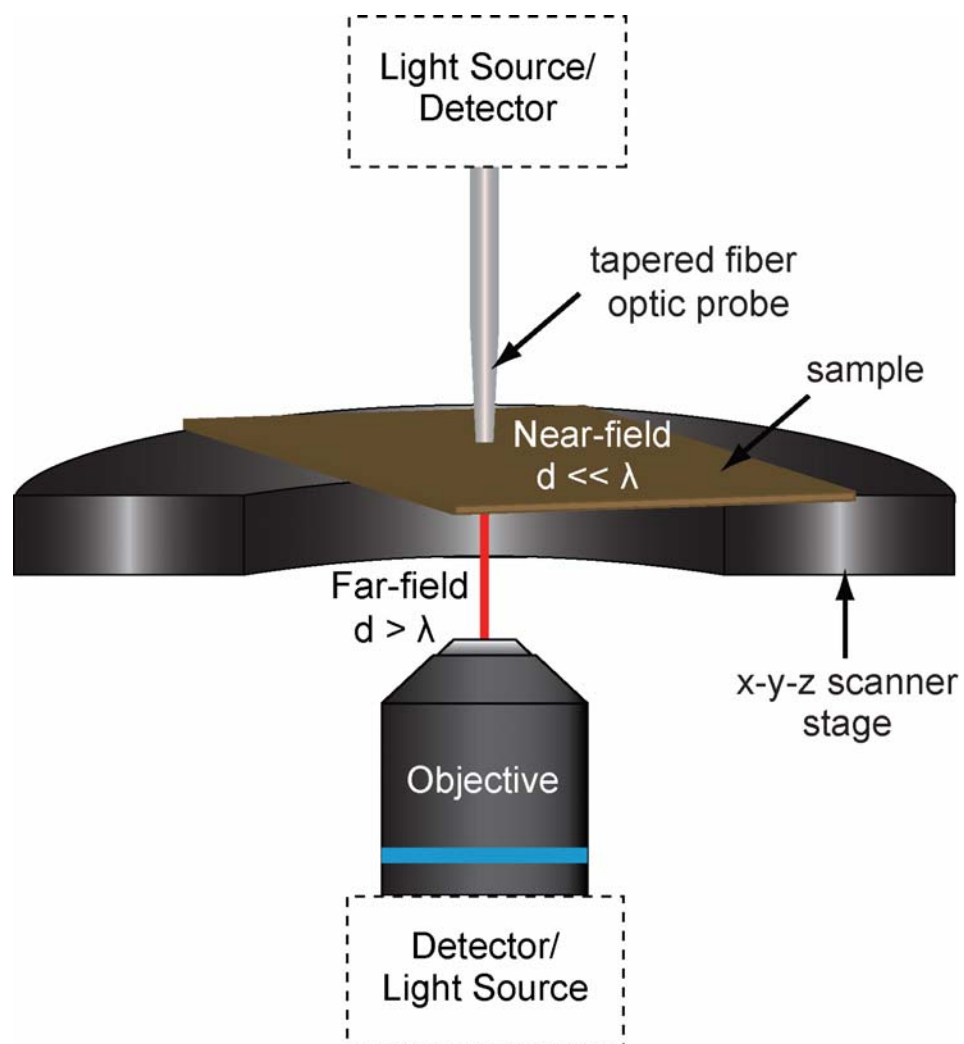
Figure 2.1. Schematic diagram of an NSOM configuration. Boxes with dashed lines indicate the components that can have two different positions.

probe distance, determines the optical resolution. There are several operating configurations (e.g. collection or illumination) for NSOM depending on the characteristics of the sample.

2.2.1 NSOM Instrumentation

All NSOM measurements in our research were performed using an Aurora 3 (Veeco) NSOM equipped with a 40X objective (NA = 0.65) (Olympus). The light from the sample was collected by an avalanche photodiode (APD) (SPCM-AQR-14, Perkin Elmer), a high quantum efficiency single photon counter. Al-coated pulled fiber probes with aperture sizes between 50-80 nm or 100-150 nm and resonant frequency of 80-100 kHz were purchased from Veeco. The uncoated prism (BRP-10) for total internal reflection (TIR) set-up was purchased from Newport and the mirror (NT45-517) was purchased from Edmund Optics.

2.2.2 NSOM Probes

NSOM probes are tapered optical fibers, which are usually fabricated either by chemical etching methods or by pulling a single mode optical fiber while heating using a CO_2 laser.[34-36] The latter methods are most commonly used because they produce probes with smaller apertures. By controlling laser power and spot size, as well as the pulling force, highly reproducible tapers and aperture diameters can be produced.[36] When the probe is created, the fiber diameter in the tapered region is reduced, and light escapes from the sides of the tip, which can be prevented by coating the probe with a thin (50-150 nm) layer of metal. Aluminum is usually used because it has the smallest skin depth (~13 nm) in the visible region.[22]

Pulled, coated probes often suffer from several problems and need to be carefully characterized. One problem that arises during the pulling process is that twin tips are often

produced, which make the correlation of topographical and optical images difficult to interpret. Another problem can be caused during thermal deposition of Al. Large grain formation in Al can lead to decreased reflectivity in the film and also cause pinhole formation, which leads to light leakage and lower throughput (Figure 2.2).

The quality of the NSOM images, just like in any scanning probe microscopy, depends strongly on the probe aperture used to deliver or collect light. Because the optical throughput of these probes is proportional to the sixth power of the aperture size,[37] large input powers are necessary for signal generation.[22] A power input that is too high, however, can cause thermal damage through absorption of light by the Al coating.[38-40] Experimental measurements have shown that the Al coating on the probe aperture can reach temperatures as high as 470 °C.[41] These harsh conditions can cause rapid probe deterioration. In collection mode experiments, we observed that when the sample was transparent (glass with patterned metal features vs. solid metal film) more light was transmitted, which heated the probe and lead to probe degradation. The heat caused the aperture to enlarge, which decreased the NSOM resolution. Therefore, the laser powers cannot be arbitrarily increased to improve the output power and should be kept on the order of 0.5-2 mW.

The ability to collect light through an NSOM probe can be improved by increasing the size of the aperture (which results in decreased resolution) or increasing the taper angle. Etched probes provide higher throughputs (at least an order of magnitude) compared to their pulled counterparts, [42] but they were not used in experiments because of the lengthy fabrication process and low resolution. NSOM measurements with pulled probes yielded resolutions on the order of
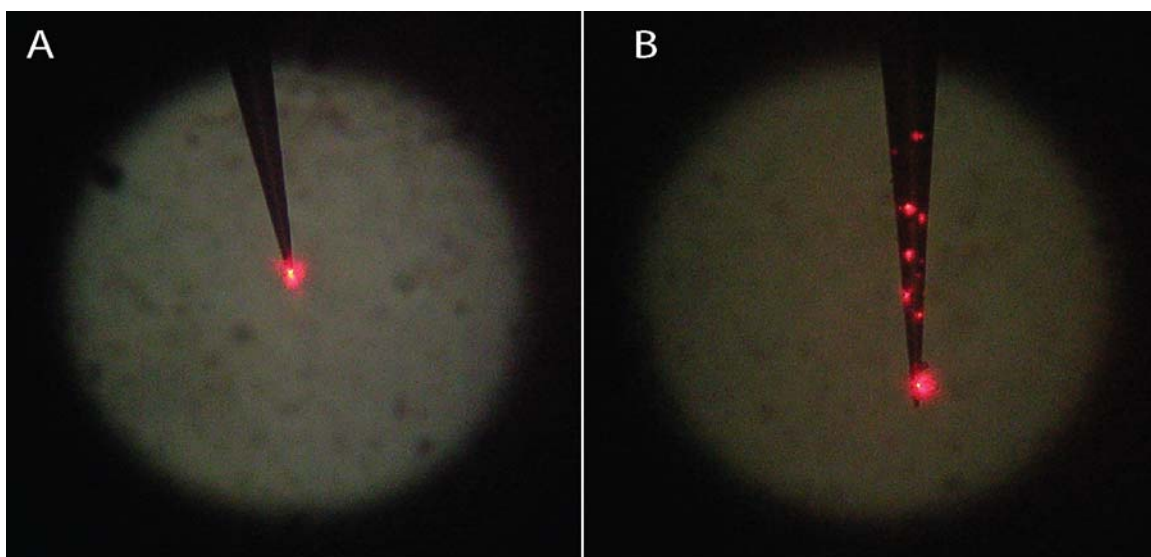
Figure 2.2. Optical micrograph of pulled NSOM probes (A) without and (B) with pinholes.

50-100 nm[22, 32, 33] although resolutions on the order of ~30 nm can be achieved with carefully fabricated probe and optimal imaging conditions.[43]

2.2.3 Illumination Mode NSOM

In the illumination configuration, a fiber optic probe delivers spatially localized light[44-47] to the sample, and the light from the sample is then collected in the far-field through an objective lens either in transmission (Figure 2.3A) or reflection (Figure 2.3B). In transmission mode, the objective lens is positioned directly below the sample, while in reflection mode the lens is at a 45° angle with respect to the sample. Transmission is often preferred over reflection because it provides maximum signal collection due to the position of the collecting optic relative to the sample; reflection mode is necessary when opaque samples are imaged.

NSOM in the illumination configuration can be used for imaging fluorescent molecules or nanoparticles.[30, 44, 48] It is the most important mode for chemical and biological applications using near-field optics[48] and is also the easiest mode of operation. For example, this mode is favored for fluorescence imaging because the chromophores are excited locally as the probe is scanned over the sample, which prevents photo-bleaching of the sample before the entire scan is completed. We used NSOM in transmission mode to image fluorescent CdSe quantum dots (QDs) (λ_{em} = 603 nm) assembled into arrays of ~ 3 μm rings (Figure 2.4) on an ITO/glass substrate. The fluorescence of the QDs was excited through the probe by 400-nm light from a Ti:Sapphire laser, and the emission from the QDs was collected using a 40x (0.65 NA) objective. Residual laser light was removed with a 530 nm long pass filter, and the fluorescence signal was detected by an APD.
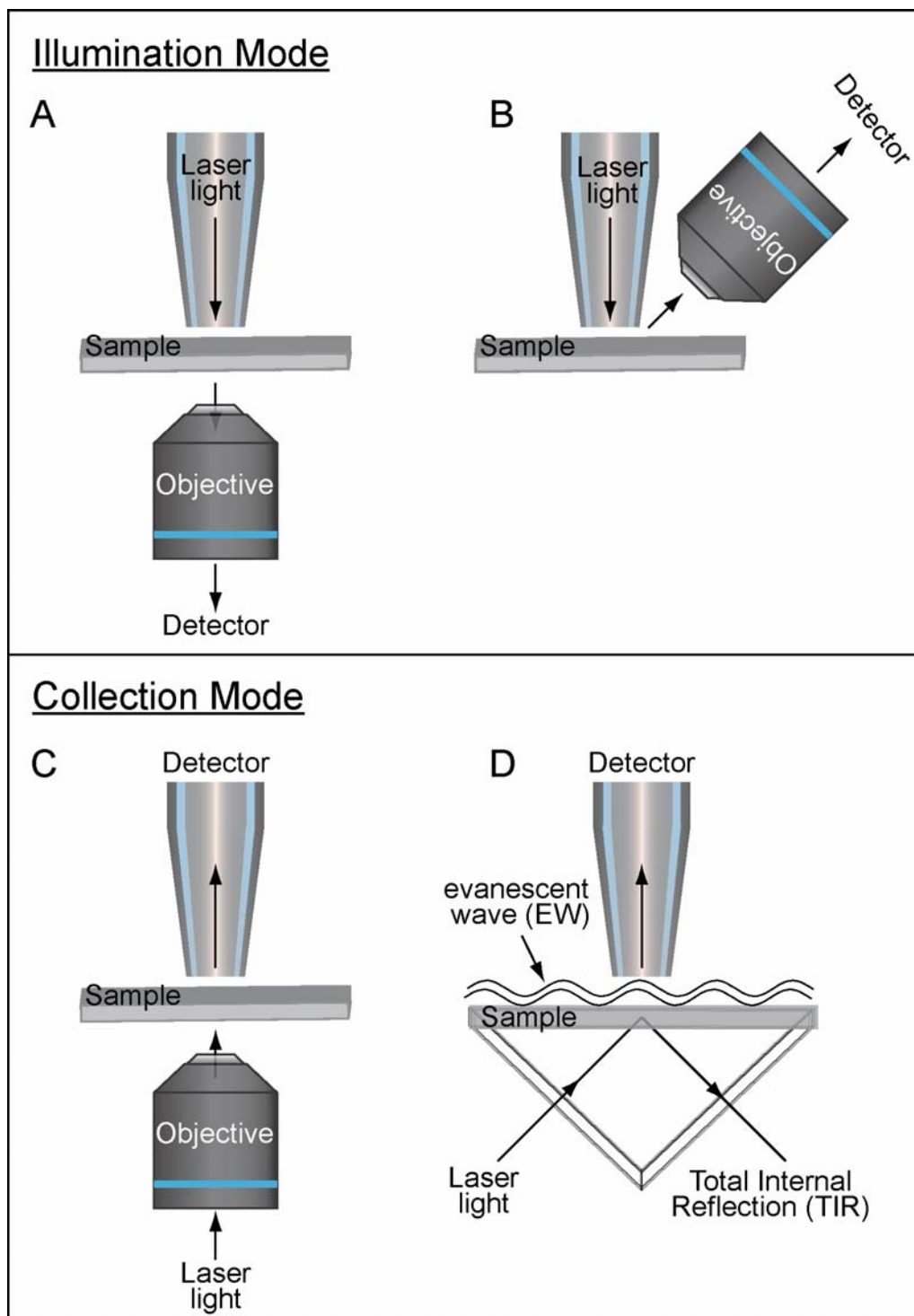
Figure 2.3. Scheme of NSOM in (A-B) illumination and (C-D) collection configurations.
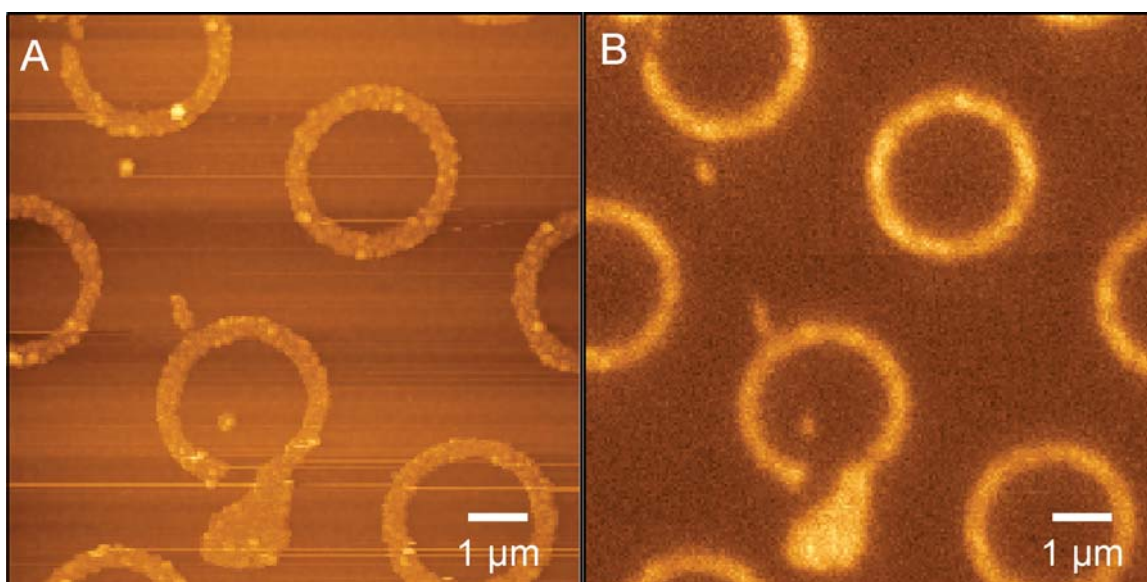
Figure 2.4. (A) Topography image of rings of 25-nm high CdSe/ZnS NCs and (B) corresponding fluorescence NSOM image.

One of the strengths of NSOM is the capability to perform local spectroscopic measurements. We have demonstrated that NSOM combined with a spectrometer can provide detailed optical information about a sample. Using transmission NSOM, 405-nm light was coupled into an uncoated fiber optic NSOM probe to excite water soluble CdSe/ZnS QDs (λ_{em} = 607 nm) on a glass substrate. The emission from these QDs was then collected by an objective lens, which coupled the light into a multimode optical fiber and routed it into a spectrometer equipped with a 600 grooves/mm grating and a LN_2-cooled CCD detector (Figure 2.5). The inset in Figure 2.5 displays the emission spectrum obtained from the QDs through the NSOM-spectrometer set-up. The emission of the QDs was slightly red-shifted (λ_{em} = 612 nm) compared to those in solution. The shift can be attributed to either the change of the dielectric environment around the QDs or to resonant energy transfer between the QDs

2.2.4 Collection Mode NSOM

Collection NSOM refers to the mode of operation where the fiber optic probe is used to collect light from the sample in the near-field, while the sample is illuminated globally through an objective lens (Figure 2.3C). This mode of operation is often used when probing evanescent waves localized near the surface of the sample. Recently, collection NSOM has been used to study surface plasmon polaritons (SPPs), which are collective charge oscillations of electrons at a metal-dielectric interface.[26, 49-51] SPPs decay exponentially normal to the surface and their propagation lengths across the surface can reach tens of microns.[25] Collection NSOM is well-suited for looking at the decay lengths of SPPs both away and across the sample. One major advantage of this mode is the uniform illumination of a relatively large area (several mm^2) of a
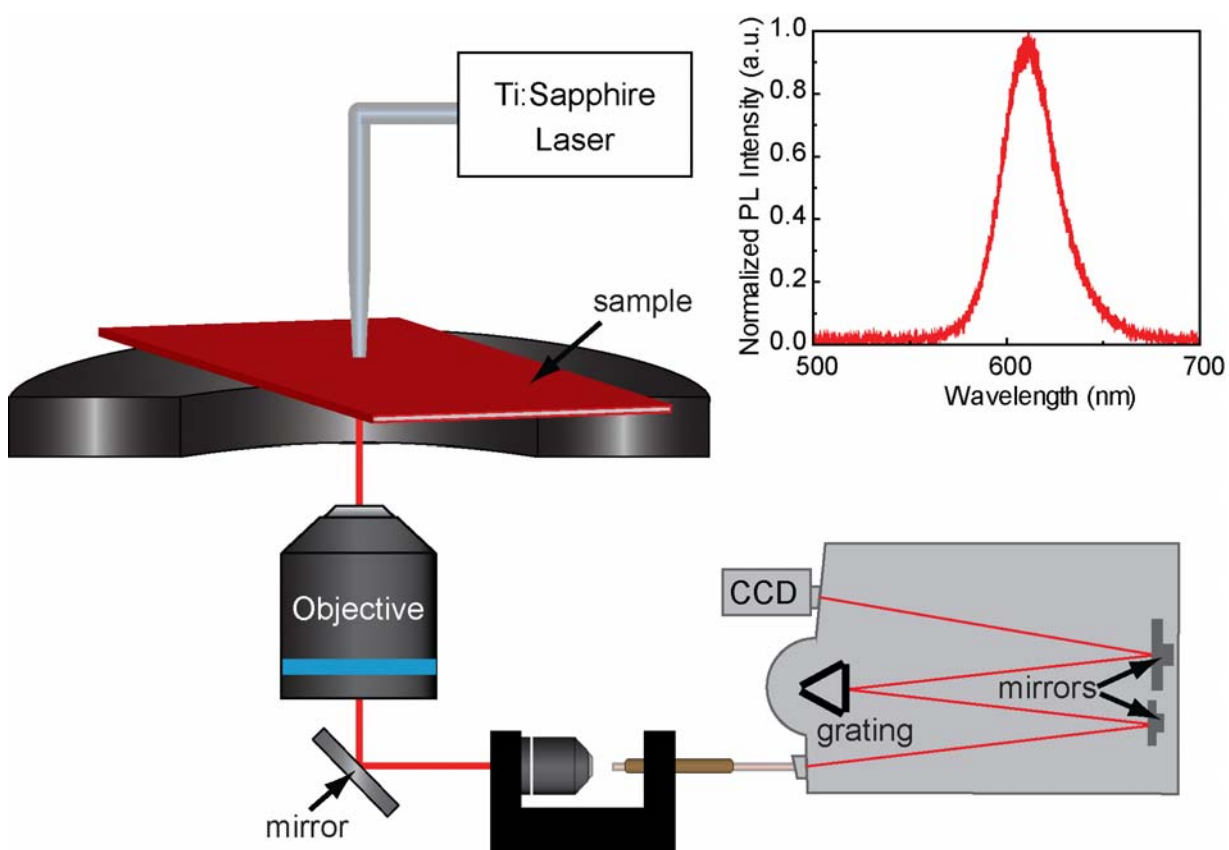
Figure 2.5. Scheme of transmission NSOM coupled with a spectrometer. Inset: photoluminescence spectra from water soluble CdSe/ZnS QDs drop-coated onto a glass slide.

sample. We have used this mode of NSOM to observe confined standing waves on dielectric surfaces.

2.2.5 Photon Scanning Tunneling Microscopy

One form of collection mode NSOM is the photon scanning tunneling microscope (PSTM), first described in 1989.[52] PSTM depends on total internal reflection (TIR), which generates exponentially decaying evanescent waves used to illuminate the sample. The fiber optic probe in the near-field is then used to detect the electromagnetic field of the sample. A typical, set-up for PSTM is shown in Figure 2.3D.

TIR can occur at an interface between materials with different refractive indices (n_1 and n_2). In order to achieve TIR, the angle of incidence θ_1 (relative to the normal) has to be greater than the critical angle (θ_c), which can be calculated using Snell's Law:

$$n_1 \sin \theta_1 = n_2 \sin \theta_2$$

where n_1 and n_2 correspond to the refractive indexes of glass and air, and θ_1 and θ_2 correspond to the angle of incident and reflected light respectfully. For BK7 glass, $n = 1.51$, which results in a θ_c of 41.5°:

$$\theta_c = \sin^{-1}\left(\frac{n_2}{n_1}\right) = \sin^{-1}\left(\frac{1.00}{1.51}\right) = 41.5°$$

Thus, for $\theta_1 > \theta_c = 41.5°$, an evanescent field is produced at the surface of the prism in the medium with smaller refractive index (i.e., air).

To perform PSTM experiments using the Aurora 3, we needed to modify the system to accommodate a prism. Because the space under the scanning stage in the Aurora 3 is limited (~ 5 cm), a holder that would accommodate the TIR prism was designed. Space constraints in the

NSOM system also required incorporation of a mirror into the holder that would reflect the laser light into the prism at angles above θ_c. The prism holder (Figure 2.6) replaced the transmission objective lens in the NSOM system, and the mirror reflected the light into the prism at an angle of 45°, which is larger than the θ_c, the condition required for TIR. Details of the holder design can be found in Appendix 1.

To verify the exponential decay of the evanescent field produced by TIR, single point spectroscopy (SPS) was used to measure the photon counts as a function of probe-distance above the sample. The sample was first mounted onto a right angle prism ($n = 1.51$) using an index matching liquid ($n = 1.52$) (F-IMF 105, Newport), and TIR was produced at the surface of the sample by shining a 400-nm light from a Ti:Sapphire laser into the prism at an incident angle of ~45°. SPS data, shown in Figure 2.7, was collected with an Al-coated probe by withdrawing the probe ~250 nm away from the probe feedback point, which is ~10-20 nm above the surface of the sample. The intensity of the evanescent field $I(z)$ decays exponentially with distance from the surface of the prism interface according to:

$$I(z) = I(0) \times e^{-z/d}$$

where $I(0)$ is the intensity at the interface, and d is the decay length for the evanescent field intensity, given by:[53]

$$d = \frac{\lambda}{4\pi}[n_1^2 \sin^2(\theta) - n_2^2]^{-1/2}$$

was calculated to be 82 nm at 45°. There was very little difference between the calculated (82 nm) and measured (61 nm) decay lengths. These numbers are within experimental error of angle measurements.
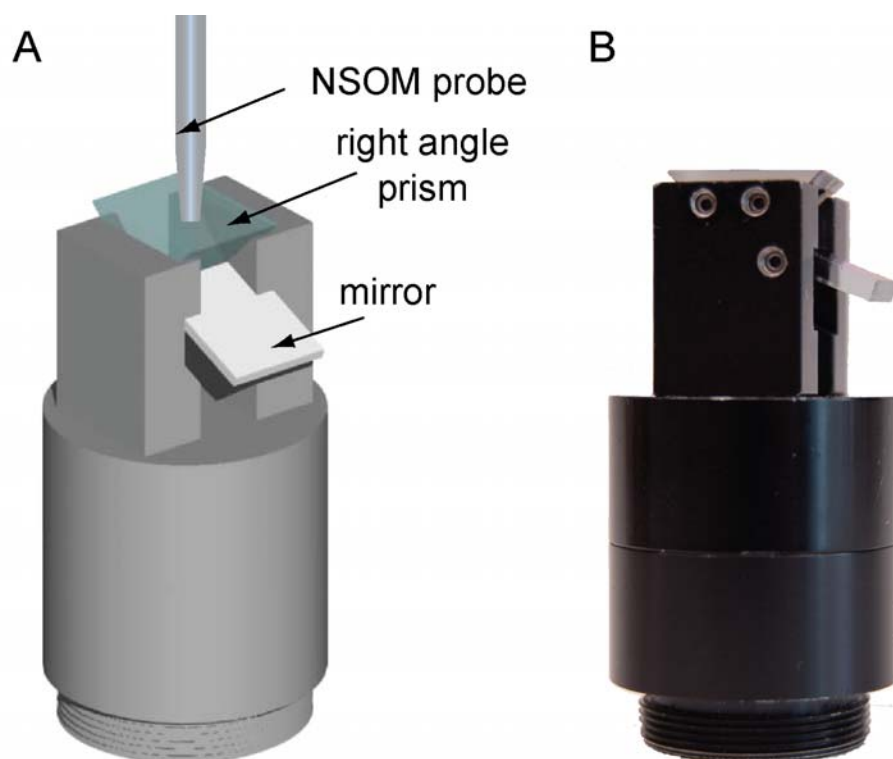
Figure 2.6. (A) Scheme and (B) optical micrograph of prism holder for PSTM set-up.
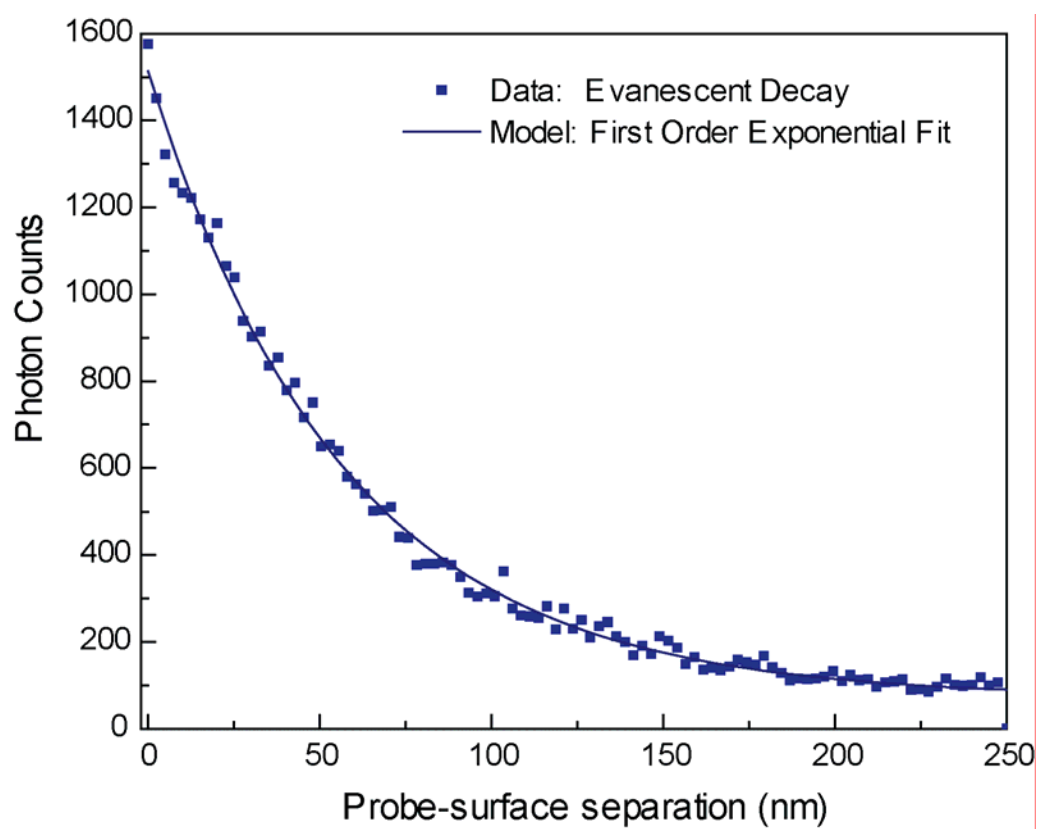
Figure 2.7. Photon counts as a function of increasing distance *z* from the sample interface. Probe-surface separation was measured from the point at which the probe was in feedback.

2.3 Overview of Single Particle Optical Spectroscopy

The optical properties of NPs strongly depend on the size, shape, and material of the particles.[27] Until recently, these properties were studied in large ensembles, but as optical microscopy techniques were refined, studies of individual metal NPs became possible.[54-56] The investigation of single NPs adds insight to conventional ensemble measurements by removing inhomogeneity in the optical signal that arises because of differences in shape, size and structure of the NPs. Although NSOM can be used to study individual particles to correlate the optical signal with topography, near-field techniques are usually limited to surfaces or surface-bound structures.

2.3.1 Set-up for Single Particle Spectroscopy

Single particle spectroscopy was performed with an inverted microscope (Nikon TE2000, Fryer Co.) coupled to a 550 mm focal length (f) imaging spectrometer (Triax 552, Jobin Yvon) with a convex lens ($f = 10$ cm) (Figure 2.8). Triax 552 has two entrance and two exit ports, which allowed the instrument to be equipped with two LN_2-cooled charge coupled device (CCD) detectors: one for VIS detection (1024x256, Symphony, Jobin Yvon) and one for near-infrared (NIR) detection (1024x1, InGaAs, Jobin Yvon). The technical advantage was that we could switch between the detectors without the need for re-alignment. A video camera (CoolSnap ES, Photometrics), used for identifying the nanoparticles and aligning them onto the CCD, was attached to the microscope.

The exit port of the microscope and the entrance port on the spectrometer were separated by 40 cm with the lens positioned half way between. This distance can be calculated using lens equation:
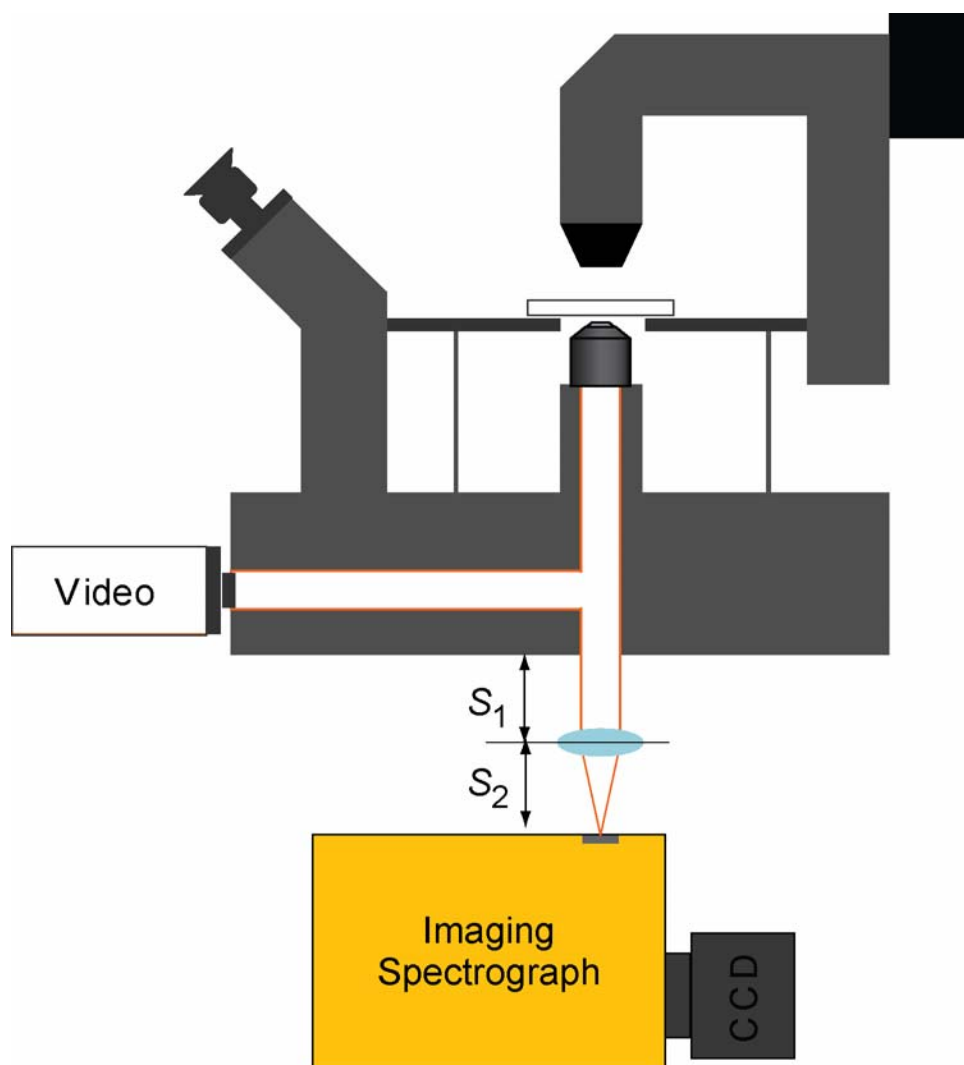
Figure 2.8. Microscope-spectrometer set-up for single particle spectroscopy.

$$\frac{1}{S_1} + \frac{1}{S_2} = \frac{1}{f}$$

where f = 10 cm, S_1 is the distance between the lens and the microscope exit port, and S_2 is the distance between the lens and the spectrometer entrance port. By changing the location of the lens, the image from the microscope that falls onto the CCD detector can be magnified or demagnified; when $S_1=S_2$ the image is not magnified. Imaging was not possible with the single-line NIR CCD (1024 x 1 pixels) detector.

2.3.2 Single Particle Spectroscopy of a Mesoscale Au Ring

Figure 2.9 illustrates a series of steps required to obtain the scattering spectrum from a single nanoparticle. First, the sample of interest (Au rings on ITO/glass substrate) was placed on the inverted microscope and illuminated with light from a dark-field (DF) condenser (NA = 0.95). A variable aperture 100X oil immersion objective (NA = 0.5-1.3) positioned below the sample. To collect the scattered light from the sample, the entrance slit on the spectrometer was opened to the maximum setting of 2 mm, and the grating was placed at zero order to project an image from the microscope onto the CCD. After the image was acquired (Figure 2.9A), one of the particles was identified and placed in the center of the imaging field. The region of interest was selected by closing the entrance slit on the spectrometer to 0.5 μm - 1 mm (Figure 2.9B) and by cutting the y-pixels on the CCD to isolate a single particle (Figure 2.9C). The NA of the objective was set below the NA of the DF condenser to collect only the scattered light. The spectrometer grating was then rotated to disperse the first-order diffracted light onto the CCD, and the spectrum was acquired (Figure 2.9D). The particle was then moved out of the selected region, and the spectrum from an empty region (area without a particle) was collected in order to
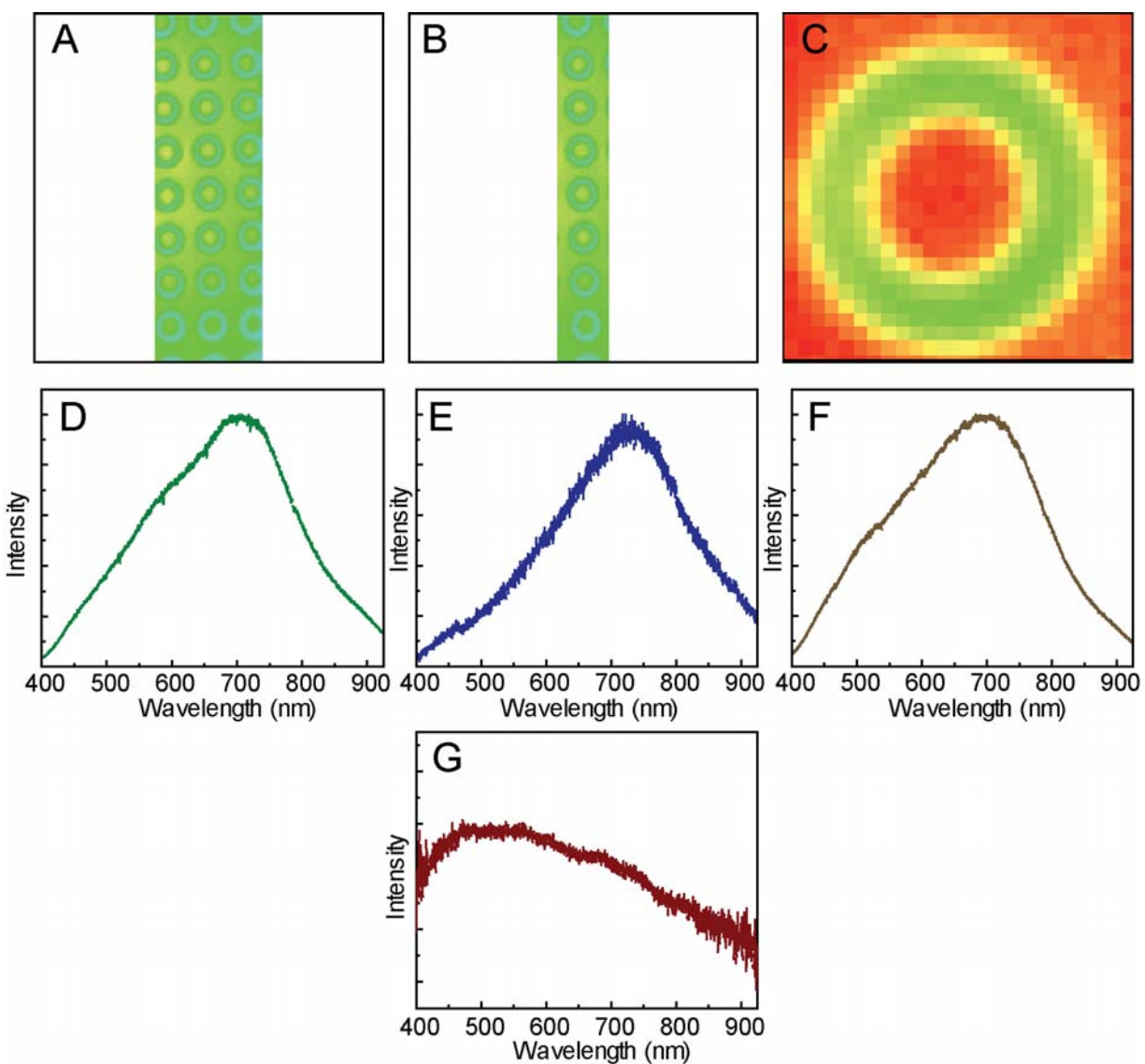
Figure 2.9. (A) Wide field (slit width = 2mm) image of 3 μm Au rings on ITO/glass substrate taken with a spectrograph with a 150 grooves/mm grating at zero order. (B) The slit of the spectrometer was closed to 0.8 mm to select only one row of particles. (C) One particle was selected by cutting down the pixels of the CCD in the software. The grating was then rotated to disperse the light and (D) raw spectrum was collected. The particle was moved and (E) background spectrum was taken. (F) The lamp profile was taken by increasing the NA of the objective lens. (G) Normalized scattering spectrum of a single Au ring.

perform background subtraction (Figure 2.9E). If desired, the background spectrum could be obtained by selecting different pixels on the CCD instead of moving the sample. To obtain the lamp profile, the NA of the objective was increased to 1.3 to collect the transmitted light (Figure 2.9F). To verify that the transmitted light spectra instead of scattered light spectra can be used for correcting the spectra against the lamp profile, the spectra of transmitted and scattered light were compared, and no differences in their spectral profiles were observed. If a variable NA objective is not available, the lamp profile can be obtained by replacing the sample with a strong white scatterer. The raw spectrum (Figure 2.9G) was processed by removing the background signal and correcting for the lamp spectral profile and CCD efficiency by using the following formula:

$$normalized\ spectrum = \frac{raw\ spectrum - background}{lamp\ profile}$$

Integration times on the order of 100 ms were necessary depending on the scattering intensity of the particles. For the lamp profile, the integration time needed to be adjusted to 5-10 ms; otherwise, the lamp intensity saturated the CCD.

To understand what parameters affected spectra quality, concepts of spectral resolution (SR), spectral coverage (SC), and signal-to-noise (S/N) are necessary. The following formulas can be used to calculate SR and SC:

SR = (linear dispersion) x (pixel width) x (slit width/pixel width)
     (nm/mm)   (mm/pixel)   (pixels)

SC = (linear dispersion) x (pixel width) x (number of pixels)
     (nm/mm)   (mm/pixel)   (pixels)

For example, for 600 grooves/mm grating with a 100-μm slit width:

SR = (3.10 nm/mm) x (0.026 mm/pixel) x (100 μm/ 26μm pixel^{-1}) = 0.5 nm

and assuming the entire CCD chip is used when acquiring the spectra:

$$SC = (3.10 \text{ nm/mm}) \times (0.026 \text{ mm/pixel}) \times (1024 \text{ pixels}) = 82.5 \text{ nm}$$

From these equations it is clear that if the grating in the spectrometer is changed to 1200 grooves/mm, resolution will increase at the expense of spectral coverage. Increasing resolution typically decreases signal-to-noise (S/N) because the same number of photons are now spread over more pixels. Other ways to improve the S/N ratio is to average multiple spectra; averaging n spectra, improves the S/N ratio by $\sqrt{n}$.

Other factors that were considered during spectra acquisition:

1. **Stray light**. Discontinuity in the spectra can arise if scattering from a neighboring particle falls into the selected region of interest. Stray light is an issue with large-area (1024x256 pixels) CCD detectors. This effect was reduced by draping a black cloth over the spectrometer to ensure all the unused entrance and exit ports were covered.

2. **Slit width**. Reducing slit width increases resolution but also decreases signal intensity.

3. **Grating**. Higher density gratings improve resolution but at the expense of spectral coverage and signal strength. For absorption, transmission, and fluorescence studies 150 grooves/mm grating had sufficient resolution and provided the highest SC. Two spectral acquisitions with this grating covered the entire visible region from 400-1000 nm (~330 nm/acquisition).

2.4 Overview of Lithography

The two lithographic methods that we used to fabricate micron-scale structures with mesoscale features included photolithography and electron beam lithography (EBL). These lithographic techniques share the same operational principle: exposure of an appropriate resist to

either UV light or an electron beam. Photolithography is a parallel technique that requires the use of a mask between the source of radiation and photosensitive material. Conventional lithography takes advantage of a hard mask to transfer the pattern on the mask into the photosensitive resist. Because of diffraction limitations and wavelength sensitivity of the resist, the resolution is usually ~500 nm. Phase-shifting photolithography (PSP),[57] a form of photolithography that takes advantage of an elastomeric phase-shifting mask patterned with μm-scale features, has made it possible to generate structures with feature sizes down to ~30-50 nm over large areas (cm^2).[58, 59] Composite polymeric masks for PSP can be generated from masters produced by conventional photolithography.

EBL is a serial, direct-write technique. By scanning a focused beam of electrons across the surface of a polymer, usually PMMA, a pattern is produced in the resist after development. Unlike optical lithography, masks are not necessary. The patterns are defined by software; therefore, arbitrary structures can be generated. One major disadvantage of EBL is the low throughput and slow nature of the process; the time required to write a 2 mm^2 area of micron-scale ellipses with ~200 nm widths was 2-4 h.

2.4.1 Materials

Photolithography: Positive tone-resist, Shipley 1805, was purchased from MicroChem. Negative tone-resist, ma-405, was purchased from MicroResist Technology. 4-methyl-2-pentanone used to dilute ma-405 was purchased from Aldrich. Resist developers, Microposit 351 (for Shipley 1805) and LDD^{TM}-26W (for ma-405) were purchased from MicroChem. Microposit 351 developer was diluted with water (1:5 vol), LDD^{TM}-26W was used as received. Fluorosilane

((tridecafluoro-1,1,2,2-tetrahydrooctyl trichlorosilane) for silanizing the masters was purchased from Gelest.

E-beam lithography: Positive tone e-beam resist, 950PMMA A3, and copolymer MMA (8.5) MAA EL6 were purchased from MicroChem. Developer solution for MMA/PMMA consisted of 1:3 dilution of methyl isobutyl ketone (MIBK) with isopropyl alcohol (IPA), which were purchased from Aldrich.

Substrates: Si (100) 3" wafers were purchased from Silicon Sense Inc. Indium tin oxide (ITO) covered glass was purchased from Thin Film Devices. The thickness of the glass was 0.4 mm, and one side covered with 150 nm of ITO coating with <30 Ω resistance.

Masks: Polydimethylsiloxane (PDMS) prepolymer kit including curing agent (Sylgard 184) for preparing soft *s*-PDMS was purchased from Dow Corning. To prepare hard *h*-PDMS the following chemicals were combined: 3.4 g VDT-731 ((7.0-8.0% vinylmethylsiloxane)-dimethylsiloxane copolymer, trimethylsiloxy terminated, 800-1,200 cs), 50 μL Pt-catalyst (platinum-divinyl tetramethyl-disiloxane complex in xylene, SPI6831.1), 1 drop modulator (2,4,6,8-tetramethyls-2,4,6,8-tetravinylcyclotetrasiloxane), and 1 g HMS-351 (25-30% methylhydrosiloxane)-dimethylsiloxane copolymer, trimethylsiloxane terminated, 25-35 cs). All chemicals for h-PDMS were purchased from Gelest.

2.4.2 Fabrication of Masters

We used conventional photolithography to generate microscale features in photoresist, which were then used as masters to mold PDMS masks for PSP. Figure 2.10A illustrates the steps involved in the fabrication of masters. A positive-tone photoresist was spin-cast on a Si wafer at 4000 rpm and baked for 3.5 min at 105 °C. Using a mask aligner (Quintel 2000), the
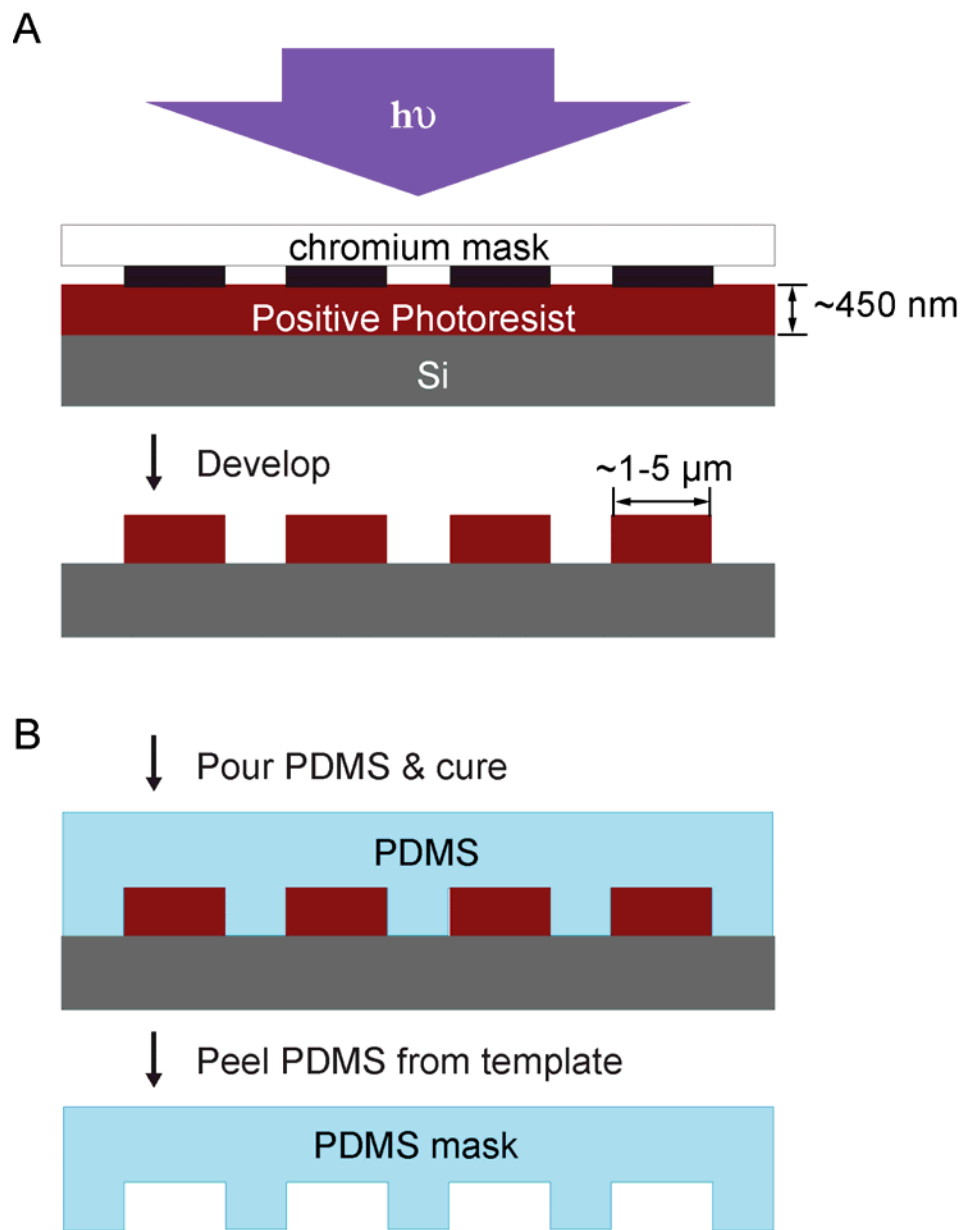
Figure 2.10. Schematic illustrations of the (A) fabrication of photoresist masters and (B) fabrication of PDMS mask.

wafer was brought into contact with a Cr mask having the desired features (e.g. 3-μm circles with center-to-center separations of 4.5 μm) and was exposed to broadband UV light (~17 mW/cm^2 at 365 nm) for several seconds. The mask was then removed, and the wafer was developed in diluted Microposit 351 to reveal solid 3-μm circular posts with the same spacing as the chromium mask.

2.4.3 Fabrication of PDMS Mask for Phase-Shifting Photolithography (PSP)

Elastomeric phase masks were prepared by casting and curing PDMS against masters consisting of patterned features (Figure 2.10B). The masters, patterned with 3-μm posts, were first protected by a silane monolayer by placing the patterned wafers with a few drops of fluorosilane in a vacuum desiccator for 2 h. A composite PDMS stamp was prepared by spin-coating a mixture of hard *h*-PDMS was on top of the patterned wafer and letting the polymer cure for couple minutes at 70 °C; then ~2 mm of soft *s*-PDMS was poured on top of *h*-PDMS and cured for 2 hours at 70 °C. The polymeric mask, patterned with recessed 3-μm cylindrical posts, was removed from the master and later used for PSP.

2.4.4 Fabrication of Resist Templates for Circular Corrals Using PSP

PSP was performed using composite PDMS masks patterned with recessed 3-μm posts spaced by 4.5-μm, with surface relief depths of ~400-500 nm and a negative tone resist (Figure 2.11A). The patterned PDMS mask was first brought into conformal contact with a layer of photoresist (~400 nm) supported on glass or ITO/glass. The substrate was then exposed to broadband ultraviolet (UV) light for 20 s. Subsequent development of the photoresist produced ~3 μm recessed rings with linewidths on the order of ~100-250 nm (Figure 2.11B).
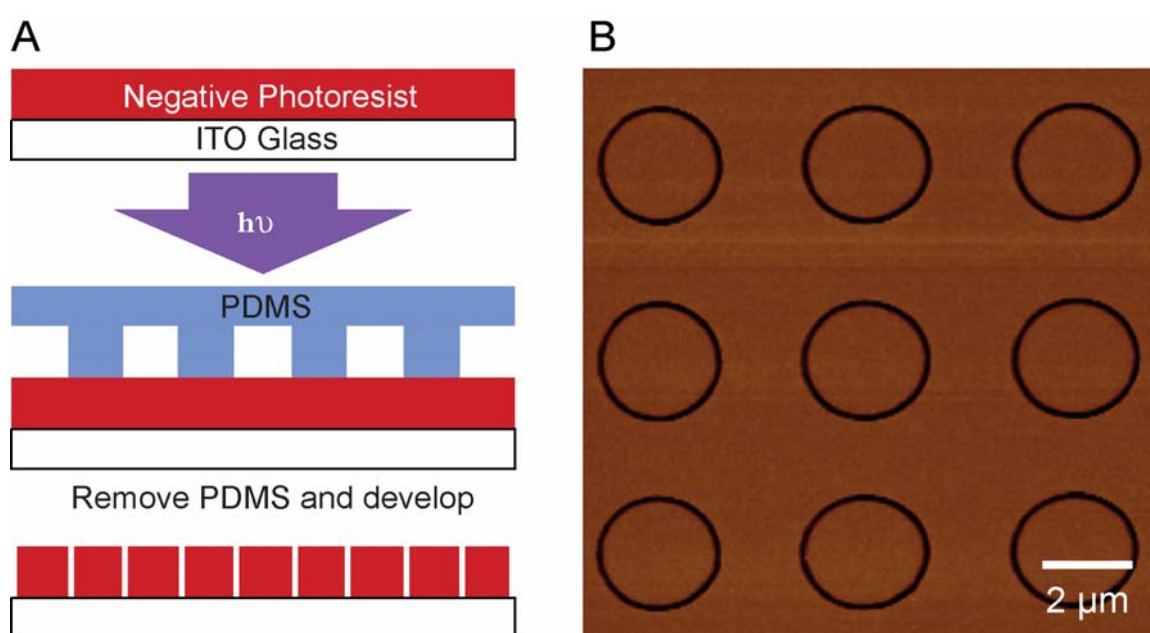
Figure 2.11. (A) Schematic illustration of PSP and (B) AFM image of recessed rings in negative tone resist produced by PSP.

2.4.5 Fabrication of Resist Templates for Elliptical Corrals Using EBL

E-beam lithography was performed using FEI Quanta environmental SEM equipped with a nanometer pattern generation system (NPGS) (Figure 2.12A). ITO/glass substrates were spin coated with MMA/PMMA, where the MMA copolymer was used to create an undercut for easy removal of the resist after metal deposition. DesignCAD LT 2000 software was used to define arrays of different size ellipses (Figure 2.12B), and the resist was exposed with a 30 kV electron beam. The line dose of the exposure was set at 4.5 nC/cm. The resist was then developed in 1:3 (vol) MIBK:IPA solution to generate elliptical patterns with ~200-250 nm linewidths. Metal was then deposited into the resist template and after lift-off the structures were imaged with SEM (Figure 2.12C).

2.5 Summary

Over the past several years, a number of exciting advances have been made in the field of nano-optics, largely due to development of fabrication and characterization methods of nanoscale structures. We have assembled near-field and far-field microscopy tools for investigation of the optical properties of nanoscale and mesoscale structures and demonstrated how these tools can be modified to improve our understanding of the nano-optical phenomena. We have also demonstrated the use of lithographic techniques for creating soft templates that can be used to create patterned arrays of optically active structures.
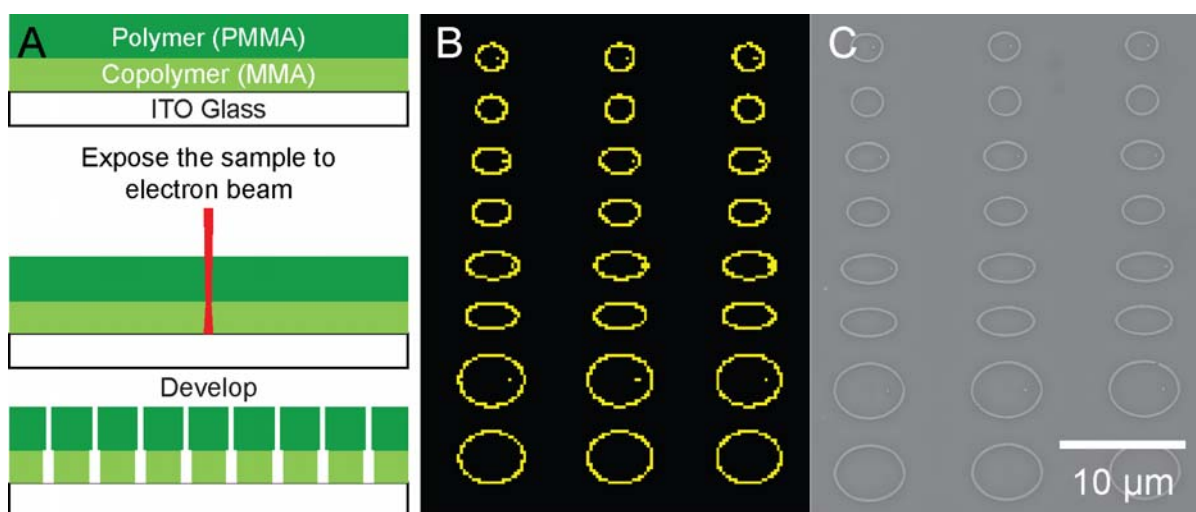
Figure 2.12. (A) Schematic illustration of e-beam lithography. (B) DesignCAD drawing of desired patterns, and (C) SEM image of metal ellipses produced after deposition and lift-off of the resist template.

Chapter 3

Templated and Hierarchical Assembly of CdSe/ZnS Quantum Dots

3.1 Introduction

Control over the patterning of functional nanomaterials is an important component in producing well-defined structures for emerging applications in photonics, electronics and sensors. Techniques that have been used to organize nanostructures on surfaces include directed growth assembly methods, self-assembly, electric field and electrostatic assembly, and template-based assembly.[60-70] The directed growth of nanostructures using patterned catalytic areas has been applied to zinc oxide nanostructures,[61, 71, 72] gallium nitride nanotubes,[73] and carbon nanotubes.[63, 64] These structures can be grown aligned and perpendicular to the substrate under proper surface and catalyst conditions.[61, 63] The latter assembly techniques are most useful for manipulating pre-formed micro- and nanostructures into well-defined positions in two (2D) and three dimensions (3D). For example, monodisperse polymeric spherical colloids have been shown to self-assemble into pre-defined templates by capillarity.[69, 74] Carbon nanotubes, semiconducting nanowires, and metallic nanorods can be aligned between arrays of electrodes by strong electric fields.[60, 67] Photoresist templates of holes and trenches have been used to assemble polystyrene microspheres, Au/SiO_2 colloids, and metallic half-shells;[65, 69, 75] molecular wires and semiconducting nanowires have also been aligned in 2D using microfluidic channels.[76, 77]

Semiconductor quantum dots (QDs) have attracted attention as potential active materials in photonics[78] and optoelectronics[71, 79] because of their tunable emission, and high fluorescence efficiency.[80-82] For example, thin layers of CdSe QDs have been used as anodes in field emission displays. Figure 3.1 shows a field emission device fabricated using CdSe QDs as the anode layer and carbon nanotubes as the filed emitting cathode layer. The ability to pattern these colloidal QDs will be important if these materials are to be incorporated into future technologies such as
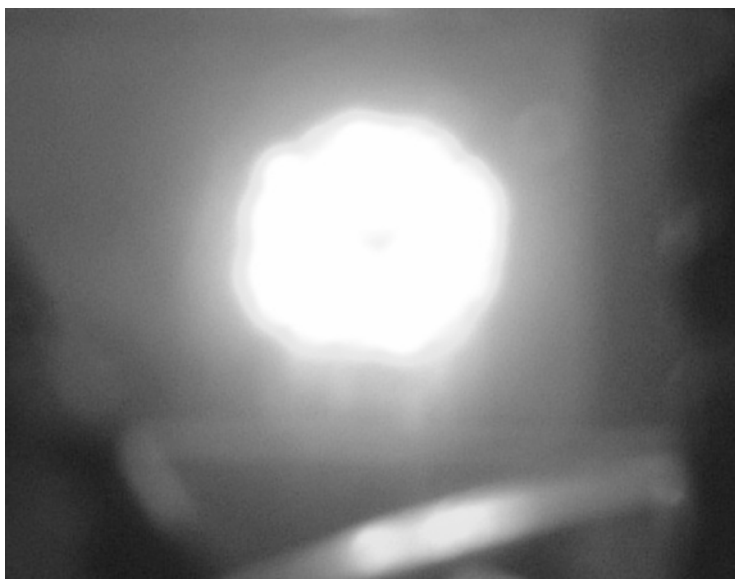
Figure 3.1. Image of light emission from CdSe anode layer from a carbon nanotube field emitter device.

photovoltaics, switches, light-emitting diodes (LEDs), and sensors.[83] Chemically synthesized colloidal semiconductor QDs self-assembled into superlattices or into close-packed solids on thin films show interesting cooperative physical properties and have potential applications in QD lasers and conducting thin films.[62, 84, 85 86] QDs packed onto 2D photonic crystal slabs have shown enhanced fluorescence intensity of up to 108 times compared with QDs on unpatterned surfaces.[87] The relative packing densities of these QDs affected the short-range and long-range[84] interactions between them. Building close-packed solids from semiconductor QDs enable the investigation of the collective optical and electronic properties of these assemblies. Therefore, it is important to construct large-area assemblies of these nanostructures with well-defined architectures so that new properties resulting from different packing densities can be investigated.

We have used soft templates to direct the assembly of CdSe/ZnS QDs into structures of different geometries. Nanofabrication techniques that can generate soft templates for the assembly of nanostructures include EBL and phase shifting photolithography (PSP). E-beam patterning has a resolution of 10 nm in PMMA, and PSP can generate feature sizes down to 30 nm in photoresist.[58, 59] For certain applications, such as field emission arrays and sensors, arrays of nanostructures patterned over large areas (cm^2) and in parallel are desirable. Soft templates prepared by PSP are thus advantageous when compared to templates patterned by the serial technique of EBL. One of the limitations, however, in generating templates of holes and trenches using optical lithography is the inherently low resolution (sub-μm) of negative-tone photoresists.[88] We have improved the resolution by using (i) composite PDMS masks for PSP,[58, 59] and (ii) a negative-tone photoresist that does not require the requisite post-baking step, which

broadens feature sizes. An additional advantage of our template-based patterning method is the ability to pattern on variety of substrates, ranging from glass to plastic.

3.2 Experimental Methods

3.2.1 Materials

Chemicals for QD Synthesis: Cadmium oxide (CdO), selenium (Se), tri-octylphosphine oxide (TOPO), tri-octylphosphine (TOP), hexadecylamine (HAD), diethylzinc in 1M heptane, hexamethyldislathiane (HMDT), thioglycolic acid (TGA), tetramethylammonium hydroxide in methanol (25% wt), tetrahydrofuran (THF), methanol, hexane were purchased from Aldrich, tetradecylphosphonic acid was purchased from Alfa Aesar. All chemicals were used as received, without further purification.

Chemicals for Photolithography: Negative-tone resist ma-405 was purchased from MicroResist Technology. 4-methyl-2-pentanone (used to dilute the resist) was purchased from Aldrich. Resist developer, LDD[TM]-26W was purchased from Microposit[TM], Rohm and Haas. Glass substrates were 25 mm diameter, No. 1 coverslips from Fisher Scientific. The substrates were cleaned with soap and rinsed with ultrapure water (18.2 MΩ/cm) from a Millipore system.

3.2.2 Synthesis of Water-soluble CdSe/ZnS Quantum Dots

CdSe Core: CdSe QDs were synthesized using previously published[89, 90] high temperature (250-310 ºC) solution phase methods. This procedure involved the decomposition of CdO in the presence of stabilizing surfactants followed by a rapid injection of Se precursor, which nucleated the growth of the QDs. In a typical synthesis of CdSe QDs, 0.4 mmol of CdO, 0.80 mmol of TDPA, and 9.76 mmol of TOPO were loaded into a three-neck flask. The reaction

mixture was heated to 310 °C under N_2 flow. The reddish CdO powder was dissolved into TDPA and TOPO and generated a colorless solution. The temperature was lowered to 270 °C and Se stock solution (0.52 mmol of Se powder dissolved in 5.46 mmol of TOP) was rapidly injected into a vigorously stirred CdO/TDPA/TOPO solution. After the injection of the Se precursor the temperature dropped slightly and was maintained between 250-260 °C throughout the reaction. Because the emission of CdSe QDs depended on the size of the particles (Figure 3.2), aliquots were taken at various times during the reaction to obtain QDs with different sizes. The emission spectra of QDs produced from this high-temperature method had narrow full-width at half maximum (FWHM). Figure 3.3 displays spectra obtained from QDs shown in Figure 3.2. The small FWHM resulted from the narrow particle size-distribution ($\sigma < 5\%$) (Figure 3.4).

ZnS Shell: The emissive properties of CdSe QDs were improved by growing a higher band gap material (ZnS) around the CdSe core to construct core-shell structures (CdSe/ZnS). It has been shown that the epitaxial growth of ZnS shells (typically 2 to 3 monolayers) not only enhances the luminescence efficiency (quantum yield ~0.9) but also increases the photostability of the core.[91-93] In a typical synthesis, to grow the ZnS shells around the CdSe cores, 0.026 g of CdSe (CdSe QDs were washed with hexane and precipitated out of methanol, followed by drying under vacuum overnight to remove excess surfactant before growing the ZnS shell) was dissolved in 5 g of TOPO and 2.5 g of HDA, and heated to 240 °C under nitrogen. The ZnS precursor solution (0.8 mmol diethylzinc in 1M heptane, 1 mmol of HMDT, and 6 mL of TOP) was prepared in the glove box and then injected dropwise into rapidly stirring CdSe/TOPO/HDA solution.[93] After the transfer of ZnS precursor was complete, the reaction was run for 1 h. ZnS

Figure 3.2. Fluorescence image of CdSe quantum dots showing an increase in QD size going from blue (~1 nm in diameter) on the left to red (~5 nm in diameter) on the right.
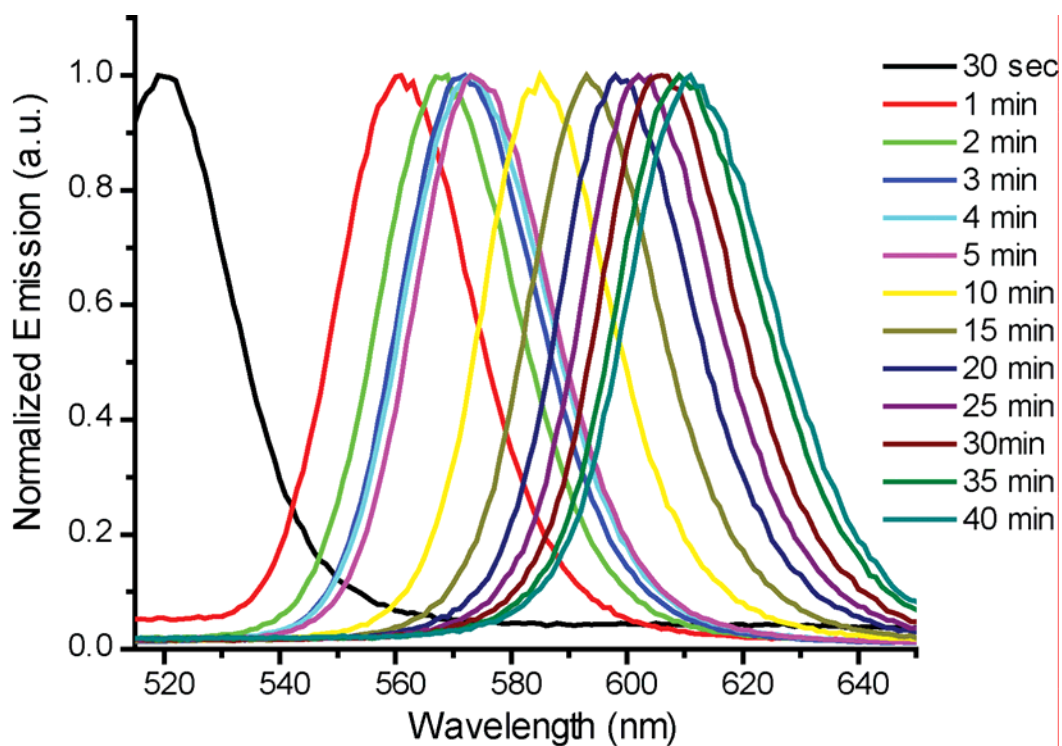
Figure 3.3. Emission spectra FWHM of ~30 nm of CdSe QDs in hexanes. Time indicates when the aliquots were taken after injection of the Se-stock. Spectra correspond to the image in Figure 1.
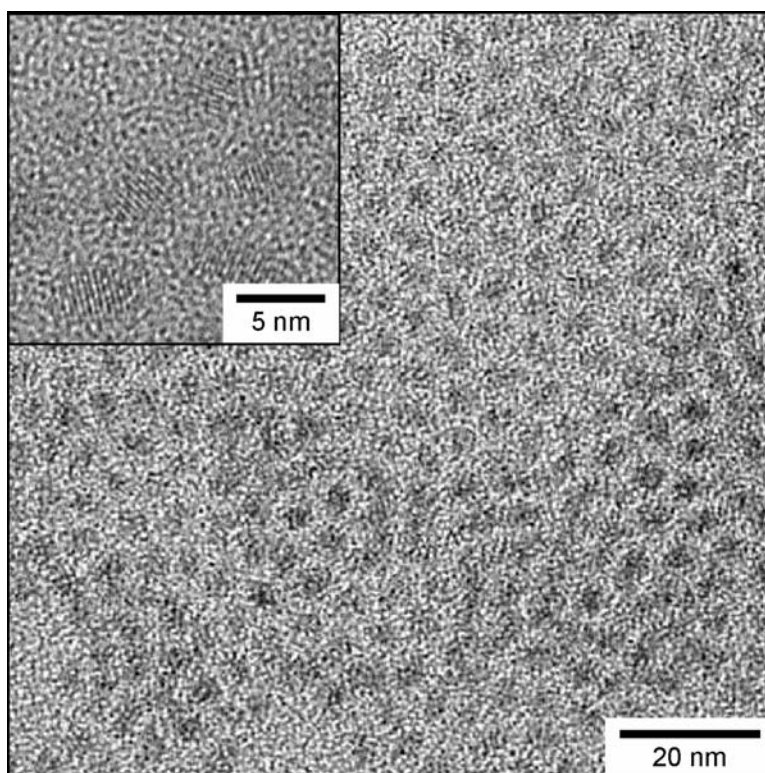
Figure 3.4. TEM micrograph of CdSe QDs. Inset : High-resolution TEM micrograph shows the crystalline and slightly oblong nature of the CdSe QDs.

passivated the surface traps and enhanced the emission properties of the QDs by forcing exciton recombination to occur within the core of the nanocrystal.

Water-soluble CdSe/ZnS: To assemble these QDs into photoresist template structures, the QDs were made water-soluble because the photoresist, which was used for the templates, was not compatible with organic solvents. Mercaptoacids are commonly used for making QDs soluble in aqueous solutions.[94, 95] The QDs were made water-soluble by functionalizing the outer shells of CdSe/ZnS QDs with TGA. In a typical synthesis, ~100 mg of TOPO capped, dry CdSe/ZnS were dispersed in 50 mL of methanol in the presence of ~0.25 mL of thioglycolic acid (TGA, Aldrich) (about 3 times the weight of QDs) and 8 mL of TMAH. The resulting solution was then allowed to reflux at 60 °C for 12 h under N_2 while stirred vigorously. As the reaction progressed the TOP/TOPO capping groups were exchanged with TGA. The final reaction volume was reduced by rotovapping off the solvent. The resulting solid was then dispersed in methanol (0.5-1 mL) followed by addition of 15-20 mL of THF. At this stage, the QDs precipitated out of the solution and were removed by centrifugation. This procedure was repeated three to four times (or until the supernatant became clear) to remove TOP/TOPO which was exchanged with the mercaptoacid. The solids were then dried under N_2 and subsequently dispersed in water.

3.2.3 Transmission Electron Microscopy of CdSe QDs

Samples for transmission electron microscopy (TEM) were prepared by placing a drop of hexane solution of CdSe QDs onto a 100 mesh copper grid purchased from Ted Pella, Inc. The solvent was allowed to evaporate overnight or under vacuum, and TEM images were acquired using a Hitachi HF2000 TEM at 200 kV accelerating voltage. Figure 3.4 shows the uniform size

distribution of the CdSe QDs, and the high resolution images (Figure 3.4, inset) demonstrate the crystalline and slightly oblong nature of the QDs.

3.2.4 Fabrication of Photoresist Templates

Photoresist-coated substrates were prepared by spinning diluted (1:1 with 4-methyl-2-pentanone) ma-405 resist at 6,000 rpm for 40 s onto cleaned glass coverslips and pre-baking the resist at 95 °C for 2 min. Composite PDMS masks,[59] patterned with recessed 3-μm posts spaced by 4.5 μm and 5-μm lines spaced by 5 μm, were used as the pattern transfer element for PSP on thin (100-200 nm) photoresist films. The substrates were exposed to broadband UV light (18.5 mW/cm^2 at 365 nm) and then developed in LDD^{TM}-26W. After development, trenches of photoresist were produced at the edges of the relief features of the mask. Figure 3.5 shows images of the trenches in photoresist acquired with an atomic force microscope (AFM). The minimum dimension of curved and straight lines in photoresist was as small as 100 nm (Figure 3.5, insets).

3.2.5 Assembly of CdSe/ZnS Quantum Dots in Photoresist Templates

Photoresist templates patterned by PSP were used to assemble CdSe/ZnS nanocrystals into patterns for investigation of their collective optical properties. Figure 3.6 summarizes the process for generating surface-patterned CdSe/ZnS mesostructures. Different sizes of water-soluble quantum dots were assembled into the template by immersing the patterned template in a concentrated solution of highly crystalline, water soluble CdSe/ZnS nanocrystals for 12-36 h. Sedimentation occurred initially along the edges of the patterned template, and then the interior of the recessed regions were filled to form a reasonably ordered solid as the templates were
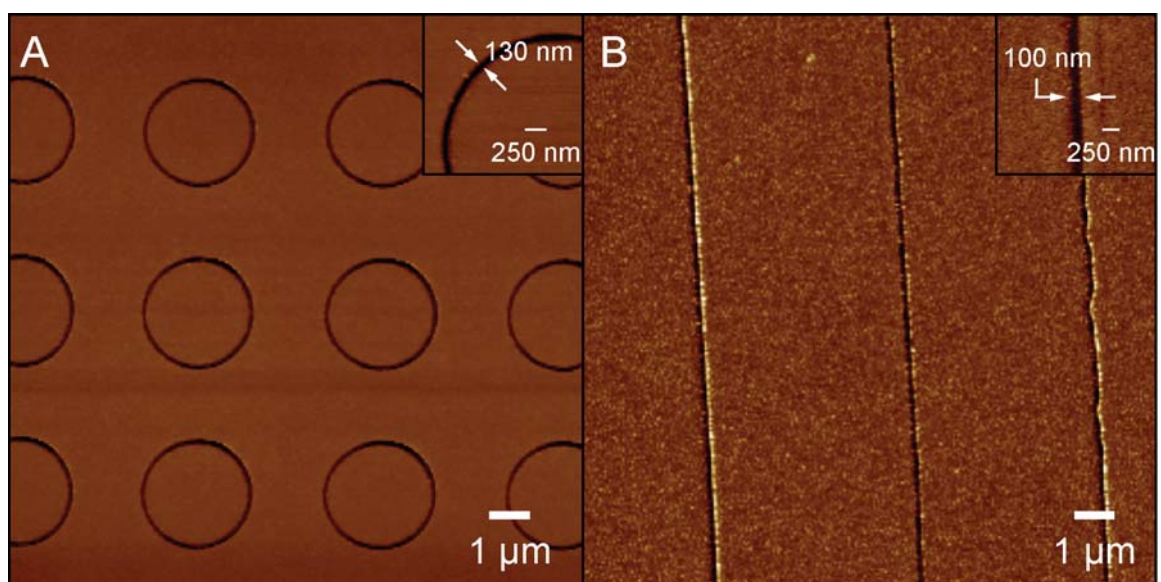
Figure 3.5. AFM images of (A) rings and (B) trenches formed in negative tone resist using phase-shifting photolithography. These linewidths can be as narrow as 100 nm.
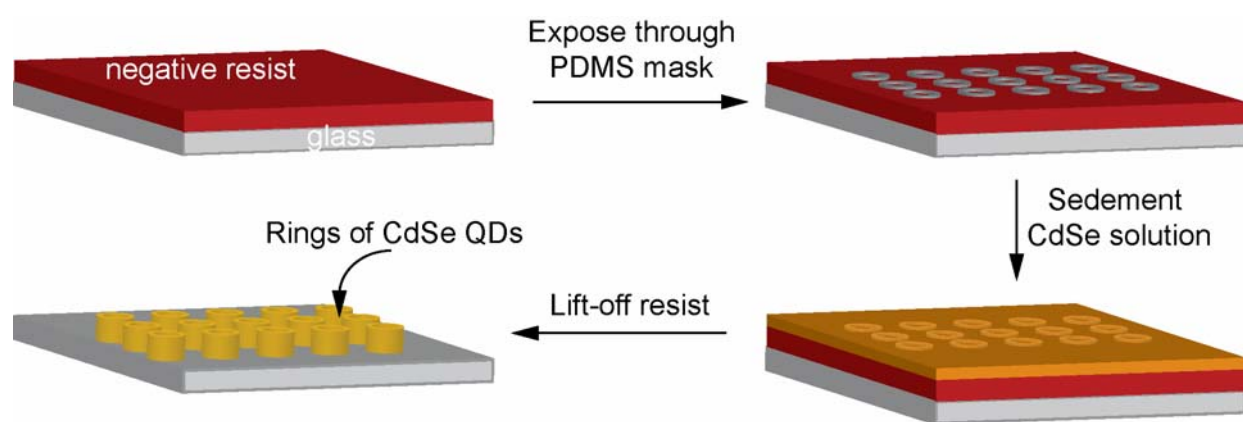
Figure 3.6. Schematic illustration for patterning chemically synthesized nanomaterials using templates made of photoresist. A pattern is produced in negative-tone resist using PSP with composite PDMS masks. The scheme depicts an example of a ring generated by PSP using a mask patterned with circular, recessed posts. The nanomaterials assembled into the recessed regions of the template by sedimentation. Removal of the photoresist generated arrays of structures in specific patterns.

immersed in the solutions of nanocrystals for longer periods of time (several days) (Figure 3.7). The substrates were removed from the solution, dried under N_2 and then placed in an oven at 180 °C for 10 min to anneal the QDs. The template was then removed by lift-off in acetone, and CdSe/ZnS mesostructures with critical feature sizes of 100 nm and 10-50 nm in height (depending on sedimentation period) were obtained.

3.2.6 Optical Characterization of Patterned CdSe/ZnS QDs

Photoluminescence (PL) spectra of CdSe/ZnS QDs in solution and patterned on substrates were collected with an excitation wavelength of 400 nm. Near-field scanning optical microscopy (NSOM) fluorescence images were acquired in transmission mode using Al-coated probes and an Aurora-3 NSOM (Veeco) with an excitation wavelength of 400 nm.

3.3 Results and Discussion

CdSe/ZnS QDs were patterned into mesostructures with curved and straight features over areas ~ 1 in^2. Red dots (PL emission in solution was 591 nm) were assembled into rings (Figure 3.8A), and yellow dots (PL emission in solution was 577 nm) were assembled into lines (Figure 3.8B). Using template-based assembly, we achieved hierarchical patterning of nanostructures—organization over nm^2 (self-assembly of dots), over μm^2 (template shape), and over cm^2 (arrays of template pattern).

One application for patterned CdSe/ZnS mesostructures is the investigation of the collective optical properties of the QDs. For example, the band-edge PL peak of CdSe and CdSe/ZnS QD solids have been observed to shift to lower energies (a red-shift in wavelength) compared to the PL peak of QDs dispersed in solution because of dipole-dipole interdot
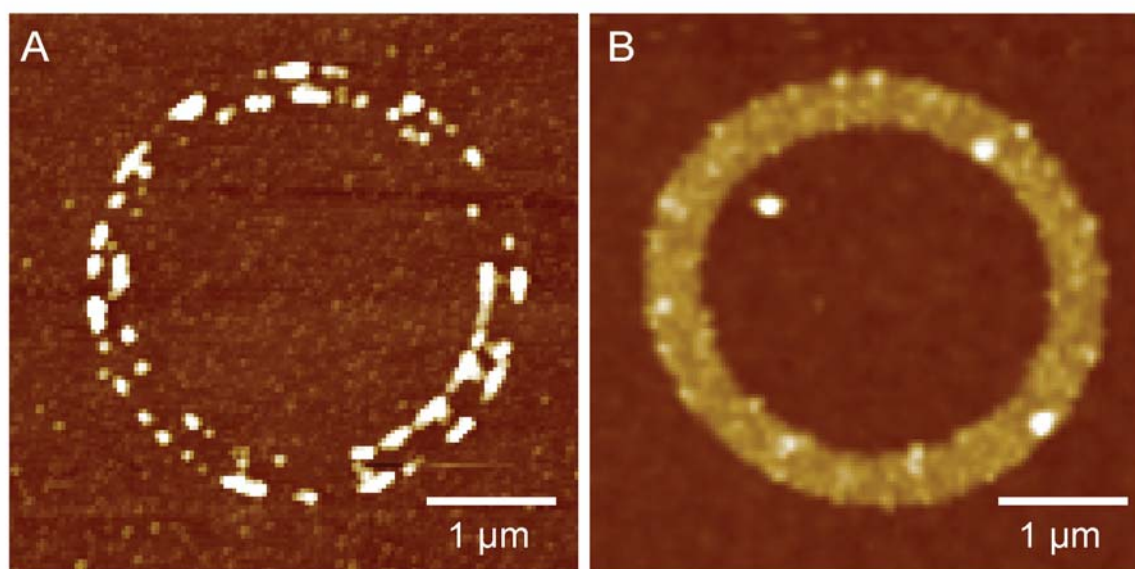
Figure 3.7. AFM images of quantum dots assembled into ring templates after (A) 12 hours and (B) two days of sedimentation.
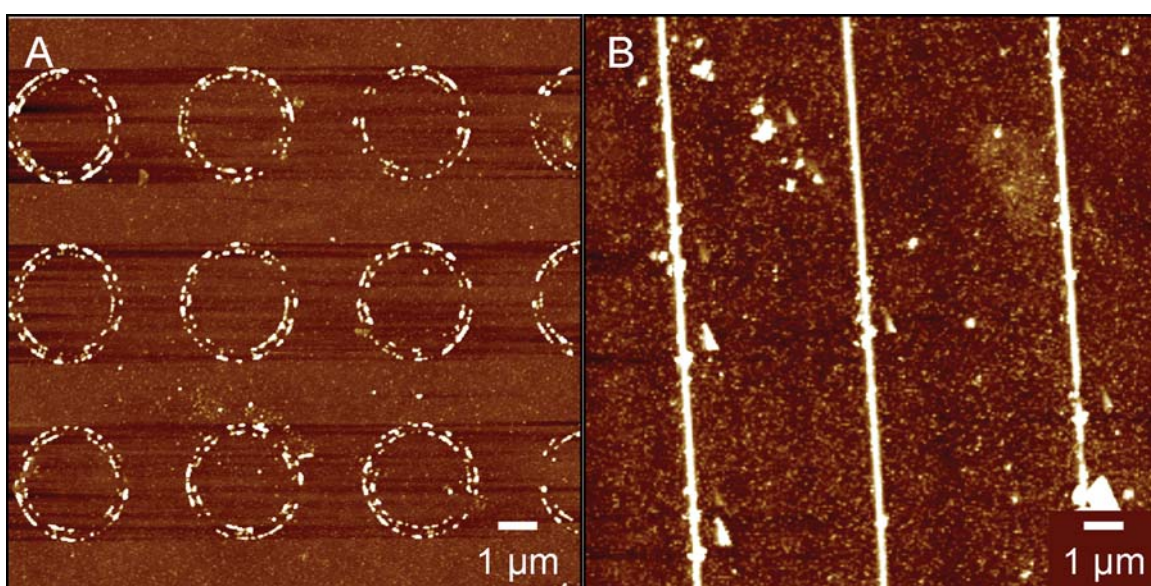
Figure 3.8. (A-B) AFM images of quantum dots patterned into rings and lines using the templates from Figure 3.4. Lines with well-packed quantum dots were as narrow as 100 nm, and the height of the quantum dot structures varied between 15-50 nm.

interactions.[62, 84] Other studies reported that the absorption edge of CdSe dots red-shifted in solution and in close-packed films because of changes in the external dielectric environment.[96] We characterized the PL of QDs patterned into arrays of rings and lines. The PL of CdSe/ZnS dots in dilute solutions compared to those patterned into rings and lines exhibited a slight (6-7 nm) red-shift in the emission wavelength (Figure 3.9). This shift was observed for the red dots, which were patterned into rings, as well as the yellow dots, which were patterned into lines. The red-shift of the PL observed from the CdSe/ZnS mesostructures is most likely because of coupling between the dots (energy transfer) and interactions between the dots and their surrounding dielectric (close-packed CdSe/ZnS dots and air/glass substrates compared to water media). We also measured a red-shift in the PL of ~10 nm for thin (200-300 nm) films of unpatterned yellow CdSe/ZnS dots supported on glass. The films were drop coated on glass and dried in air overnight. The thickness of the films was determined by the use of an AFM. The magnitude of the red-shift that we observe falls between the reported red-shifted wavelengths for solids of CdSe/ZnS dots (40 nm) and CdSe dots (~1 nm) composed of same sized particles. [78, 84, 96, 97]

We characterized the localized emission from QD structures using NSOM to demonstrate that the CdSe/ZnS QDs retain their luminescence properties after patterning. The quantum dots were excited through the NSOM tip with the 488 nm line from a continuous wave Ar-ion laser, and the emission was collected through a holographic edge filter at 488 nm and focused onto an avalanche photodiode. Figure 3.10 shows the spatially resolved emission of the patterned quantum dots; the inset depicts the amplitude image. As expected, the emission from the CdSe/ZnS mesostructures is strongest when the density of the quantum dots inside the patterned
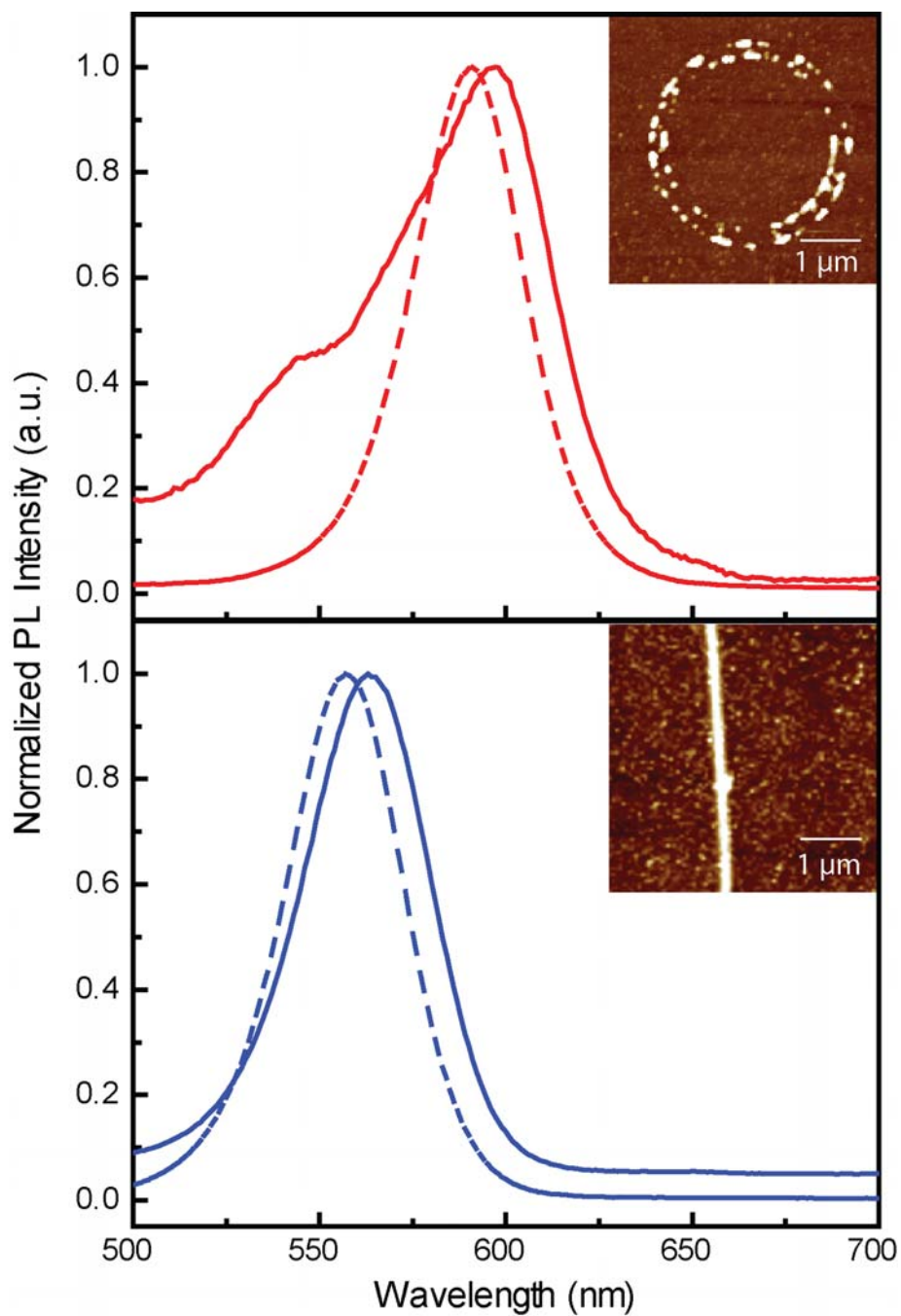
Figure 3.9. Photoluminescence (PL) spectra of CdSe/ZnS nanocrystals in aqueous solutions (dashed lines) and patterned on substrates (solid lines) from Figure 3.6. Both (A) larger dots patterned into rings and (B) smaller dots patterned into lines exhibited a red-shift in the PL compared to the same dots in dilute solutions. The insets represent the mesoscale patterns of the CdSe/ZnS dots from which the PL was measured.
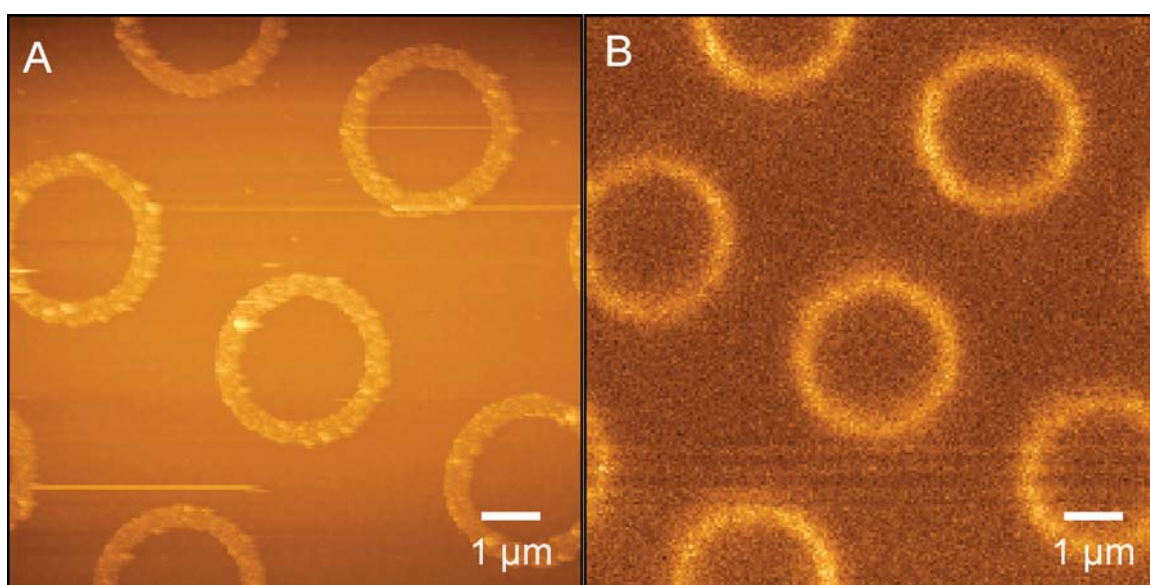
Figure 3.10. (A) Topography image of rings of 25 nm high CdSe/ZnS dots and (B) corresponding fluorescence NSOM image of arrays of quantum dots patterned into ring structures.

areas is highest. We plan to improve the contrast between the rings and the background by using an excitation source with lower wavelengths (< 400 nm).

3.4 Conclusions

This chapter demonstrated that soft templates in photoresist, generated by PSP through composite PDMS masks, can be used to assemble optically functional nanomaterials in 2D. The templates have critical feature sizes as narrow as 100 nm, can be patterned over areas as large as 1 in^2, and can be used to assemble nanoparticles of any size and shape into mesoscale patterns. This technique is most useful for manipulating nanomaterials dispersed in aqueous solutions because polar and organic solvents (typically used for the synthesis of colloids and nanoparticles) will dissolve the photoresist template. Moreover, patterned CdSe/ZnS mesostructures with increased packing densities can provide insight for investigations of long-range interactions in mixed QD solids composed of small and large QDs; these studies can provide an important first step towards controlling energy transfer in QD assemblies.

Chapter 4

Confinement of Standing Waves in Optical Corrals

4.1 Introduction

Recent advances in nanoscience and the discovery of size-dependent optical properties of nanomaterials have generated interest in structures that can confine and manipulate light. This interest has been fueled by the potential of these structures in emerging applications, such as optoelectronics,[5] photonics,[1, 5, 98] and chemical and biological sensing.[27, 99] Significant effort has been directed towards understanding light propagation, in the form of surface plasmon polartions (SPPs), on metallic surfaces.[5] SPPs, which are collective charge oscillations that result from resonant interactions between electrons and photons at the interface of metallic and dielectric structures, have the ability to guide light on surfaces over length scales of tens of microns.[5, 15] Metallic films with perforations have been fabricated and studied for their ability to manipulate and guide light on surfaces.[26, 50, 98, 100]

Attention has also been directed towards studying dielectric structures with mesoscale (100-1000 nm) features because of predictions that they can exhibit analogous behavior with structures on the nanometer scale. For example, photonic crystals, dielectric materials with periodic, ordered structures (repeat unit hundreds of nanometers), control the propagation of photons in much the same way as semiconductors control the propagation of electrons.[12] There is a forbidden gap in the photonic band structure that prohibits the existence of specific optical frequencies along certain crystal directions. Understanding how light can be manipulated on dielectric and metallic surfaces can be important for creating functional optoelectronic devices.

One type of structure that has been especially helpful in understanding light confinement on dielectric surfaces is an optical corral,[17] a microscale (1-10 μm) analog of the nanoscale (~7 nm) quantum corral.[20] To generate quantum corrals, a scanning tunneling microscope (STM) was

used to manipulate individual atoms on metallic surfaces into circular structures. The walls of the quantum corrals were built from Fe atoms, which were individually positioned on the Cu (111) surface by the STM tip. These circular structures confined the surface free electrons, which resulted in standing wave patterns from the strong scattering that occurred at the boundary made of Fe atoms. This work demonstrated that when electrons were confined to length scales approaching the de Broglie wavelength (71.3 Å), their behavior was dominated by quantum mechanical effects. The realization of the optical analog to the quantum can enable testing of analogous behavior of confined light and electrons.

Calculations performed on an optical corral made from dielectric pads arranged in a ~3-μm circle have shown that it is possible to confine electromagnetic (EM) waves within corral structures to generate patterns that resembled those produced in their electronic counterparts.[17] Recent results demonstrated the first experimental observations of confinement of photonic states using gold posts (100 nm high and 100 nm in diameter) arranged in a 3.6-μm diameter circle on an ITO substrate.[18] In the optical corral, specific patterns of light were present inside the circular structures depending on the size of the corral and the excitation wavelength of light. Experimental realization of confined EM waves within a 4 μm x 2 μm stadium structure, composed of 100-nm gold posts on an ITO substrate, was also demonstrated. [18]

Optical corrals make possible new fundamental studies of light propagation in confined geometries on dielectric surfaces. In particular, the optical analog to the quantum corral also allows the exploration of the differences between the scattering of EM waves and electrons from the corral structures. Advances in lithographic techniques have enabled the construction of micron-scale corrals with 100-nm scale features. The advantage of using top-down lithographic

approaches for the generation of these optical corrals is that arrays of circular and elliptical corrals with different sizes and shapes can be patterned, which provides an opportunity to tune the patterns of the EM waves inside of the corrals. Additionally, unlike in the case of the quantum corral, polarization effects can be used to control the patterns of the standing waves. This chapter describes how EM standing wave patterns can be tailored within metallic corrals on dielectric surfaces by controlling: (i) the size and shape of the corrals, (ii) the wavelength of light used for excitation, and (iii) the polarization of the incident light.

4.2 Experimental Methods

4.2.1 Materials

Substrates: Indium tin oxide (ITO)-coated glass was purchased from Thin Film Devices. The thickness of the glass was 0.4 mm; one side of the glass was covered with 150 nm of ITO having <30 Ω sheet resistance.

4.2.2 Fabrication of Circular and Elliptical Corrals

Templates for the corral structures (circular and elliptical) were fabricated using lithographic techniques described in Chapter 2. Templates with arrays of circular rings with ~250 nm widths and inner diameters of ~2.23 μm and ~4.8 μm were fabricated using phase-shifting photolithography (PSP). The center-to-center spacing for the smaller corrals was 4.5 μm and 15 μm for the larger corrals. Electron-beam lithography (EBL) was used to fabricate the templates for the elliptical corrals with ~250-nm widths and the following eccentricities (*e*): 0.6, 0.75, and 0.86. The eccentricity values for the elliptical corrals were chosen to mimic the sizes of the

quantum mirage structures.[101] EBL was used instead of PSP for the elliptical corrals because it allowed us to make structures of different sizes on the same substrate.

The corrals (circular and elliptical) were produced by depositing 50-60 nm of gold (Au) into the resist templates defined by PSP and EBL (Figure 4.1A and Figure 4.2) and then performing lift-off. The height of the structures was chosen to be larger than the skin depth of Au at optical wavelengths (~25 nm).[102] Unlike structures made of Au posts, corrals with solid walls confine light more efficiently inside of the structures. Metal deposition was done with an electron beam evaporator (PVD 75, Kurt J. Lesker) (base pressure of 10^{-7}- 10^{-6} Torr). The thickness of the film and the deposition rate, which was maintained at ~1 Å/s to create a smooth film, were monitored using 6 MHz gold microbalance (Kurt J. Lesker). The substrates were sonicated in acetone or Shipley remover 1165 to remove the resist and leave metal structures on ITO/glass. Circular corrals made from silver (Ag), and alumina (Al_2O_3) were also fabricated (Figure 4.1B and C). For Au and Ag structures, 5 nm of chromium (Cr) was deposited as an adhesion layer.

4.2.3 Instrumentation

NSOM experiments were carried out using an Aurora 3 (Veeco) instrument using Al-coated, pulled, fiber optic probes with 100-150 nm apertures and 80-100 kHz resonant frequencies (Veeco). Figure 4.3 illustrates the detailed set-up of NSOM in collection mode. The samples were uniformly illuminated through a 40X objective lens (Olympus), and the light from the sample was collected through the probe into a high quantum efficiency avalanche photodiode (APD) (SPCM-AQR-14, Perkin Elmer). A focusing lens was positioned before the objective lens in order to decrease the divergence of the light and to create <0.5 mm uniform
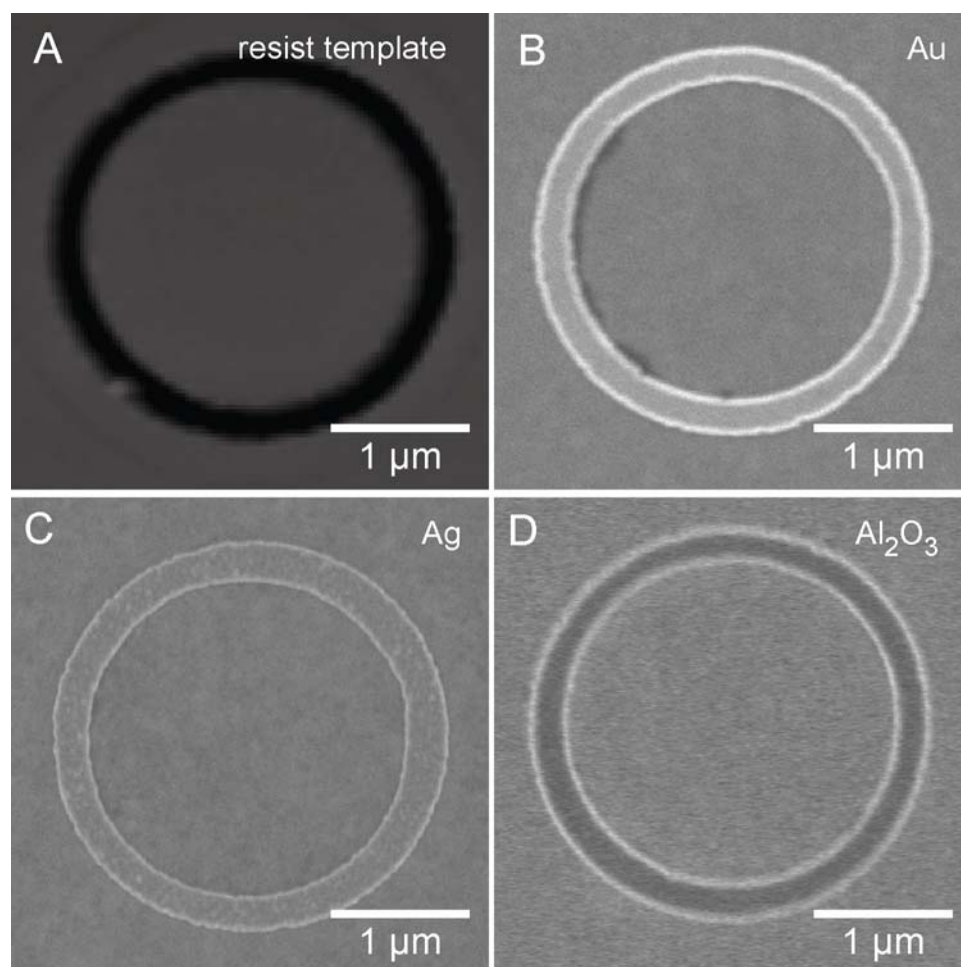
Figure 4.1. AFM image of (A) photoresist template for circular corrals and SEM images of (B) Au, (C) Ag, and (D) Al_2O_3 rings on ITO/glass substrate.
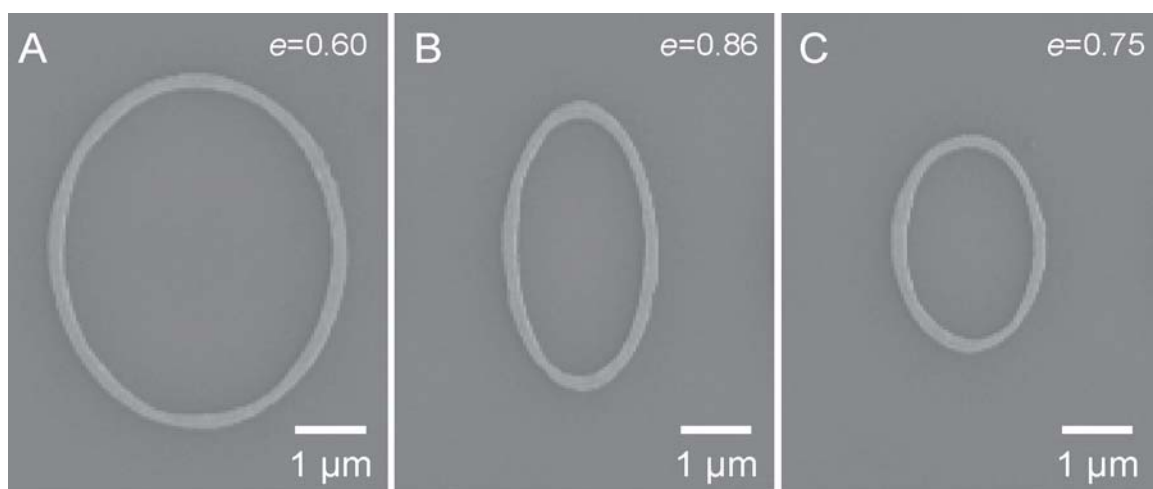
Figure 4.2. SEM image of Au ellipses with eccentricities (*e*) of (A) 0.60, (B) 0.86, and (C) 0.75.
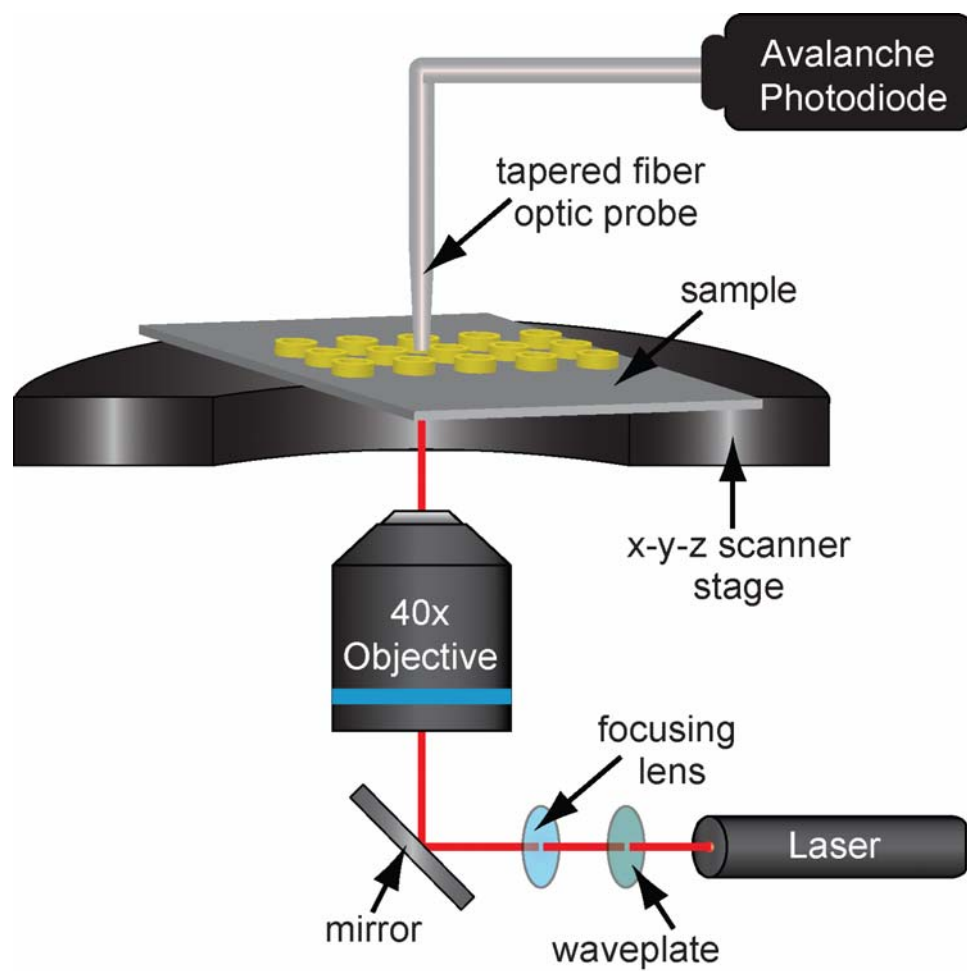
Figure 4.3. Scheme of collection mode NSOM set-up used for imaging the corrals.

illumination spot on the surface of the sample. Three different laser sources were used for illumination: 457 nm Ar-ion (2-10 mW, LaserPhysics), 543 nm HeNe (5 mW, Melles Griot) and 633 nm HeNe (15 mW, Melles Griot) lasers. Both linearly polarized and circularly polarized light was used to investigate the optical properties of the corrals. Linearly polarized laser light was converted into circularly polarized light by placing a ¼-waveplate in front of the laser source; a ½-waveplate was also used to change the angle of polarization with respect to the sample.

4.3 Optical Characterization of Corrals

4.3.1 Circular Corrals

Arrays of circular corrals made of Au with inside diameters of 4.8 μm and center-to-center spacing of 15 μm were imaged using collection mode NSOM (Figure 4.4A). When the structures were illuminated under normal incidence with circularly polarized 633-nm light from a HeNe laser, evanescent EM waves were localized at the surface of the sample. The evanescent nature of the EM waves, which extended ~200-250 nm above the surface, was confirmed by single-point NSOM spectroscopy. These circular structures confined the localized waves, which scattered from the walls of the corrals to generate patterns of standing waves inside and outside of the structures (Figure 4.4B). The pattern inside of the corral consisted of ripples. Concentric, circular fringes outside of the corrals were also observed. The measured wavelength was 633 nm, which was identical to the wavelength of light used for imaging of the structures.

To investigate the effect of the size of the structures on the patterns inside and outside of the corrals, we fabricated arrays of circular corrals with smaller inner diameters (2.23 μm) and center-to-center separations (5 μm) (Figure 4.5A). When these structures were imaged using
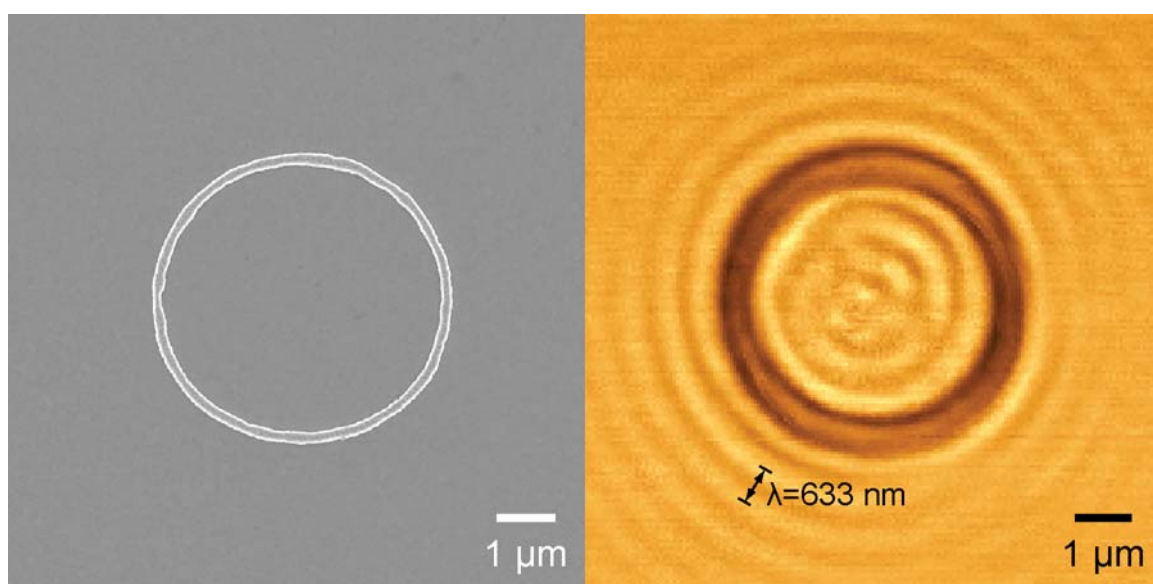
Figure 4.4. SEM image of (A) 4.8-µm Au ring and (B) corresponding optical NSOM taken with circularly polarized 633-nm light.
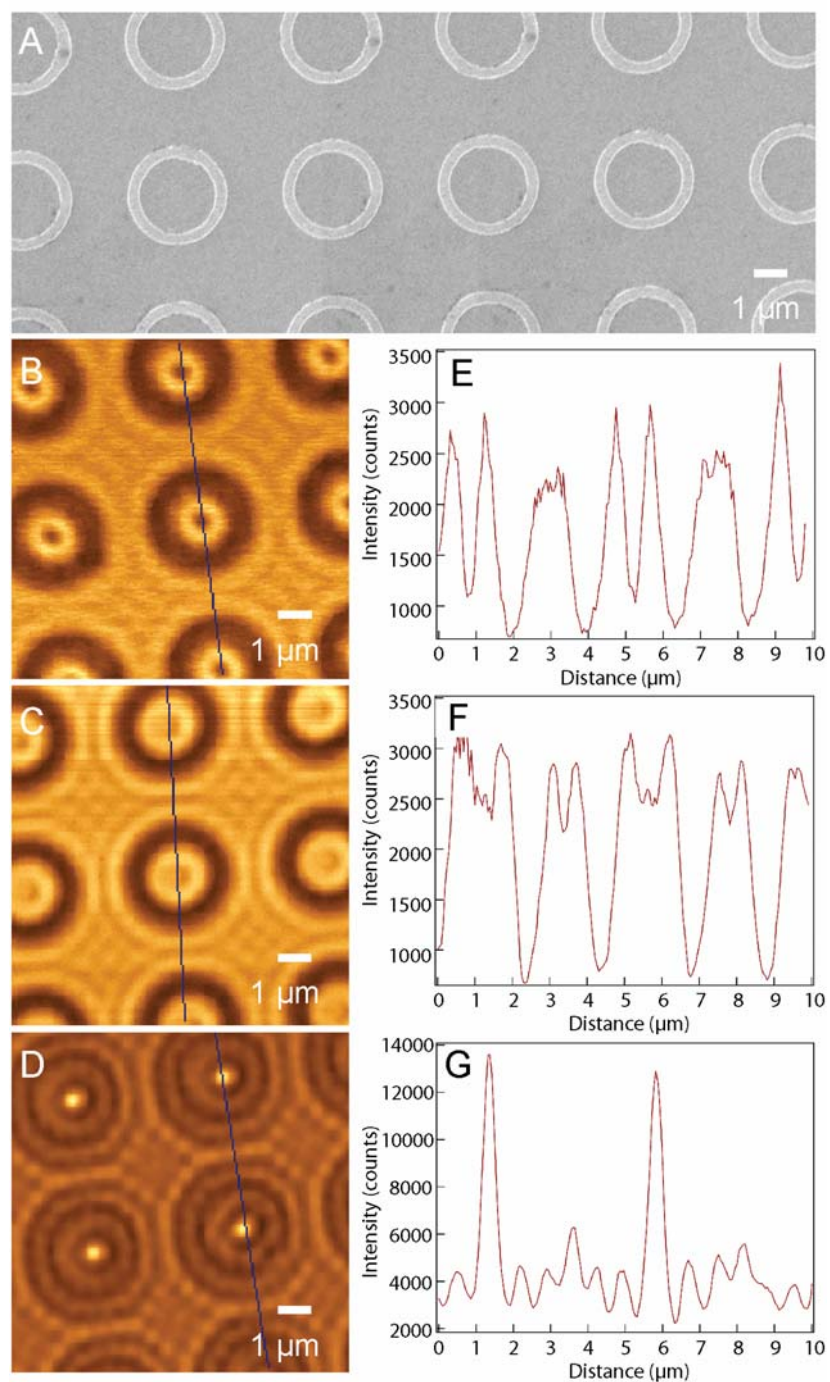
Figure 4.5. (A) SEM image arrays of 2.35-μm Au rings. Collection mode NSOM images of 3-μm rings imaged with (B) 633 nm, (C) 543 nm, (C) 457 nm light and their corresponding cross sections (E-G).

circularly polarized 633-nm light, we noticed that the number of internal ripples decreased as expected (Figure 4.5B), and the central spot inside of the corral became dark. Because the center-to-center spacings of the rings was only 4.5 μm, EM waves that scattered from the outside walls interfered in a constructive and destructive manner to generate intricate patterns of standing waves outside of the corrals.

Variations in the patterns in response to a change in the wavelength of the excitation light were also observed. Therefore, the 2.23-μm Au rings were excited and imaged using two additional wavelengths (457 nm and 543 nm). When the 633-nm light was replaced with 543-nm and then with 457-nm light, the dark spot in the middle of the corral gradually switched to a bright spot (Figure 4.5B-D). Cross sections of the optical images (Figure 4.5E-G) clearly illustrate this observation. The intensity of the bright spot, which resulted after the corrals were irradiated with 457-nm light, was ~6 times higher than the lowest intensity on the pattern. This observation suggested that only certain wavelengths of light were optimally sustained inside of the rings to produce a spot with high intensity in the middle of the structures. Interestingly, the patterns formed within the optical corrals resembled the patterns of electronic standing waves in the quantum corrals.[20, 101, 103]

To investigate how the material of the corral affected the patterns formed inside the structures, we fabricated circular corrals with metallic (Au and Ag) and dielectric (Al_2O_3) walls with inside diameters of 2.35 μm (Figure 4.6A-C). When the different corrals were excited with circularly polarized 633-nm light, identical patterns were produced inside of the metallic and the dielectric structures (Figure 4.6D-F). One noticeable difference was that the dielectric rings were brighter than the metallic ones, which was expected because Al_2O_3 is transparent. Another
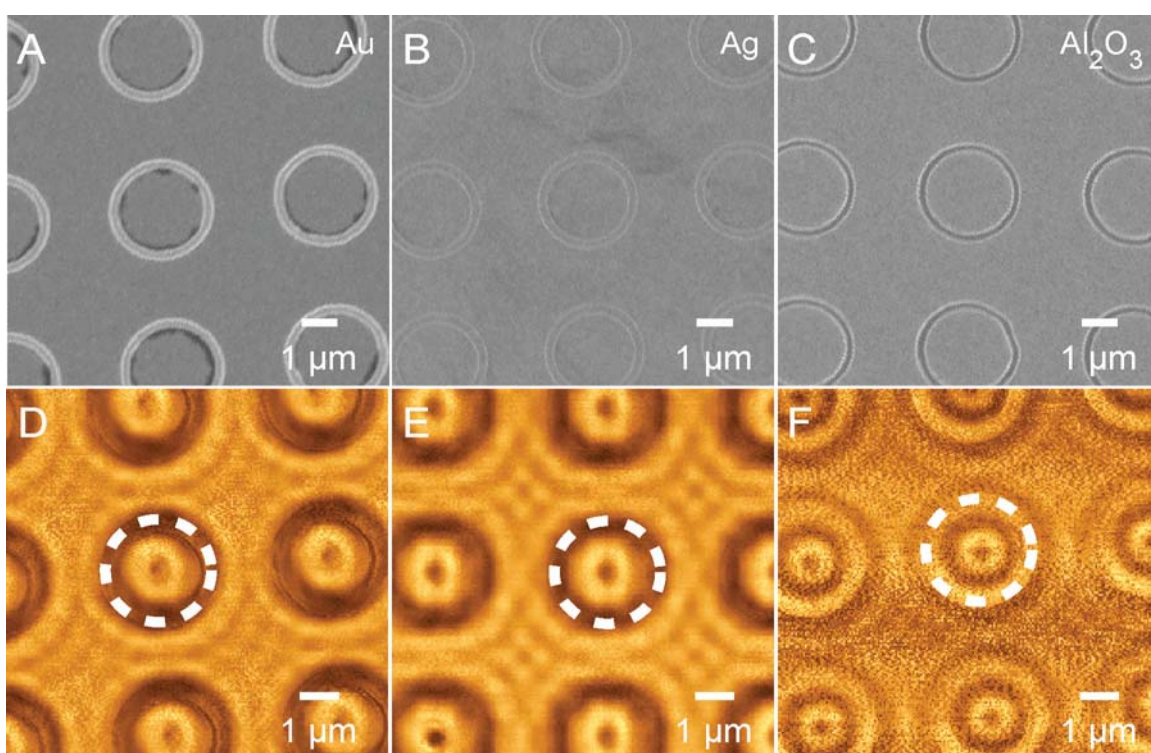
Figure 4.6. SEM images of (A) Au, (B) Ag, and (C) Al$_2$O$_3$ rings on ITO/glass and their corresponding collection mode NSOM images (D-F). White dashed rings on the NSOM images indicate the position of the ring structures.

variation among the optical images was the contrast of the patterns of the standing waves. The dielectric structures had the lowest contrast, as expected, because the reflectivity of Al_2O_3 compared to the metals is lower at 633 nm. Among the two metals, Ag had a slightly better contract because it has ~5% higher reflectivity at 633 nm than Au.[104] Thus, we discovered that the pattern formed in the inside and outside of the corrals depended not only on the size of the circular corrals but also on the materials of the corral structures.

4.3.2 Elliptical Corrals

Although circular corrals provide a simple platform for studying the optical analog to the quantum corral, complex structures such as ellipses would provide more interesting ways to control light on surfaces. One advantage of using structures with lower symmetries (ellipses vs. rings) is the potential opportunity to study effects of polarization on light localization within the corral structures. Ellipses with three different eccentricities: $e = 0.6$ ($a = 2.5$ μm, $b = 2$ μm), $e = 0.86$ ($a = 4$ μm, $b = 1$ μm), and $e = 0.75$ ($a = 1.5$ μm, $b = 1$ μm) were studied (Figure 4.7A-C). Upon illumination of the $e = 0.6$ ellipses with circularly polarized 457-nm light, complex patterns, which resembled the image obtained from the quantum corrals of similar eccentricity,[103] were formed inside of the structures (Figure 4.7D). To verify the effect of the shape of the structure on the internal pattern of the EM waves, two other ellipses with larger eccentricities $e = 0.86$ and $e = 0.75$ were also imaged with the same wavelength of light (Figure 4.7E-F). Interestingly, for these ellipses, light at the focal points was suppressed (dark spots were present), while the ellipse with $e = 0.6$ did not. To investigate whether this phenomenon was related to the structure of the corral or to the wavelength of light used for imaging, the ellipses were imaged with 543-nm and 633-nm light (Figure 4.7G-L) This time, the ellipses with larger
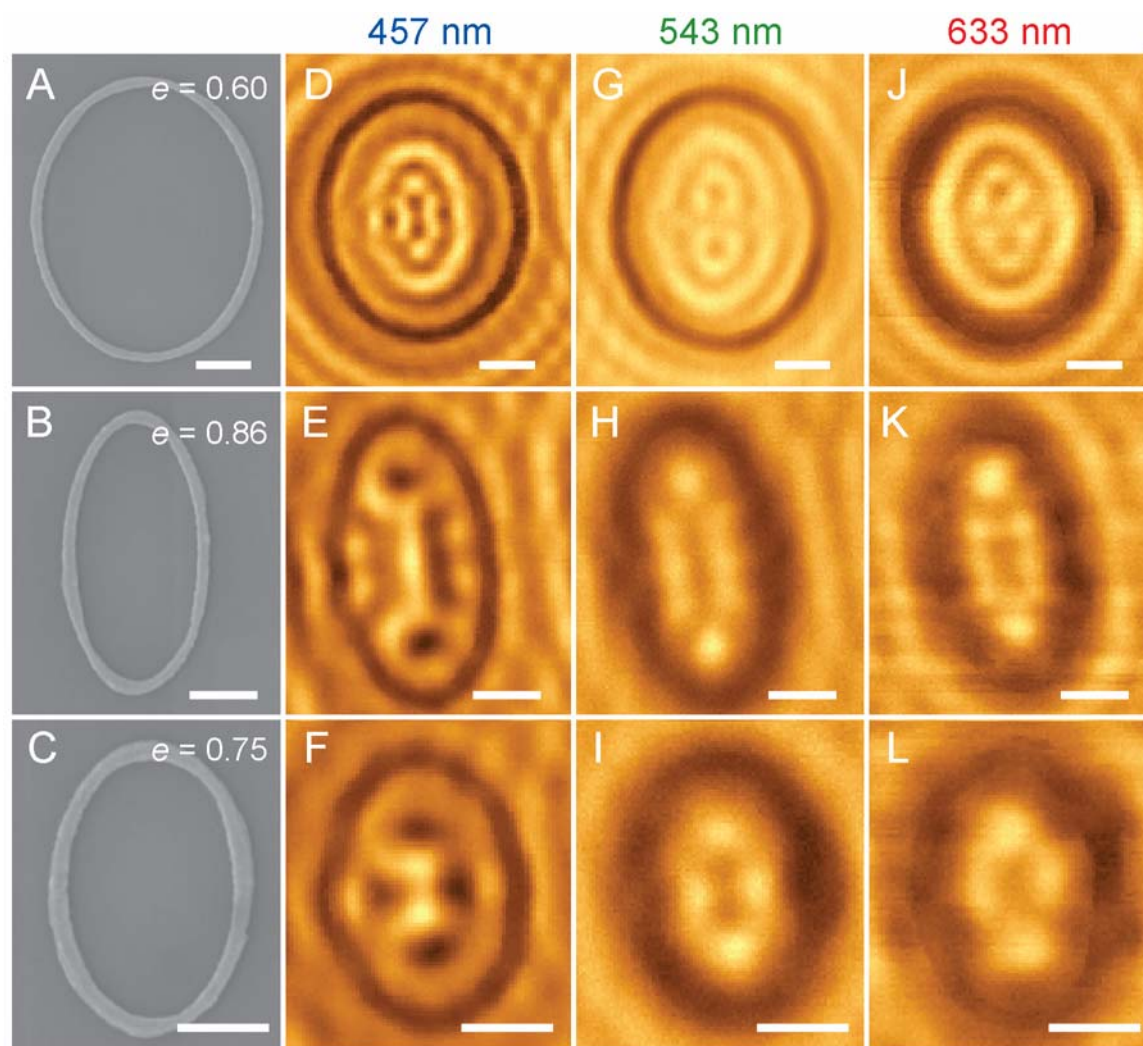
Figure 4.7. SEM images of ellipses with eccentricity of (A) 0.60, (B) 0.86, and (C) 0.75 imaged with (D-F) 457-nm, (G-I) 543-nm, and (J-L) 633-nm light. All the optical images were acquired with circularly polarized light. All scale bars are 1 μm.

eccentricities revealed bright spots (higher light intensity) at the focal points. We believe that the pattern formed inside of the corrals was a collective effect that resulted from the reflection of the EM waves from the walls of the corrals.

Because of the low symmetry of the elliptical corrals, we expected the EM waves confined within the elliptical structures to exhibit polarization dependence. Two ellipses ($e = 0.6$ and $e = 0.86$) were imaged using circularly and linearly polarized (along short and long axis) 543-nm light. Figure 4.8 demonstrates that the EM waves confined inside of the corrals displayed a different pattern depending on the polarization of light. This result confirms that the standing wave patterns inside of the corrals can be tailored by simply changing the polarization of the incident light.

4.4 Conclusions

We have presented a method for confining EM waves in artificial structures and demonstrated that it is possible to create an optical analog to the quantum coral. Using circular corrals, we showed that only certain wavelengths of light are efficiently sustained within circular structures of specific diameters to produce a bright spot at the center of the structure. The ability to modify the EM wave patterns inside of the corrals was further investigated in elliptical structures, which allowed the patterns to be tailored by simply changing the polarization of the incident light. Wavelength-dependent changes on the patterns were also observed. Ellipses with different eccentricities were investigated to understand the size and shape-dependence of the corral structure on the patterns. Interestingly, ellipses with larger eccentricities showed that light can either be suppressed or enhanced at the focal points of the corrals, depending on the excitation wavelength. The experimental realization of these optical corrals will not only
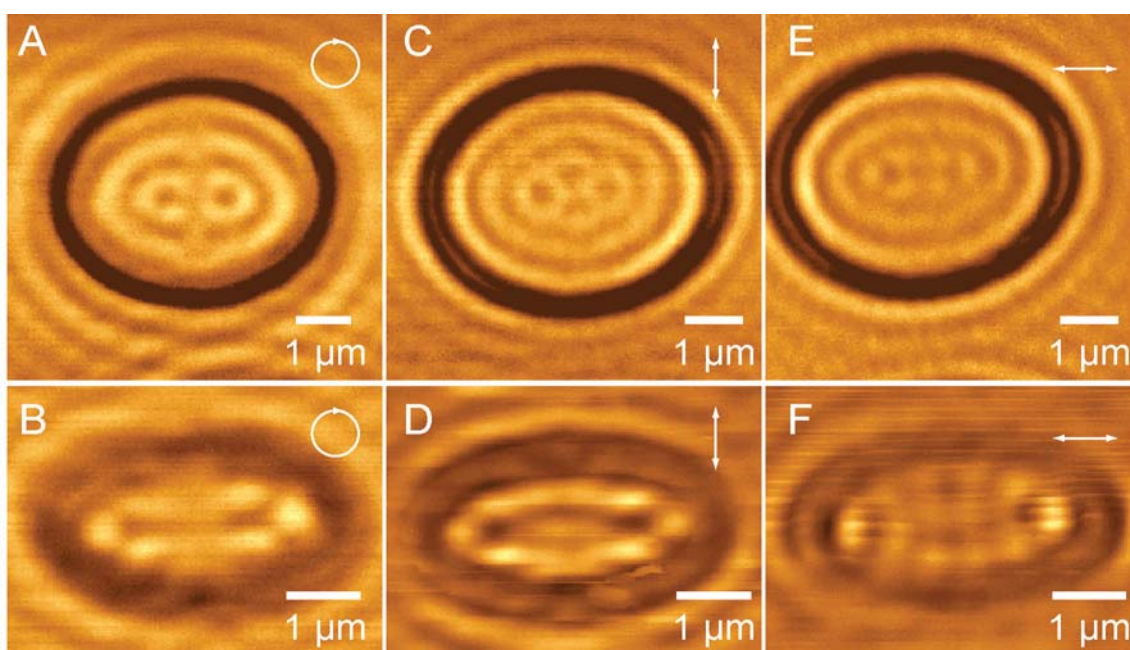
Figure 4.8. Ellipses with *e* of 0.6 and 0.86 imaged using 543-nm light with (A-B) circular polarization, (C-D) linear polarization along the long axis, and (E-F) linear polarization along the short axis.

improve our understanding of light propagation on dielectric surfaces but will also allow to manipulate light on planar surfaces.

Chapter 5

Benchtop Nanoscale Patterning Using Soft Lithography

5.1 Introduction

Unlike previous chapters that give accounts of laboratory research projects, this chapter addresses work in the area of nanoscience education. Recent advances in nanoscience and the discovery of size-dependant properties of nanomaterials have generated interest in developing new methods to create nanoscale (sub-100 nm) structures. Specifically, microelectronics and optoelectronics have been a driving force for miniaturization and the development of new micro- and nanofabrication techniques. Educational institutions have responded to this increased importance of nanotechnology by developing relevant undergraduate coursework and degree programs.[105-108] Nanopatterning techniques however have not received much attention in the form of laboratory curriculum because of the expense and expertise involved in the hands-on training.

Through the support of the first nanoscale center for learning and teaching (NCLT) headquartered at Northwestern Univerisity, we have developed several benchtop nanoscale experiments[109] in response to the increasing need for laboratory exercises to supplement lecture-only courses on nanotechnology. These experiments provide students hands-on experience in nanopatterning techniques. Typically, nanofabrication techniques fall into two categories: bottom-up and top-down. In bottom-up methods, larger structures are assembled from smaller building blocks (e.g. atoms and molecules), while in top-down approaches, structures are reduced from the macroscale into the nanoscale. Many laboratory experiments for undergraduate curricula have been developed based on bottom-up approaches,[110, 111] while top-down techniques have been limited to macroscale analogies, such as: (i) using PDMS stamps with mm-scale features for micro-contact printing (μCP) of self-assembled monolayers (SAMs);[112] (ii) using 1-

in nylon spheres in contact with photosensitive paper and a UV lamp to illustrate nanosphere lithography;[113] (iii) using projection lithography to create microscale circuits;[114] and (iv) using photolithography to demonstrate the concept of microchip fabrication.[115]

Our work is distinct from the above examples because it outlines experiments in which students use soft lithographic techniques to fabricate and replicate nanoscale features (110 nm). The experiments outlined in this chapter can be incorporated into undergraduate laboratories or advanced high school curricula because of the simplicity and the inexpensive nature of the patterning methods. The nanopatterning techniques described here include replica molding (RM), micro-molding in capillaries (MIMIC), and micro-contact printing (μCP) and etching.[116, 117] These simple experiments were designed to require only readily available and inexpensive materials such as compact discs (CDs), glass microscope slides, poly(dimethylsiloxane) (PDMS), and polyurethane (PU). These soft lithographic methods can be used to generate both polymeric and metallic nanostructures. Importantly, we have also created an online, recipe-style, video manual, which can be found on the NCLT *NanoED Portal* at http://www.nanoed.org/courses/nano_experiments_menu.html, to provide step-by-step instructions for the students.

5.2 Soft Lithography

Soft lithography consists of a suite of techniques that use only a patterned elastomeric material, such as polydimethylsiloxane (PDMS), as a "soft mold or stamp" to replicate and transfer patterns from a master onto a surface.[116] This inherently parallel process offers the ability to (i) pattern complex molecules, (ii) control chemical structure of surfaces, (iii) create channels for microfluidics, and (iv) pattern features over large areas (> 50 cm^2) on non-planar

surfaces using ordinary lab facilities. Depending on the patterning technique, either molecular layers or three dimensional structures can be created in soft and hard materials such as polymers and metals. In general, the soft lithography process consists of three steps: (i) the fabrication of a master; (ii) the generation of a PDMS mold (or stamp) from the master; and (iii) the use of the patterned PDMS mold (or stamp) to create features defined by its relief structure. Conventional masters for pattern replication are generated using microfabrication techniques such as photolithography, electron-beam writing, and micromachining.[117-119] While these techniques are versatile, they are very expensive, time consuming and require specialized instrumentation and expertise. Because of these requirements, access to patterning techniques is typically limited to a select group of users. In contrast, soft lithography is not subject to these limitations and thus experiments based on these techniques can be accessible to college and high school students.

5.2.1 Fabrication of Masters

Introduction

The fabrication of masters usually involves expensive instrumentation and facilities. An inexpensive and readily available master with sub-500 nm features can be obtained from data storage devices such as CDs or digital versatile discs (DVDs). Conventional CDs store digital data in a series of indentations packed in a long spiral track starting at the center of the disc. The discs have a pattern imprinted into a polycarbonate (PC) layer covered with a reflective aluminum (Al) coating, which in turn is covered by a transparent protective acrylic layer. Figure 5.1 shows a cross section of a CD. Each indentation in the PC layer is 110- nm deep. The PC layer is comprised of 1.2-μm wide and 110-nm tall indentations that are spaced by 690 nm; these features are pre-molded onto the CD during manufacturing. The Al recording layer that is in
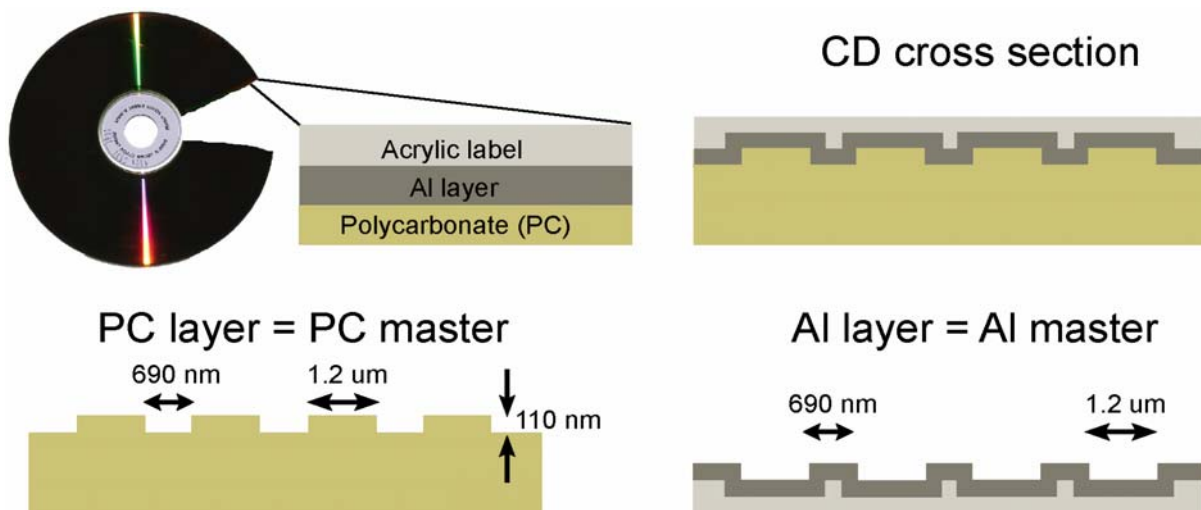
Figure 5.1. Cross section of a CD.

contact with the PC substrate has the inverse features. These two layers, PC and Al, can be used to create two types of masters with complementary features.

Procedure for Students

1. Obtain a CD-R and use scissors to cut out a piece ~ 1x1 in^2.

2. Peel off the Al layer from PC layer using tweezers. The layers should separate easily from each other. When the layers are separated, place the patterned side facing up into petri dish and label the containers. Both Al and PC layers can now be used as separate masters.

3. Use an atomic force microscope (AFM) to image the surfaces of Al and PC layers (Figure 5.2). Compare the width and height of the patterns.

Notes for Instructors

1. A piece of Scotch$^®$ Magic tape can be placed on the Al layer before peeling it from the PC layer to prevent flaking and curling of the thin Al sheet.

2. An optical microscope can be used to visualize the patterns on the Al and the PC layers if an AFM is not available.

5.2.2 Fabrication of PDMS Molds

Introduction

An elastomeric mold, a key pattern transfer element in soft lithography, can be generated by casting a heat-curable pre-polymer against a master (in this case the PC or Al layer from a CD). The material most commonly used for fabricating molds or stamps for soft lithography is
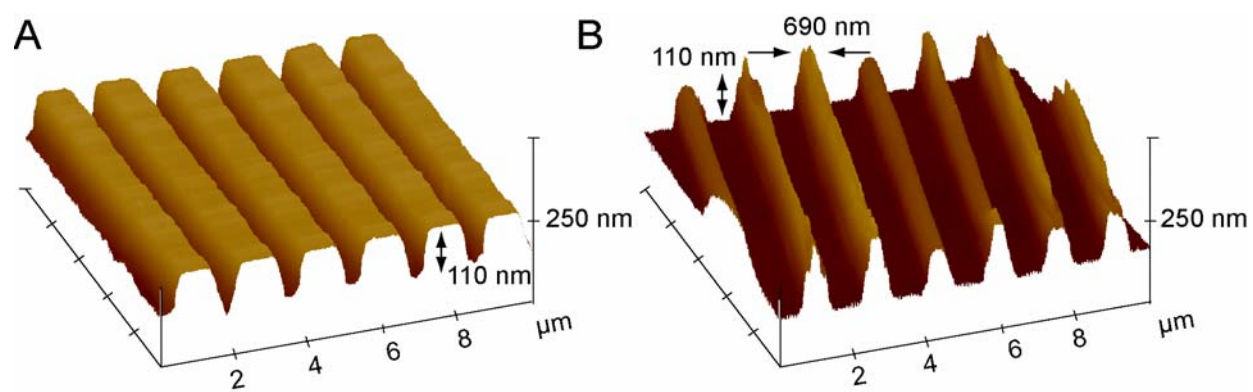
Figure 5.2. AFM images of (A) PC layer and (B) Al layer obtained from a CD-R.

PDMS – an optically transparent, silicone-based, organic polymer. Because of its low surface free energy, PDMS conforms easily to three dimensional (3D) surfaces and thus can also be used for patterning on curved surfaces. PDMS molds are formed by casting two component pre-polymer (Sylgard 184 silicon rubber base and curing agent) over the patterned master, cross-linking the elastomer by thermal curing and then peeling the PDMS off the mold (Figure 5.3). The mold is patterned with inverse features of the master. For example, if the PC master was used to generate the PDMS mold, then the mold will have features similar to the Al master. Many elastomeric molds can be prepared from one master, and each mold can be used repeatedly for different patterning experiments.

Procedure for Students

1. Weigh out ~20 g of the Sylgard 184 pre-polymer into a plastic cup. To the same cup, add 2 g of curing agent (10:1 weight ratio of pre-polymer to curing agent).

2. Mix the pre-polymer/curing agent mixture vigorously with a plastic fork until it is full of bubbles (1-2 min).

3. Place the cup with the polymer mixture into a desiccator to degas (remove the bubbles) the PDMS for 20-40 min (or until all bubbles have disappeared).

4. Pour PDMS over the PC and Al masters obtained from the CD; be careful not to create bubbles in the polymer.

5. Place the masters covered with PDMS into an oven to cure at 70 °C for 1-2 h.

6. Using a scalpel, gently and evenly cut out a piece of the patterned PDMS from each master.
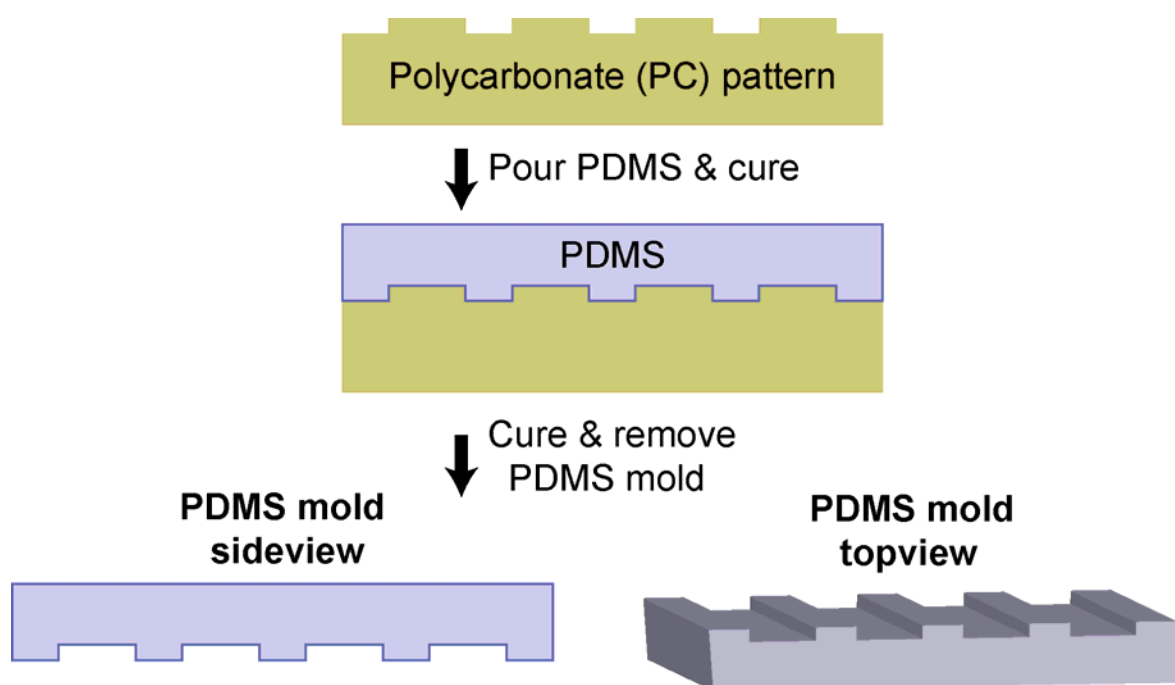
Figure 5.3. Scheme for making PDMS mold using PC layer.

7. Remove the PDMS mold from the surfaces using tweezers and place it patterned-side down on a clean glass slide. Label the molds and image them using AFM (Figure 5.4).

Questions

1. What is the relationship between the patterns of the Al and the PC masters?

2. What is the relationship between the patterns of the PDMS molds and the masters?

Notes for Instructors

1. Make sure the PDMS mixture is thoroughly mixed and completely degassed; no bubbles should be present in the PDMS before removing it from the desiccator. If the students remove the PDMS from the desiccator before all the bubbles have disappeared, they can put it back and degas for another 5-10 min. Use of a desiccator can be avoided by degassing the PDMS in air for a longer period of time (~ 2 h). To speed up the degassing of the PDMS in air, it can be stirred for 4-5 min instead of 2 min.

2. Students should avoid leaving the PDMS in the desiccator for more than 2 h because it will become very viscous and difficult to pour over the masters.

3. PDMS should not be tacky after curing. If it is not cured completely after 1-2 h, it can be placed back in the oven until completely cured.

4. PDMS molds should be relatively thin (~2-3 mm) so that conformal contact between the mold and the surface can be achieved.

5. If the PDMS mold becomes dirty, they can be cleaned by rinsing with ethanol and drying under nitrogen or by placing a piece of Scotch® Magic tape over the patterned side of the
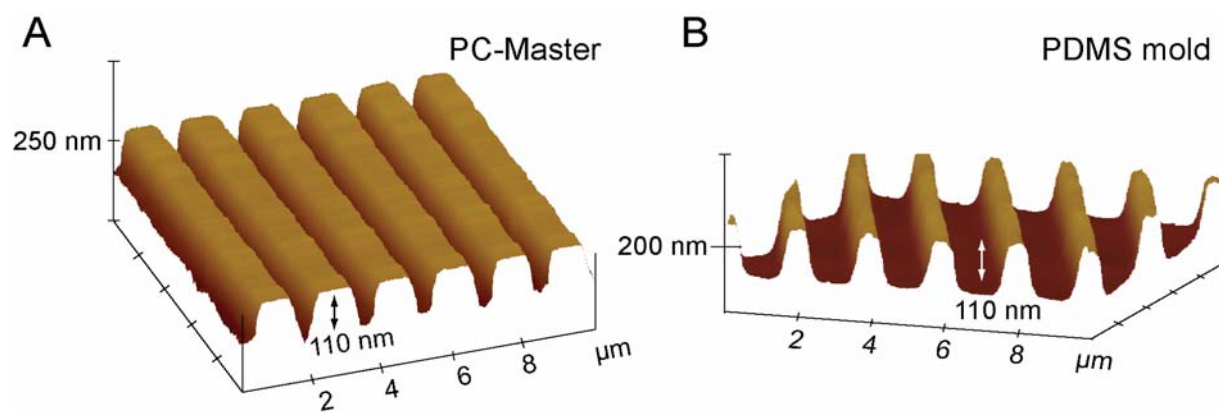
Figure 5.4. AFM image of (A) PC-master and (B) PDMS mold formed from (A).

PDMS and peeling the tape off the surface (after the tape is removed, the mold should be rinsed with ethanol and dried with nitrogen).

5.2.3 Replica Molding (RM)

Replica molding is a technique that involves casting organic polymers against a PDMS mold to produce a pattern (or replica) that is identical to the master. Feature sizes as small as 30-nm wide and 5-nm tall are possible with this technique,[120] which has found widespread application in the manufacturing of structures such as compact discs and diffraction gratings. Figure 5.5 illustrates the general procedure behind RM. A drop of liquid pre-polymer, such as PU, is placed between a substrate (e.g., a microscope slide) and a PDMS mold that comes into conformal contact with the substrate. After the PU is cured under UV light, the PDMS can be carefully peeled off to reveal a PU-replica of the master on the glass surface.

This technique has the capability to generate multiple replicas of nanostructures starting from a single master. The simplicity, low cost and versatility of this technique confirm its potential use in patterning nanostructures. Advantages of RM include its ability to replicate 3D topologies in a single step and to provide high fidelity structure replication with accuracy down to the size of large molecules (~ 2 nm).

Procedure

1. Clean a glass slide using soap and water. Rinse the slide with ethanol and dry with a stream of nitrogen.

2. Place 2-3 drops of liquid PU on a glass slide to create a puddle with an area not larger than the PDMS mold.
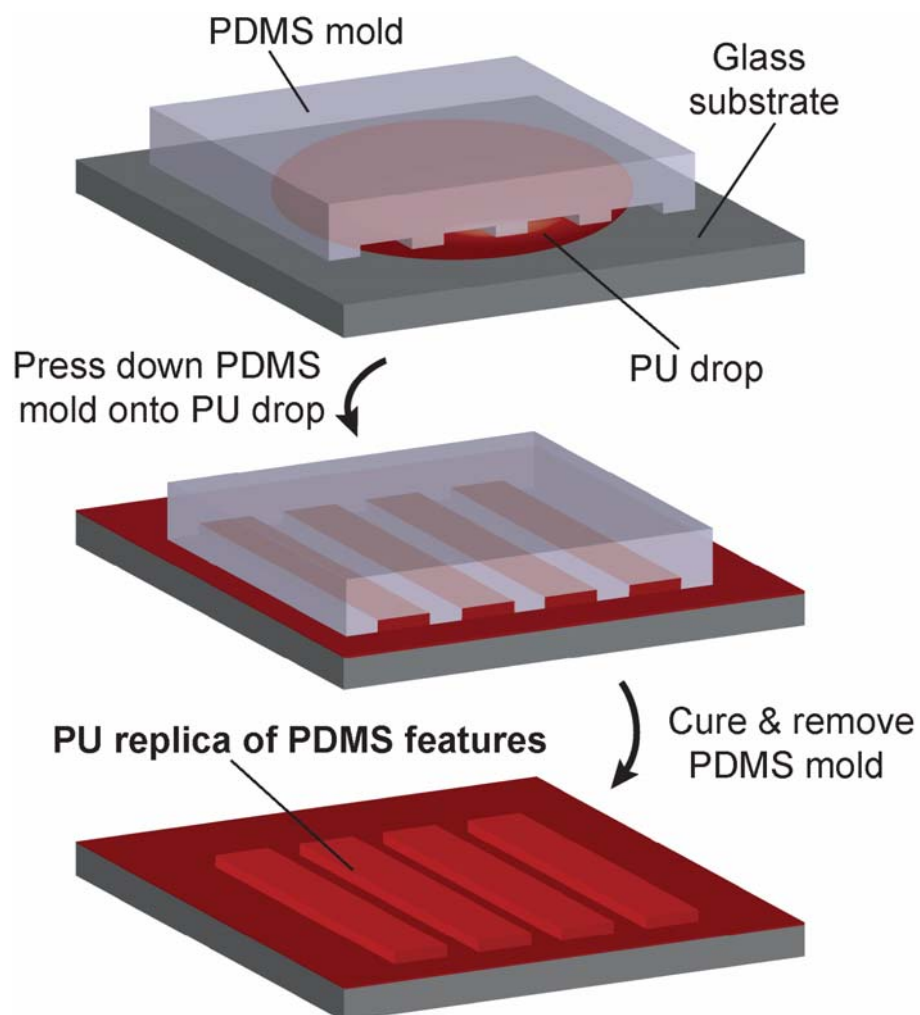
Figure 5.5. Scheme of RM.

3. Pick up the PDMS mold (either from the Al or the PC master) with tweezers and bring the patterned side of the mold in contact with the PU drop. Press down lightly on the mold with tweezers to ensure that the mold makes contact with the glass.

4. Place the sample ~5 inches under UV lamp and let the PU cure for 10 min.

5. Remove the mold with tweezers and store it on a clean glass side with the patterned side down.

6. To visualize the PU pattern look at it with an optical microscope or AFM (Figure 5.6).

Questions

1. Characterize your RM sample and compare it to your PDMS mold. How well did the pattern transfer?

2. In molding techniques, how does the pattern compare with the pattern of the mold? How could you obtain the exact pattern as the one on the mold?

3. What are the limitations of RM?

Note for Instructors

1. Make sure the students do not use too much PU. They only need 1-2 drops of PU for a 4-cm^2 sized mold.

5.2.4 Micro-Molding in Capillaries (MIMIC)

One type of RM is micro-molding in capillaries (MIMIC), a soft lithographic technique based on the spontaneous filling of a fluid in capillaries formed between two surfaces. Figure 5.7 illustrates the general procedure of MIMIC. A PDMS mold is placed on the surface of a substrate (e.g., a microscope slide) to form a network of empty channels. At the ends of the channels, a
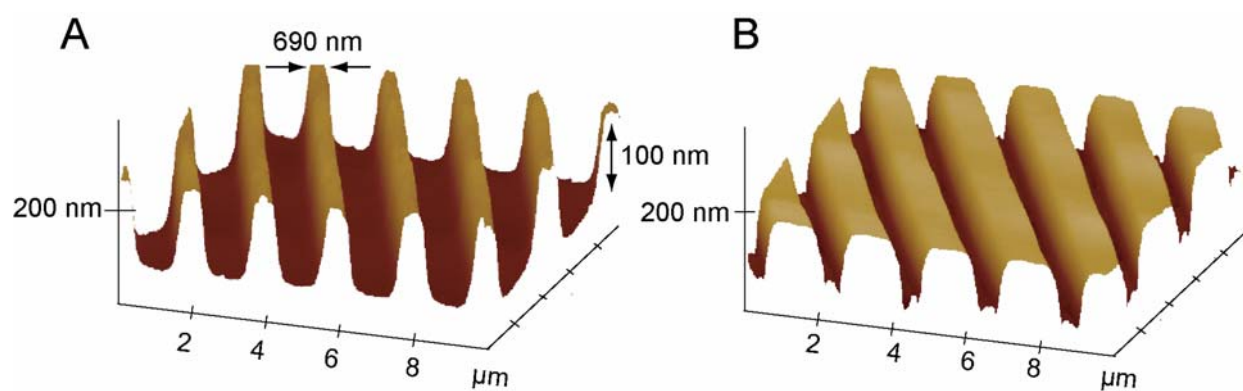
Figure 5.6. AFM images of (A) PDMS mold from PC layer and (B) polyurethane replica of PC layer formed by curing PU against the mold in (A).
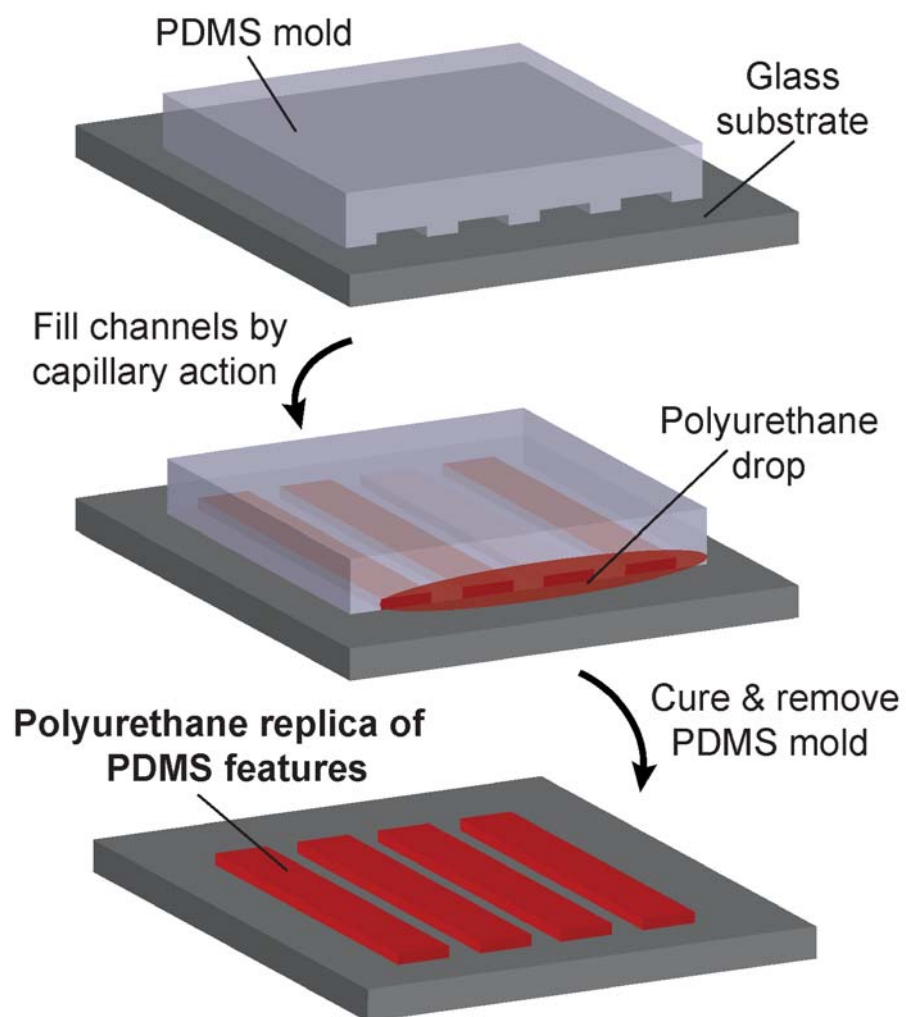
Figure 5.7. Scheme for MIMIC.

drop of low-viscosity photocurable fluid (such as PU) can be placed; the fluid will spontaneously be drawn into the channels by capillary forces. After the PU is cured under UV light, the PDMS mold is removed to leave behind a network of polymeric features on the substrate. Similar to RM, the polyurethane features very closely replicate the size and shape of the features of the master. The application of capillary molding is limited by the viscosity of the liquid precursors, and it remains a challenge to fill channels with dimensions less than 100 nm.

Procedure for Students

1. Clean a glass slide with soap and water. Rinse the slide with ethanol and dry with a stream of nitrogen.

2. Pick up one of the PDMS molds (if you used the PDMS from the Al master for the RM experiment, use the mold from the PC master for this experiment). Determine the direction of the lines on the mold by shining light from a laser pointer through a PDMS mold (patterned side facing down) held above a piece of white paper. Make sure you understand how the diffraction pattern relates to the direction of the lines on the mold. **WARNING:** *Exercise care when working with a laser pointer. Do not place your head directly above the sample.*

3. Place the mold on a cleaned glass slide with the patterned side facing down.

4. To create nanochannels, trim the ends of the PDMS mold by pressing down vertically with a razor blade on the ends that are perpendicular to the direction of the lines.

5. Place a drop or two of liquid PU at one of the open ends of the channels and wait for ~10 min for the channels to fill by capillary action.

6. Place the sample ~ 5 in below a UV lamp and let the PU cure for 10 min.

7. Remove the mold and place it facedown on a clean glass slide.

8. Hold the sample with tweezers and rotate it to see the diffraction pattern, which indicates that pattern generation was successful.

9. Look at the PU sample under an optical microscope or AFM (Figure 5.8).

Questions

1. Characterize your MIMIC sample and compare it to your PDMS mold. How well did the pattern transfer?

2. Compare and contrast the two molding techniques – RM and MIMIC. What are their advantages and disadvantages?

3. Which technique produced the best replication of the CD pattern from the PDMS mold?

4. In molding techniques, how does the pattern compare with the pattern of the mold? How could you obtain the exact pattern as the one on the mold?

Note for Instructors

1. When trimming the ends of the mold, the students should not drag the razor along the lines, otherwise the channels will collapse and prevent the flow of PU into the channels.

2. If, after properly trimming the edges of the PDMS, filling the channels with PU, and curing the sample under UV light students do not see a diffraction pattern in the cured PU, they can repeat the experiment by placing the sample in the desiccator to help fill the channels by vacuum.

3. Make sure that the students do not shine the laser in their eyes when they check for the diffraction pattern.
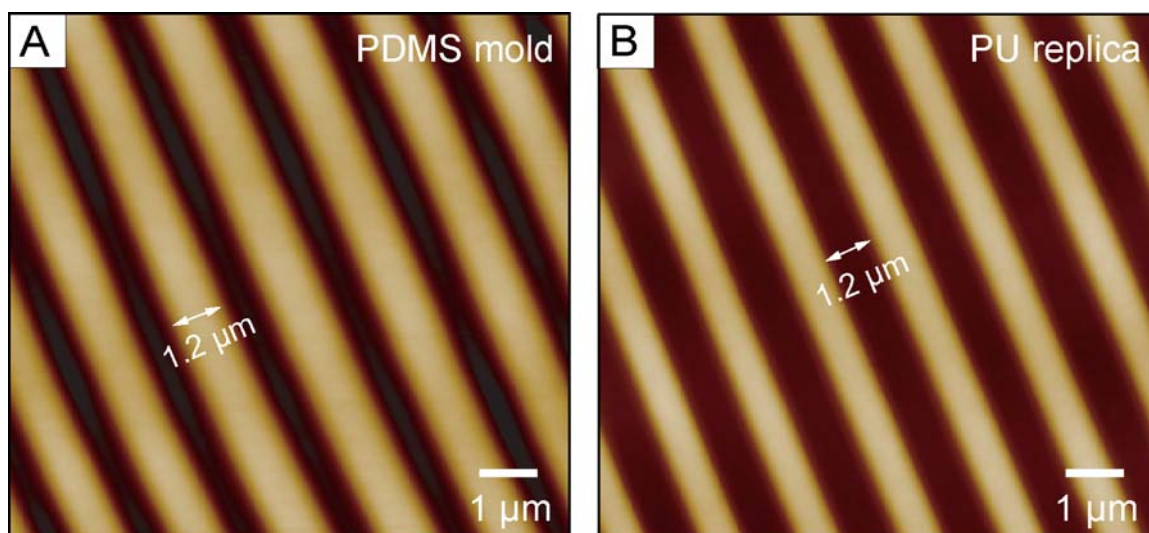
Figure 5.8. AFM images of (A) PDMS mold from Al-layer and (B) PU-replica of the Al-layer after MIMIC. Dark regions correspond to recessed features, and bright regions correspond to raised features.

4. The laser pointer should be 1-2 in away from the sample, which in turn should be held 2-4 in above a piece of white paper.

5. Diffraction lines produced will be perpendicular to the patterned lines.

5.2.5 Micro-Contact Printing (µCP) and Etching

Micro-contact printing is a flexible method for creating patterned self-assembled monolayers (SAMs) and for functionalized surfaces with a variety of organic molecules. A patterned, elastomeric element is used as a stamp (the word 'stamp' is used instead of 'mold' in this section to refer to the printing functionality of the PDMS) to transfer 'ink' to metal substrates. When the PDMS stamp comes into conformal contact with a metal surface, the molecules are transferred from the stamp to the surface in the areas where the stamp is in contact with the metal. The most frequently used inks are alkanethiols, which react strongly with gold surfaces to form SAMS. These SAMs can act like masks or wet etch resists to protect the underlying metal surface. µCP can be combined with etching to produce nanostructures with the same features as the PDMS mask. The physical dimensions of the features on the stamp primarily determine the minimum feature sizes of the patterns that can be generated with this technique. One advantage of µCP over RM and MIMIC is that this technique can be used to produce not only polymeric but also metallic features. Although µCP is extremely useful for a wide range of applications, its resolution encounters practical limits around 100-200 nm, because of the combined effects of: (i) surface diffusion of molecular inks; (ii) disorder at the edges of the printed SAMs; and (iii) the isotropic nature of many of the etching and deposition methods used to convert the patterned SAMs into functional materials.[117, 121]

Thin films of coinage metals such as Au, Ag, Cu, and Pd can be used for µCP, although the most widely used system involves patterning alkanethiol molecules on Au. In an earlier report, vinyl gold films (used in the signage industry) were employed as substrates for the formation of SAMs of thiol molecules.[112] The procedure to obtain Au surfaces suitable for µCP, however, required many laborious steps. For our experiments, archival gold CD-Rs from Diversified Systems Group, Inc. are used. The CDs can be treated with nitric acid to remove the protective polymer coating and expose the patterned Au surface.

The basic steps involved in µCP are outlined in Figure 5.9. A patterned stamp is coated with the "ink" solution and then brought into conformal contact with an Au film for several seconds. The stamp is then removed from the surface to leave behind a patterned SAM on Au. These patterned SAMs can also be used to generate metallic structures with the same pattern as the PDMS stamp because the SAMs can act like a mask or etch resist to protect the underlying metal surface (Figure 5.9, left).

Besides nanostructures of Au lines (or other patterns depending on the PDMS mask), more complex patterns can be produced by µCP on patterned Au surfaces. For example, after µCP with a PDMS stamp patterned with lines at an angle to the Au lines of the CD, the sample can be exposed to an Au etchant to remove the unprotected Au-areas and produce a checkerboard pattern (Figure 5.9, right). Thus, µCP combined with wet chemical etching can provide a way to generate complicated metallic nanostructures.
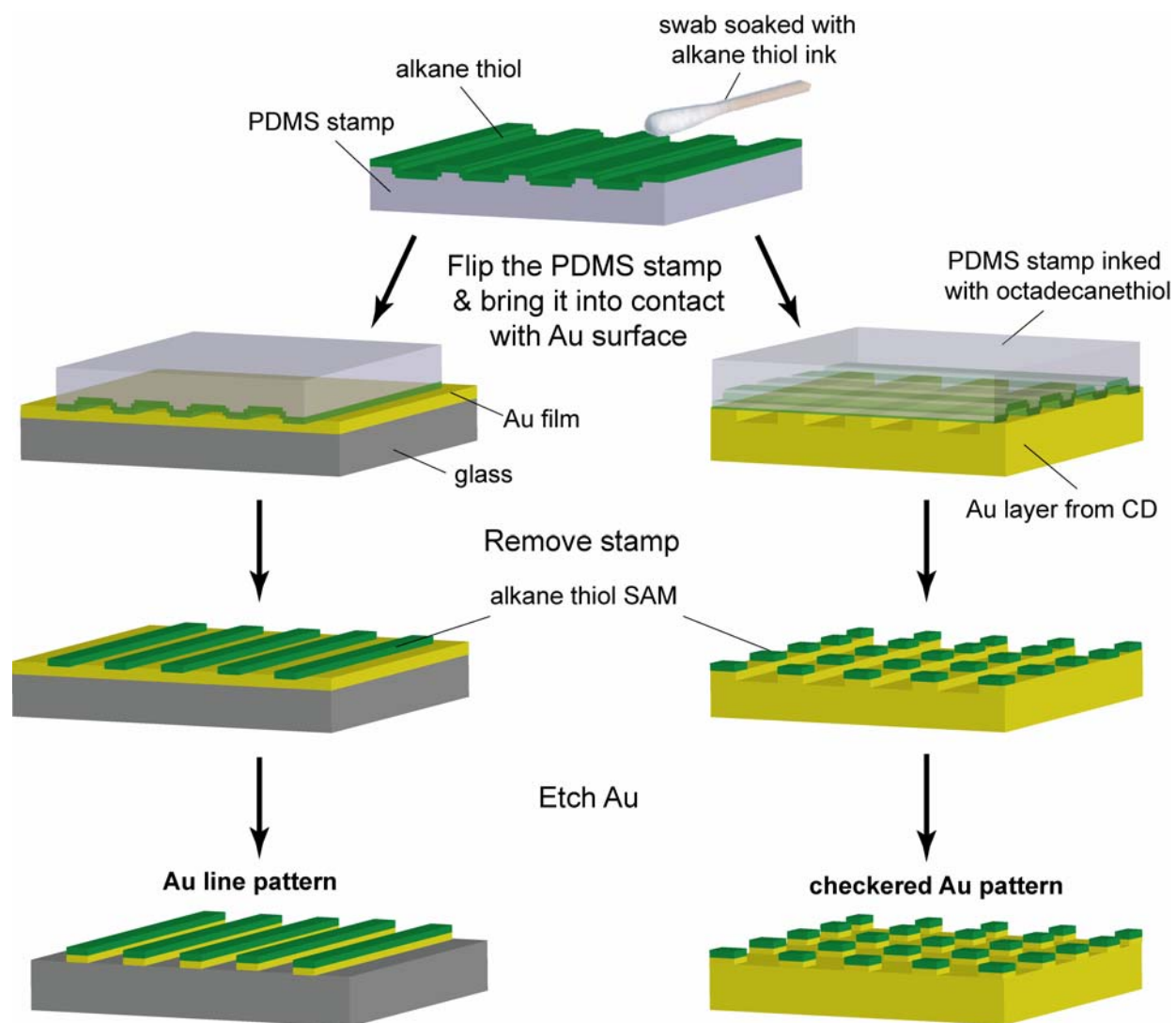
Figure 5.9. Procedure for micro-contact printing and etching of a Au film (left) and a Au-CD (right).

Procedure for Students

A. Preparing Au CD Samples

1. Using scissors cut out a piece of Au recordable archival CD.

2. Pour ~20 mL of concentrated HNO_3 into a small beaker. **WARNING:** *HNO_3 is highly corrosive and can cause severe burns. Handle with care.* Place the dull side of the CD facedown into a beaker, making sure the CD is completely immersed in the acid. The acid treatment will remove the protective layer from the CD.

3. Remove the CD from the beaker using plastic hemostats, rinse with water and dry with nitrogen. The protective layer should peel off to reveal a patterned Au surface. Pour the acid into an appropriately labeled waste container.

B. Micro-Contact Printing Using PDMS Stamps

1. Make a 1 mM solution of octadecanethiol in ethanol, which will be the "ink" solution.

2. Dip a cotton swab into the ink solution and rub it back and forth across the patterned side of the PDMS stamp (generated from the either the PC or Al layers of the CD) for 10 s.

3. Remove excess ink from the stamp by drying it under a stream of nitrogen for 30 s.

4. Place the stamp into conformal contact (you might have to slightly press on the stamp from the top) with the Au surface such that the lines on the stamp are perpendicular to the lines on the Au substrate. To determine which way the lines are patterned on the CD, you can use the laser diffraction method described earlier. Leave the stamp on the substrate for 10 s and then remove it with tweezers. This process will transfer your thiol ink onto the Au surface.

5. To visualize the ink transfer from the stamp to the Au sample, breathe on the Au sample. A diffraction pattern should be visible to indicate successful ink transfer.

C. SAMs as Etch Resists

1. Dilute commercial Au etchant (Transene) with deionized water (1:3 v/v) to make 15 mL of solution and stir.

2. Using plastic hemostats, place your patterned Au sample into the etching solution for 40-45 s. Remove the sample, rinse it with water and dry under a nitrogen stream.

3. Place the sample under a microscope or use the laser diffraction method to visualize the Au checkerboard pattern produced (Figure 5.101).

Questions

1. Compare the etched and unetched patterns by looking at the diffraction pattern from the sample by shining a laser pointer onto the sample. What does the diffraction look like from each sample?

2. What are the limitations of micro-contact printing? How does diffusion of the "ink" play a role?

3. Is micro-contact printing followed by etching a good way to make micro- or nanostructures? Why or why not?

Notes for Instructors

1. Hexadecanethiol or any other long chain alkanethiol can be used instead of octadecanethiol. Octadecanethiol is solid at room temperature and might take more time
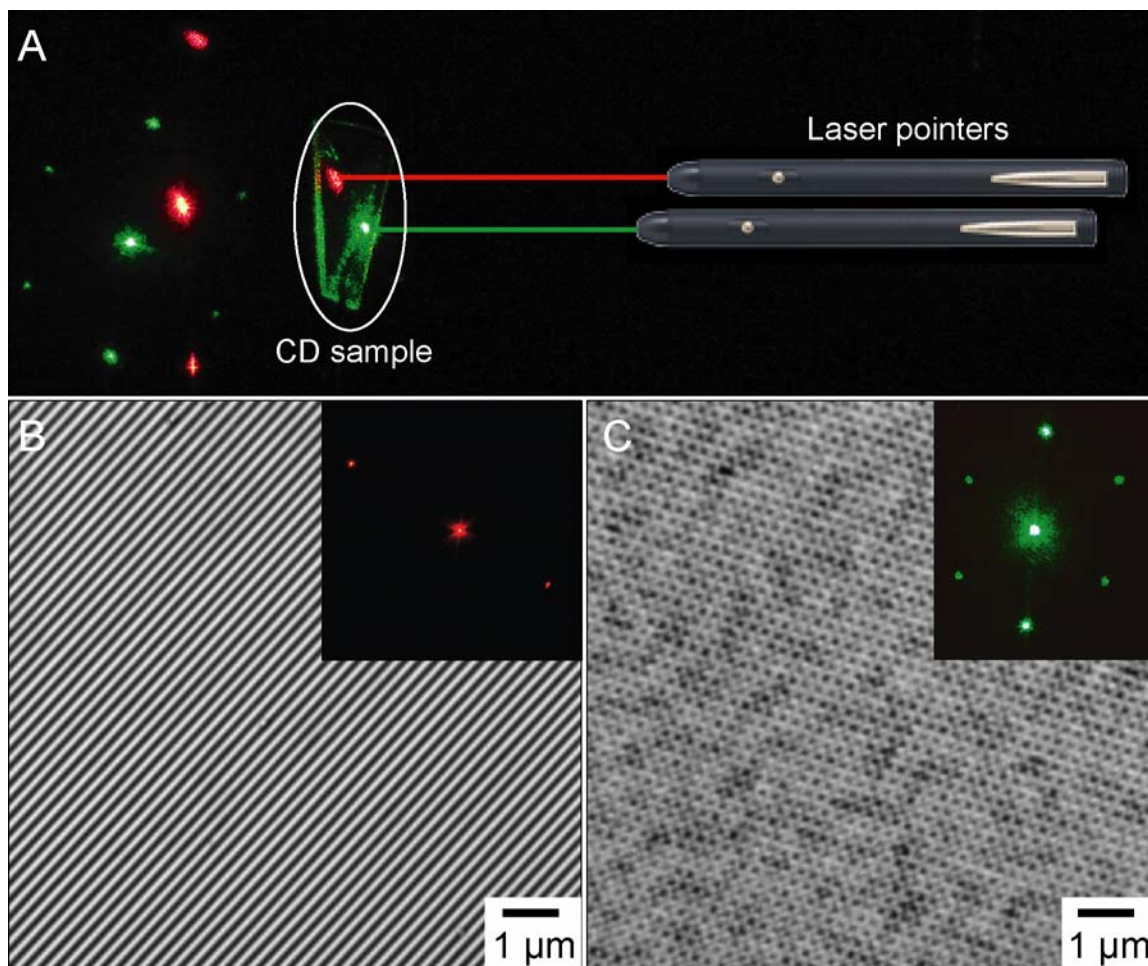
Figure 5.10. (A) Patterns on the CD can be visualized by shining a laser pointer onto the sample and observing the diffraction produced from the pattern. The red laser pointer is incident on the unetched Au line pattern (B) and creates a linear diffraction pattern (B, inset). The green laser pointer is incident on the etched checkerboard pattern (C) and creates a hexagonal diffraction pattern (C, inset). In the optical micrographs of (B) and (C), dark regions correspond to recessed features, and bright regions correspond to raised features.

to dissolve in ethanol. Hexadecanethiol is a liquid at RT and will dissolve faster in ethanol.

2. If octadecanethiol or other longer chain alkanethiol is used, make sure that the thiol is dissolved completely in ethanol. It might help to heat the solution but do not let the ethanol evaporate.

3. The thiol solution should be prepared fresh immediately prior to use. A fresh thiol solution produces better SAMs.

Students should dry the stamp after applying the ink to the stamp to remove any excess of thiol solution; otherwise, the excess ink will diffuse outside of the features, and no pattern will be produced.

4. If the stamp does not go into conformal contact with the substrate on its own, the students can press lightly on the top of the stamp with tweezers.

5. Students can print SAMs on top of Au substrate in different patterns by placing the PDMS line stamp on top of the Au lines at different angles; after etching different metal patterns corresponding diffraction patterns will be produced.

6. To visualize the patterns on the archival grade gold CD-Rs, students can shine a laser pointer onto the sample and look at the diffraction pattern transmitted through the CD on a white piece of paper. The diffraction pattern from a blank CD will consist of a line of spots and the diffraction from the etched area will result in a hexagonal pattern of spots. If two different color laser pointers (green and red) are available, students can shine them simultaneously at different spots on the sample.

7. Students may need to dim the lights in the room to see the diffraction patters from the etched sample because some of the diffractions spots are weak.

8. If students cannot see the change in the diffraction pattern after etching the sample, they can try varying the distance between the sample and the paper. If the sample is too close to the paper, they might not see the additional diffraction spots that were produced by etching.

9. Note: students can also visualize the diffraction pattern through the Au-CD before the removal of the protective layer with nitric acid, although the intensity will not be as bright. Diffraction through a Sony® CD-R (with Al layer) is harder to visualize by looking at the transmitted light because the Al layer is relatively thick. The diffraction pattern on CDs with Al layers can still be obtained by looking at the light that is reflected by the CD. Care must be taken so that this reflected light does not enter the eyes.

10. If the students do not obtain a checkered pattern after etching, they can repeat the experiment and vary the time that the stamp is in contact with the Au CD (anywhere from 5-30 s).

5.3 Conclusion

The feasibility of these labs was demonstrated by including them as part of a two-quarter, research-based course on nanoscience and technology at Northwestern University (NU). The classroom size was limited to 12 students, but the experiments were intended to require only minimal supervision and can be scaled easily for larger class sizes. Prior to classroom implementation, these experiments were also tested in our laboratory by three undergraduate students.

To demonstrate that these activities are also accessible to high school science students we invited approximately 60-70 students and 2-3 teachers from New Trier Township High School (NTTHS) in Winnetka, IL to participate in "What is Nanosciene/technology?" event at NU. The event included presentations by graduate students on "What is Nanotechnology?", a tour of microscope and laser labs, including demonstration of an AFM and scanning electron microscope (SEM), and hands-on activities involving the benchtop nanopattering described earlier in the chapter. The students had an opportunity to practice μCP and etching techniques and look at the samples they prepared using different microscopy tools.

Because of the success of this event and teacher interest in introducing the material in their classrooms, we expanded our partnership with NTTHS to educate not only the students but also to provide the teachers with resources and training to allow introduction of our materials into their classrooms. We hosted a group of seven science (chemistry, biology, and physics) teachers from NTTHS. The teachers were exposed to the benchtop nanopatterning experiments through lecture and hands-on activities along with a demonstration of state-of-the-art instruments used in nanoscience. We provided them with the information and training necessary to incorporate our nanopatterning experiments into their classrooms.

References

1.   Ozbay, E., Plasmonics: Merging photonics and electronics at nanoscale dimensions. *Science* **2006,** 311, (5758), 189-193.

2.   Birner, A.; Wehrspohn, R. B.; Gosele, U. M.; Busch, K., Silicon-based photonic crystals. *Advanced Materials* **2001,** 13, (6), 377-388.

3.   Soukoulis, C. M., *Photonic crystals and light localization in the 21st century*. Kluwer Academic Publishers: Crete, Greece, 2000; Vol. 563.

4.   Ogawa, S. P.; Imada, M.; Yoshimoto, S.; Okano, M.; Noda, S., Control of light emission by 3d photonic crystals. *Science* **2004,** 305, (5681), 227-229.

5.   Barnes, W. L.; Dereux, A.; Ebbesen, T. W., Surface plasmon subwavelength optics. *Nature* **2003,** 424, (6950), 824-830.

6.   Maier, S. A.; Friedman, M. D.; Barclay, P. E.; Painter, O., Experimental demonstration of fiber-accessible metal nanoparticle plasmon waveguides for planar energy guiding and sensing. *Applied Physics Letters* **2005,** 86, (7), 071103/071101-071103/071103.

7.   Nie, S. M.; Emery, S. R., Probing single molecules and single nanoparticles by surface-enhanced raman scattering. *Science* **1997,** 275, (5303), 1102-1106.

8.   Kneipp, K.; Wang, Y.; Kneipp, H.; Perelman, L. T.; Itzkan, I.; Dasari, R.; Feld, M. S., Single molecule detection using surface-enhanced raman scattering (sers). *Physical Review Letters* **1997,** 78, (9), 1667-1670.

9.   Maier, S. A.; Atwater, H. A., Plasmonics: Localization and guiding of electromagnetic energy in metal/dielectric structures. *Journal of Applied Physics* **2005,** 98, (1), 011101/011101-011101/011110.

10.   Fink, Y.; Winn, J. N.; Fan, S. H.; Chen, C. P.; Michel, J.; Joannopoulos, J. D.; Thomas, E. L., A dielectric omnidirectional reflector. *Science* **1998,** 282, (5394), 1679-1682.

11.   Russell, P., Photonic crystal fibers. *Science (Washington, DC, United States)* **2003,** 299, (5605), 358-362.

12.   Joannopoulos, J. D.; Meade, R. D.; Winn, N. J., *Photonic crystals, molding the flow of light*. Princeton University Press: Princeton, NJ, 1995.

13.   Gates, B.; Xia, Y. N., Photonic crystals that can be addressed with an external magnetic field. *Advanced Materials* **2001,** 13, (21), 1605-1608.

14.   Charbonneau, R.; Berini, P.; Berolo, E.; Lisicka-Shrzek, E., Experimental observation of plasmon-polariton waves supported by a thin metal film of finite width. *Optics Letters* **2000,** 25, (11), 844-846.

15.   Berini, P.; Charbonneau, R.; Lahoud, N.; Mattiussi, G., Characterization of long-range surface-plasmon-polariton waveguides. *Journal of Applied Physics* **2005,** 98, (4), 043109/043101-043109/043112.

16.   Dionne, J. A.; Sweatlock, L. A.; Atwater, H. A.; Polman, A., Plasmon slot waveguides: Towards chip-scale propagation with subwavelength-scale localization. *Physical Review B* **2006,** 73, (3), 035407/035401-035407/035409.

17.   Colas des Francs, G.; Girard, C.; Weeber, J.-C.; Chicane, C.; David, T.; Dereux, A.; Peyrade, D., Optical analogy to electronic quantum corrals. *Physical Review Letters* **2001,** 86, (21), 4950-4953.

18.   Chicanne, C.; David, T.; Quidant, R.; Weeber, J. C.; Lacroute, Y.; Bourillot, E.; Dereux, A.; Colas des Francs, G.; Girard, C., Imaging the local density of states of optical corrals. *Physical Review Letters* **2002,** 88, (9), 097402/097401-097402/097404.

19.   Dereux, A.; Girard, C.; Chicanne, C.; des Francs, G. C.; David, T.; Bourillot, E.; Lacroute, Y.; Weeber, J. C., Subwavelength mapping of surface photonic states. *Nanotechnology* **2003,** 14, (8), 935-938.

20.   Crommie, M. F.; Lutz, C. P.; Eigler, D. M., Confinement of electrons to quantum corrals on a metal surface. *Science (Washington, DC, United States)* **1993,** 262, (5131), 218-220.

21.   Lamprecht, B.; Krenn, J. R.; Schider, G.; Ditlbacher, H.; Salerno, M.; Felidj, N.; Leitner, A.; Aussenegg, F. R.; Weeber, J. C., Surface plasmon propagation in microscale metal stripes. *Applied Physics Letters* **2001,** 79, (1), 51-53.

22.   Dunn, R. C., Near-field scanning optical microscopy. *Chemical Reviews (Washington, D. C.)* **1999,** 99, (10), 2891-2927.

23.   Weeber, J. C.; Krenn, J. R.; Dereux, A.; Lamprecht, B.; Lacroute, Y.; Goudonnet, J. P., Near-field observation of surface plasmon polariton propagation on thin metal stripes. *Physical Review B* **2001,** 64, 045411/045411 -045411/045419.

24.   Krenn, J. R.; Weeber, J. C., Surface plasmon polaritons in metal stripes and wires. *Philosophical Transactions of the Royal Society of London, Series A: Mathematical, Physical and Engineering Sciences* **2004,** 362, (1817), 739-756.

25.   Raether, H., *Surface plasmons on smooth and rough surfaces and on gratings*. Springers, Ed.: Berlin, 1988.

26.   Gao, H.; Henzie, J.; Odom, T. W., Direct evidence for surface plasmon-mediated enhanced light transmission through metallic nanohole arrays. *Nano Letters* **2006,** 6, (9), 2104-2108.

27.   Haes, A. J.; Haynes, C. L.; McFarland, A. D.; Schatz, G. C.; van Duyne, R. P.; Zou, S., Plasmonic materials for surface-enhanced sensing and spectroscopy. *MRS Bulletin* **2005,** 30, (5), 368-375.

28.   Bohren, C. F.; Huffman, D. R., *Absorption and scattering of light by small particles*. Wiley: New York, 1983.

29.   Haynes, C. L.; McFarland, A. D.; Zhao, L.; Van Duyne, R. P.; Schatz, G. C.; Gunnarsson, L.; Prikulis, J.; Kasemo, B.; Kaell, M., Nanoparticle optics: The importance of radiative dipole coupling in two-dimensional nanoparticle arrays. *Journal of Physical Chemistry B* **2003,** 107, (30), 7337-7342.

30.   Ianoul, A.; Bergeron, A., Spatially inhomogeneous enhancement of fluorescence by a monolayer of silver nanoparticles. *Langmuir* **2006,** 22, (24), 10217-10222.

31.   Ash, E. A.; Nicholls, G., Super-resolution aperture scanning microscope. *Nature* **1972,** 237, (5357), 510-512.

32.   Pohl, D. W.; Denk, W.; Lanz, M., Optical stethoscopy: Image recording with resolution $\lambda/20$. *Applied Physics Letters* **1984,** 44, 651-653.

33.   Lewis, A.; Isaacson, M.; Harootunian, A.; Murray, A., Development of a 500 å spatial resolution light microscope. I. Light is efficiently transmitted through $\lambda/16$ diameter apertures. *Ultramicroscopy* **1984,** 13, 227.

34.   Betzig, E.; Trautman, J. K.; Harris, T. D.; Weiner, J. S.; Kostelak, R. L., Breaking the diffraction barrier: Optical microscopy on a nanometric scale. *Science (Washington, D. C.)* **1991,** 251, 1468-1470.

35.   Zeisel, D.; Nettesheim, S.; Butoit, B.; Zenobi, R., Pulsed laser-induced desorption and optical imaging on a nanometer scale with scanning near-field microscopy using chemically etched fiber tips. *Applied Physics Letters* **1996,** 68, (18), 2491-2492.

36.   Valaskovic, G. A.; Holton, M.; Morrison, G. H., Parameter control, characterization, and optimization in the fabrication of optical fiber near-field probes. *Applied Optics* **1995,** 34, (7), 1215-1228.

37.   Bethe, H. A., *Physical Review Letters* **1944,** 66, 163.

38.   Kurpas, V.; Libenson, M.; Martsinovsky, G., Laser heating of near-field tips. *Ultramicroscopy* **1995,** 61, 187-190.

39.   Yakobson, B. I.; LaRosa, A.; Hallen, H. D.; Paesler, M. A., Thermal/optical effects in nsom probes. *Ultramicroscopy* **1995,** 61, (1-4, Selected Papers from the 3rd International Conference on Near-Field Optics and Related Techniques, 1995), 179-185.

40.   Dickenson Nicholas, E.; Erickson Elizabeth, S.; Mooren Olivia, L.; Dunn Robert, C., Characterization of power induced heating and damage in fiber optic probes for near-field scanning optical microscopy. *Rev Sci Instrum FIELD Full Journal Title:The Review of scientific instruments* **2007,** 78, (5), 053712.

41.   Stahelin, M.; Bopp, M. A.; Tarrach, G.; Meixner, A. J.; Zschokke-Granacher, I., *Applied Physics Letters* **1996,** 68, 2603.

42.   Hoffmann, P.; Dutoit, B.; Salathe, R.-P., Comparison of mechanically drawn and protection layer chemically etched optical fiber tips. *Ultramicroscopy* **1995,** 61, 165-170.

43.   McNeill, J. D.; O'Connor, D. B.; Barbara, P. F., Imaging organic device function with near-field scanning optical microscopy. *Journal of Chemical Physics* **2000,** 112, (18), 7811-7821.

44.   Harootunian, A.; Betzig, E.; Isaacson, M.; Lewis, A., Super-resolution fluorescence near-field scanning optical microscopy. *Applied Physics Letters* **1986,** 49, (11), 674-676.

45.   Betzig, E.; Finn, P. L.; Weiner, J. S., Combined shear force and near-field scanning optical microscopy. *Applied Physics Letters* **1992,** 60, (20), 2484-2486.

46.   Fischer, U. C.; Pohl, D. W., Observation of single-particle plasmons by near-field optical microscopy. *Physical Review Letters* **1989,** 62, (4), 458-461.

47.   Novotny, L.; Pohl, D. W.; Regli, P., Near-field, far-field and imaging properties of the 2d aperture snom. *Ultramicroscopy* **1995,** 57, (2/3), 180-188.

48.   Monson, E.; Merritt, G.; Smith, S.; Langmore, J. P.; Kopelman, R., Implementation of an nsom system for fluorescence microscopy. *Ultramicroscopy* **1995,** 57, (2/3), 257-262.

49.   Yin, L.; Vlasko-Vlasov, V. K.; Pearson, J.; Hiller, J. M.; Hua, J.; Welp, U.; Brown, D. E.; Kimball, C. W., Subwavelength focusing and guiding of surface plasmons. *Nano Letters* **2005,** 5, (7), 1399-1402.

50. Yin, L.; Vlasko-Vlasov, V. K.; Rydh, A.; Pearson, J.; Welp, U.; Chang, S. H.; Gray, S. K.; Schatz, G. C.; Brown, D. B.; Kimball, C. W., Surface plasmons at single nanoholes in au films. *Applied Physics Letters* **2004,** 85, (3), 467-469.

51. Liu, Z.; Steele, J. M.; Srituravanich, W.; Pikus, Y.; Sun, C.; Zhang, X., Focusing surface plasmons with a plasmonic lens. *Nano Letters* **2005,** 5, (9), 1726-1729.

52. Reddick, R. C.; Warmack, R. J.; Ferrell, T. L., New form of scanning optical microscopy. *Physical Review B: Condensed Matter* **1989,** 39, 767-770.

53. Harlepp, S.; Robert, J.; Darnton, N. C.; Chatenay, D., Subnanometric measurements of evanescent wave penetration depth using total internal reflection microscopy combined with fluorescent correlation spectroscopy. *Applied Physics Letters* **2004,** 85, (17), 3917-3919.

54. McFarland, A. D.; Van Duyne, R. P., Single silver nanoparticles as real-time optical sensors with zeptomole sensitivity. *Nano Letters* **2003,** 3, (8), 1057-1062.

55. Raschke, G.; Kowarik, S.; Franzl, T.; Soennichsen, C.; Klar, T. A.; Feldmann, J.; Nichtl, A.; Kuerzinger, K., Biomolecular recognition based on single gold nanoparticle light scattering. *Nano Letters* **2003,** 3, (7), 935-938.

56. Nehl, C. L.; Liao, H.; Hafner, J. H., Optical properties of star-shaped gold nanoparticles. *Nano Letters* **2006,** 6, (4), 683-688.

57. Rogers, J. A.; Paul, K. E.; Jackman, R. J.; Whitesides, G. M., Generating .Apprx.90 nanometer features using near-field contact-mode photolithography with an elastomeric phase mask. *Journal of Vacuum Science & Technology, B: Microelectronics and Nanometer Structures* **1998,** 16, (1), 59-68.

58. Odom, T. W.; Thalladi, V. R.; Love, J. C.; Whitesides, G. M., Generation of 30-50 nm structures using easily fabricated, composite pdms masks. *Journal of the American Chemical Society* **2002,** 124, (41), 12112-12113.

59. Odom, T. W.; Love, J. C.; Wolfe, D. B.; Paul, K. E.; Whitesides, G. M., Improved pattern transfer in soft lithography using composite stamps. *Langmuir* **2002,** 18, (13), 5314-5320.

60. Duan, X.; Huang, Y.; Cui, Y.; Wang, J.; Lieber, C. M., Indium phosphide nanowires as building blocks for nanoscale electronic and optoelectronic devices. *Nature* **2001,** 409, (6816), 66-69.

61. Huang, M. H.; Mao, S.; Feick, H.; Yan, H.; Wu, Y.; Kind, H.; Weber, E.; Russo, R.; Yang, P., Room-temperature ultraviolet nanowire nanolasers. *Science* **2001,** 292, (5523), 1897-1899.

62.   Kagan, C. R.; Murray, C. B.; Nirmal, M.; Bawendi, M. G., Electronic energy transfer in cdse quantum dot solids. *Physical Review Letters* **1996,** 76, (9), 1517-1520.

63.   Kempa, K.; Kimball, B.; Rybczynski, J.; Huang, Z. P.; Wu, P. F.; Steeves, D.; Sennett, M.; Giersig, M.; Rao, D. V. G. L. N.; Carnahan, D. L.; Wang, D. Z.; Lao, J. Y.; Li, W. Z.; Ren, Z. F., Photonic crystals based on periodic arrays of aligned carbon nanotubes. *Nano Letters* **2003,** 3, (1), 13-18.

64.   Kong, J.; Soh, H. T.; Cassell, A. M.; Quate, C. F.; Dai, H., Synthesis of individual single-walled carbon nanotubes on patterned silicon wafers. *Nature* **1998,** 395, (6705), 878-881.

65.   Love, J. C.; Gates, B. D.; Wolfe, D. B.; Paul, K. E.; Whitesides, G. M., Fabrication and wetting properties of metallic half-shells with submicron diameters. *Nano Letters* **2002,** 2, (8), 891-894.

66.   Qin, D.; Xia, Y.; Xu, B.; Yang, H.; Zhu, C.; Whitesides, G. M., Fabrication of ordered two-dimensional arrays of micro- and nanoparticles using patterned self-assembled monolayers as templates. *Advanced Materials* **1999,** 11, (17), 1433-1437.

67.   Smith, P. A.; Nordquist, C. D.; Jackson, T. N.; Mayer, T. S.; Martin, B. R.; Mbindyo, J.; Mallouk, T. E., Electric-field assisted assembly and alignment of metallic nanowires. *Applied Physics Letters* **2000,** 77, (9), 1399-1401.

68.   Vlasov, Y. A.; Yao, N.; Norris, D. J., Synthesis of photonic crystals for optical wavelengths from semiconductor quantum dots. *Advanced Materials* **1999,** 11, (2), 165-169.

69.   Yin, Y.; Lu, Y.; Gates, B.; Xia, Y., Template-assisted self-assembly: A practical route to complex aggregates of monodispersed colloids with well-defined sizes, shapes, and structures. *Journal of the American Chemical Society* **2001,** 123, (36), 8718-8729.

70.   Lu, N.; Chen, X.; Molenda, D.; Naber, A.; Fuchs, H.; Talapin, D. V.; Weller, H.; Mueller, J.; Lupton, J. M.; Feldmann, J.; Rogach, A. L.; Chi, L., Lateral patterning of luminescent cdse nanocrystals by selective dewetting from self-assembled organic templates. *Nano Letters* **2004,** 4, (5), 885-888.

71.   Wang, X.; Summers, C. J.; Wang, Z. L., Large-scale hexagonal-patterned growth of aligned zno nanorods for nano-optoelectronics and nanosensor arrays. *Nano Letters* **2004,** 4, (3), 423-426.

72.   Greyson, E. C.; Babayan, Y.; Odom, T. W., Directed growth of ordered arrays of small-diameter zno nanowires. *Advanced Materials* **2004,** 16, (15), 1348-1352.

73.   Goldberger, J.; He, R.; Zhang, Y.; Lee, S.; Yan, H.; Choi, H.-J.; Yang, P., Single-crystal gallium nitride nanotubes. *Nature* **2003,** 422, (6932), 599-602.

74.   Yin, Y. D.; Lu, Y.; Xia, Y. N., A self-assembly approach to the formation of asymmetric dimers from monodispersed spherical colloids. *Journal of the American Chemical Society* **2001,** 123, (4), 771-772.

75.   Yin, Y.; Xia, Y., Self-assembly of monodispersed spherical colloids into complex aggregates with well-defined sizes, shapes, and structures. *Advanced Materials* **2001,** 13, (4), 267-271.

76.   Huang, Y.; Duan, X.; Wei, Q.; Lieber, C. M., One-dimensional nanostructures into functional networks. *Science* **2001,** 291, (5504), 630-633.

77.   Messer, B.; Song, J. H.; Yang, P., Microchannel networks for nanowire patterning. *Journal of the American Chemical Society* **2000,** 122, (41), 10232-10233.

78.   Achermann, M.; Petruska, M. A.; Crooker, S. A.; Klimov, V. I., Picosecond energy transfer in quantum dot langmuir-blodgett nanoassemblies. *Journal of Physical Chemistry B* **2003,** 107, (50), 13782-13787.

79.   Bakkers, E. P. A. M.; Vanmaekelbergh, D., Resonant electron tunneling through semiconducting nanocrystals in a symmetrical and an asymmetrical junction. *Physical Review B: Condensed Matter and Materials Physics* **2000,** 62, (12), R7743-R7746.

80.   Kasuya, A.; Sivamohan, R.; Barnakov, Y. A.; Dmitruk, I. M.; Nirasawa, T.; Romanyuk, V. R.; Kumar, V.; Mamykin, S. V.; Tohji, K.; Jeyadevan, B.; Shinoda, K.; Kudo, T.; Terasaki, O.; Liu, Z.; Belosludov, R. V.; Sundararajan, V.; Kawazoe, Y., Ultra-stable nanoparticles of cdse revealed from mass spectrometry. *Nature Materials* **2004,** 3, (2), 99-102.

81.   Alivisatos, A. P., Semiconductor clusters, nanocrystals, and quantum dots. *Science* **1996,** 271, (5251), 933-937.

82.   Manna, L.; Scher, E. C.; Alivisatos, A. P., Synthesis of soluble and processable rod-, arrow-, teardrop-, and tetrapod-shaped cdse nanocrystals. *Journal of the American Chemical Society* **2000,** 122, (51), 12700-12706.

83.   Somers, R. C.; Bawendi, M. G.; Nocera, D. G., Cdse nanocrystal based chem-/bio-sensors. *Chemical Society Reviews* **2007,** 36, (4), 579-591.

84.   Kagan, C. R.; Murray, C. B.; Bawendi, M. G., Long-range resonance transfer of electronic excitations in close-packed cdse quantum-dot solids. *Physical Review B: Condensed Matter* **1996,** 54, (12), 8633-8643.

85.   Klimov, V. I.; Mikhailovsky, A. A.; Xu, S.; Malko, A.; Hollingsworth, J. A.; Leatherdale, C. A.; Eisler, H. J.; Bawendi, M. G., Optical gain and stimulated emission in nanocrystal quantum dots. *Science* **2000,** 290, (5490), 314-317.

86.   Murray, C. B.; Kagan, C. R.; Bawendi, M. G., Self-organization of cdse nanocrystallites into three-dimensional quantum dot superlattices. *Science* **1995,** 270, (5240), 1335-1358.

87.   Ganesh, N.; Zhang, W.; Mathias, P. C.; Chow, E.; Soares, J. A. N. T.; Malyarchuk, V.; Smith, A. D.; Cunningham, B. T., Enhanced fluorescence emisison from quantum dots on a photonic crystal surface. *Nature Nanotechnology* **2007,** 2, 515-520.

88.   Shaw, J. M.; Gelorme, J. D.; Labianca, N. C.; Conley, W. E.; Holmes, S. J., Negative photoresists for optical lithography. *IBM Journal of Research and Development* **1997,** 41, (1/2), 81-94.

89.   Murray, C. B.; Sun, S.; Gaschler, W.; Doyle, H.; Betley, T. A.; Kagan, C. R., Colloidal synthesis of nanocrystals and nanocrystal superlattices. *IBM Journal of Research and Development* **2001,** 45, 47-56.

90.   Peng, Z. A.; Peng, X., Formation of high-quality cdte, cdse, and cds nanocrystals using cdo as precursor. *Journal of the American Chemical Society* **2001,** 123, (1), 183-184.

91.   Dabbousi, B. O.; Rodriguez-Viejo, J.; Mikulec, F. V.; Heine, J. R.; Mattoussi, H.; Ober, R.; Jensen, K. F.; Bawendi, M. G., (cdse)zns core-shell quantum dots: Synthesis and optical and structural characterization of a size series of highly luminescent materials. *Journal of Physical Chemistry B* **1997,** 101, (46), 9463-9475.

92.   Hines, M. A.; Guyot-Sionnest, P., Synthesis and characterization of strongly luminescing zns-capped cdse nanocrystals. *Journal of Physical Chemistry* **1996,** 100, (2), 468-471.

93.   Talapin, D. V.; Rogach, A. L.; Kornowski, A.; Haase, M.; Weller, H., Highly luminescent monodisperse cdse and cdse/zns nanocrystals synthesized in a hexadecylamine-trioctylphosphine oxide-trioctylphosphine mixture. *Nano Letters* **2001,** 1, (4), 207-211.

94.   Chan, W. C.; Nie, S., Quantum dot bioconjugates for ultrasensitive nonisotopic detection. *Science* **1998,** 281, (5385), 2016-2018.

95.   Mattoussi, H.; Mauro, J. M.; Goldman, E. R.; Anderson, G. P.; Sundar, V. C.; Mikulec, F. V.; Bawendi, M. G., Self-assembly of cdse-zns quantum dot bioconjugates using an engineered recombinant protein. *Journal of the American Chemical Society* **2000,** 122, (49), 12142-12150.

96.   Leatherdale, C. A.; Bawendi, M. G., Observation of solvatochromism in cdse colloidal quantum dots. *Physical Review B: Condensed Matter and Materials Physics* **2001,** 63, (16), 165315/165311-165315/165316.

97.   Crooker, S. A.; Hollingsworth, J. A.; Tretiak, S.; Klimov, V. I., Spectrally resolved dynamics of energy transfer in quantum-dot assemblies: Towards engineered energy flows in artificial materials. *Physical Review Letters* **2002,** 89, (18), 186802/186801-186802/186804.

98.   Ebbesen, T. W.; Lezec, H. J.; Ghaemi, H. F.; Thio, T.; Wolff, P. A., Extraordinary optical transmission through sub-wavelength hole arrays. *Nature* **1998,** 391, (6668), 667-669.

99.   Willets, K. A.; Van Duyne, R. P., Localized surface plasmon resonance spectroscopy and sensing. *Annual Review of Physical Chemistry* **2007,** 58, 267-297.

100.   Henzie, J.; Lee, M. H.; Odom, T. W., Multiscale patterning of plasmonic metamaterials. *Nature Nanotechnology* **2007,** 2, (9), 549-554.

101.   Manoharan, H. C.; Lutz, C. P.; Eigler, D. M., Quantum mirages formed by coherent projection of electronic structure. *Nature* **2000,** 403, (6769), 512-515.

102.   Dawson, P.; Boyle, M. G., Light emission from scanning tunnelling microscope on polycrystalline au films-what is happening at the single-grain level? *Journal of Optics A: Pure and Applied Optics* **2006,** 8, (4), S219-S226.

103.   Fiete, G. A.; Heller, E. J., Colloquium: Theory of quantum corrals and quantum mirages. *Review of Modern Physics* **2003,** 75, (3), 933-948.

104.   JK Consulting, T. F. D. A. High reflectors. http://www.kruschwitz.com/HR's.htm#Metal%20Coatings (November 20, 2007).

105.   Blum, J. Tech first to offer nanotech undergrad degree. http://cenit.latech.edu/cenit/news/index.asp?name=view&article=20050225 (October 9, 2007).

106.   Hersam, M.; Lauhon, L., J Degree programs and courses. http://www.nclt.us/programs_nanocourses.htm (October 9, 2007).

107.   Odom, T. W. Junior research seminar: Nanoscale patterning and systems. http://chemgroups.northwestern.edu/odom/juniorseminar.htm (October 9, 2007).

108.   Porter, L. A., Jr., Chemical nanotechnology: A liberal arts approach to a basic course in emerging interdisciplinary science and technology. *Journal of Chemical Education* **2007,** 84, (2), 259-264.

109. Viswanathan, M.; Babayan, Y.; Odom, T. W., Benchtop nanoscale patterning using soft lithography. *Journal of Chemical Education* **2007,** 84, (11), 1795-1798.

110. Winkler, L. D.; Arceo, J. F.; Hughes, W. C.; DeGraff, B. A.; Augustine, B. H., Quantum dots: An experiment for physical or materials chemistry. *Journal of Chemical Education* **2005,** 82, (11), 1700-1702.

111. Bentley, A. K.; Farhoud, M.; Ellis, A. B.; Lisensky, G. C.; Nickel, A.-M. L.; Crone, W. C., Template synthesis and magnetic manipulation of nickel nanowires. *Journal of Chemical Education* **2005,** 82, (5), 765-768.

112. McKenzie, L. C.; Huffman, L. M.; Parent, K. E.; Hutchison, J. E.; Thompson, J. E., Patterning self-assembled monolayers on gold. Green materials chemistry in the teaching laboratory. *Journal of Chemical Education* **2004,** 81, (4), 545-548.

113. Haynes, C. L.; McFarland, A. D.; Van Duyne, R. P.; Godwin, H. A., Nanopatterning with lithography. *Journal of Chemical Education* **2005,** 82, (5), 768A-768B.

114. Stelick, S. J.; Alger, W. H.; Laufer, J. S.; Waldron, A. M.; Batt, C. A., Hands-on classroom photolithography laboratory module to explore nanotechnology. *Journal of Chemical Education* **2005,** 82, (9), 1361-1364.

115. Berkowski, K. L.; Plunkett, K. N.; Yu, Q.; Moore, J. S., Introduction to photolithography: Preparation of microscale polymer silhouettes. *Journal of Chemical Education* **2005,** 82, (9), 1365-1369.

116. Xia, Y.; Whitesides, G. M., Soft lithography. *Angewandte Chemie, International Edition* **1998,** 37, (5), 550-575.

117. Gates, B. D.; Xu, Q.; Stewart, M.; Ryan, D.; Willson, C. G.; Whitesides, G. M., New approaches to nanofabrication: Molding, printing, and other techniques. *Chemical Reviews* **2005,** 105, (4), 1171-1196.

118. Bratton, D.; Yang, D.; Dai, J.; Ober, C. K., Recent progress in high resolution lithography. *Polymers for Advanced Technologies* **2006,** 17, (2), 94-103.

119. Harriott, L. R.; Hull, R., Nanolithography. *Introduction to Nanoscale Science and Technology* **2004**, 7-40.

120. Xia, Y.; McClelland, J. J.; Gupta, R.; Qin, D.; Zhao, X. M.; Sohn, L. L.; Celotta, R. J.; Whitesides, G. M., Replica molding using polymeric materials. A practical step toward nanomanufacturing. *Advanced Materials* **1997,** 9, (2), 147-149.

121. Biebuyck, H. A.; Larsen, N. B.; Delamarche, E.; Michel, B., Lithography beyond light: Microcontact printing with monolayer resists. *IBM Journal of Research and Development* **1997,** 41, (1/2), 159-170.
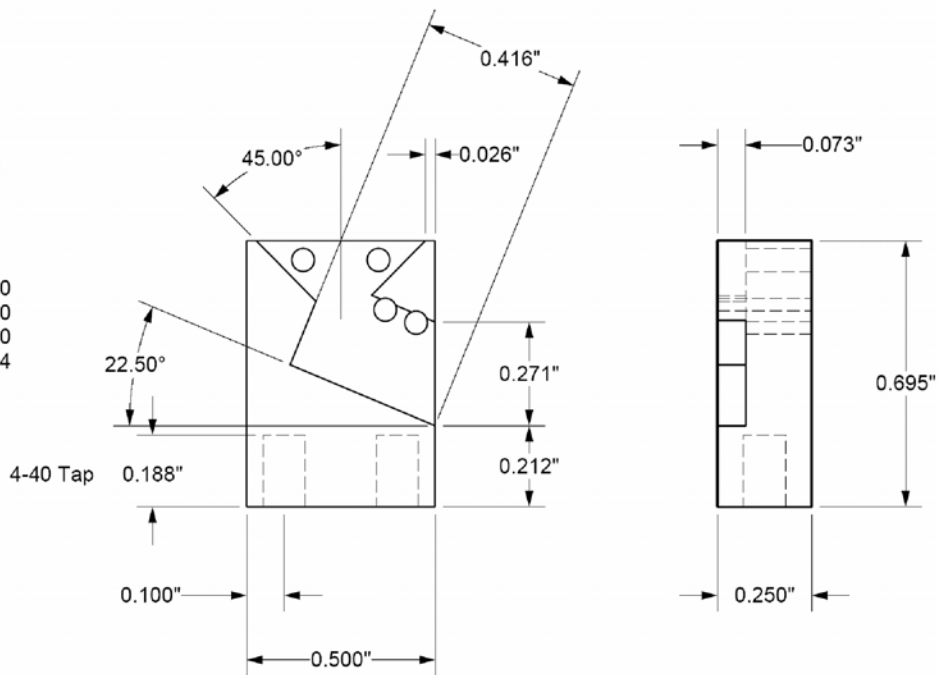
Appendix 1

Prism Holder Design for PSTM

Prism Holder, Piece #1
Scale: 3:1
Aluminum

0-80 Tapped Thru
Locations from
Top Right Corner

X	Y
-0.350	-0.050
-0.150	-0.050
-0.132	-0.180
-0.050	-0.214

0.416"

45.00°   0.026"

0.073"

22.50°

0.271"

0.695"

0.212"

4-40 Tap   0.188"

0.100"

0.500"

0.250"

Prism Holder, Piece #2
Scale: 3:1
Aluminum

0.416"

0.026"   45.00°

0.073"

0.271"

22.50°

0.695"

0.212"

0.188" 4-40 Tap

0.100"

0.500"

0.250"
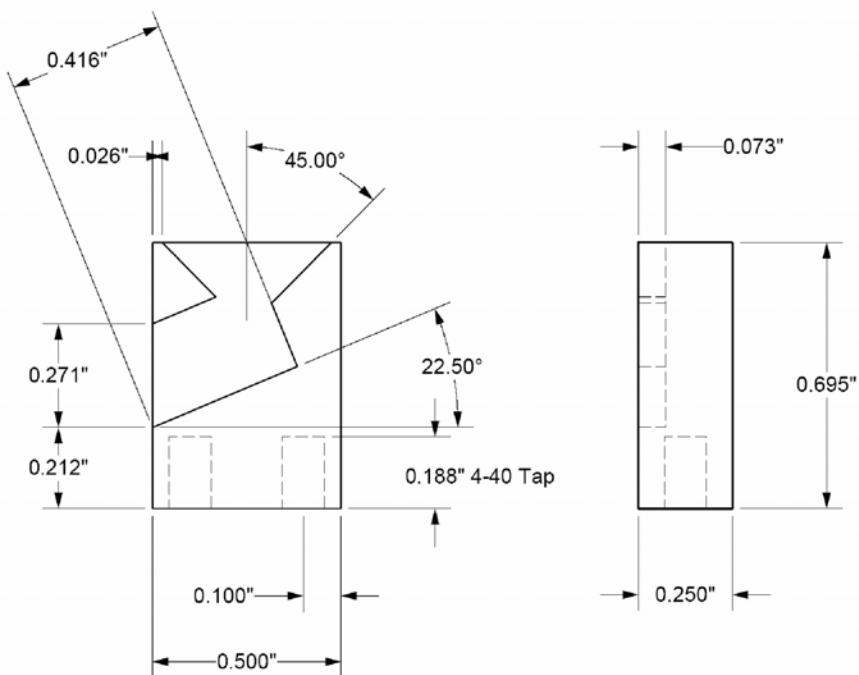
Figure A1.1. CAD drawings of piece 1 and piece 2 of prism holder.

Prism Holder, Piece #3
Scale: 3:1
Aluminum

Countersink 4-40

0.250"

4-40 Tap

0.500"

0.300"

0.300"

1.000"

0.300"

0.500"
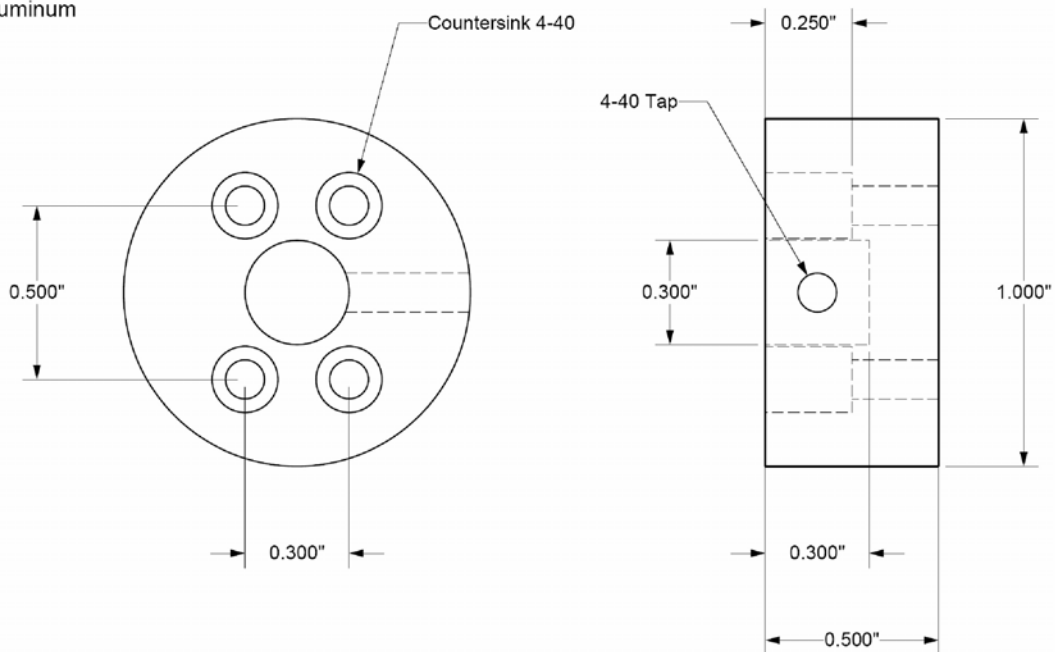
Prism Holder, Piece #4
Scale: 3:1
Aluminum

Ø 1.000"

Ø 0.300"

0.800" 36 TPI

0.300"

0.500"

0.187"
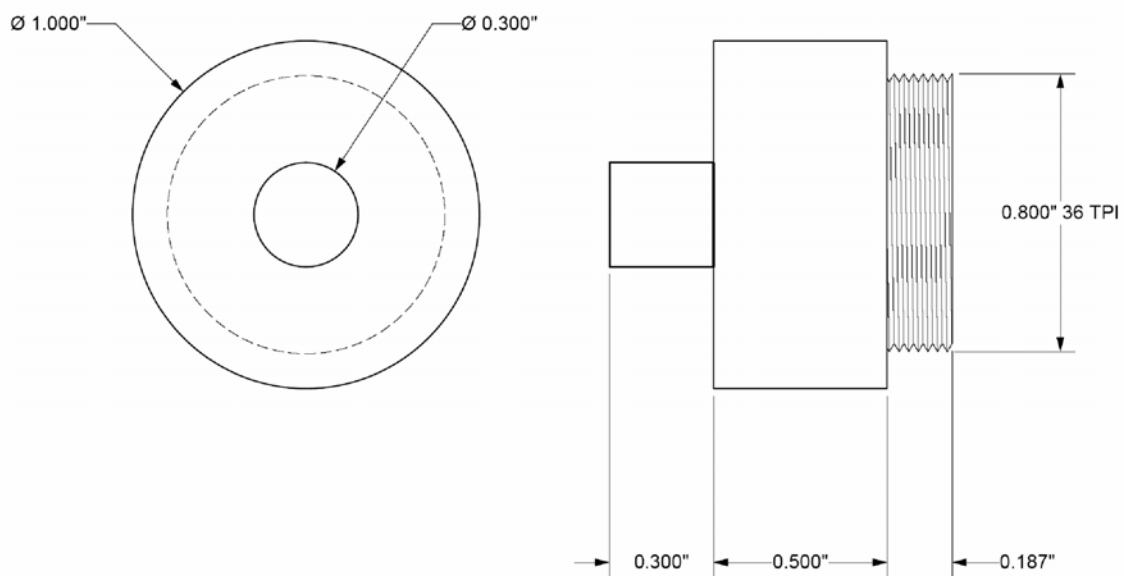
Figure A1.2. CAD drawings of piece 3 and piece 4 of prism holder.

right angle
prism

mirror

Figure A1.3. Components of prism holder.

Figure A1.4. Diagram showing the mirror position with respect to the prism.

Appendix 2

Instructions for Single Point Spectroscopy with NSOM
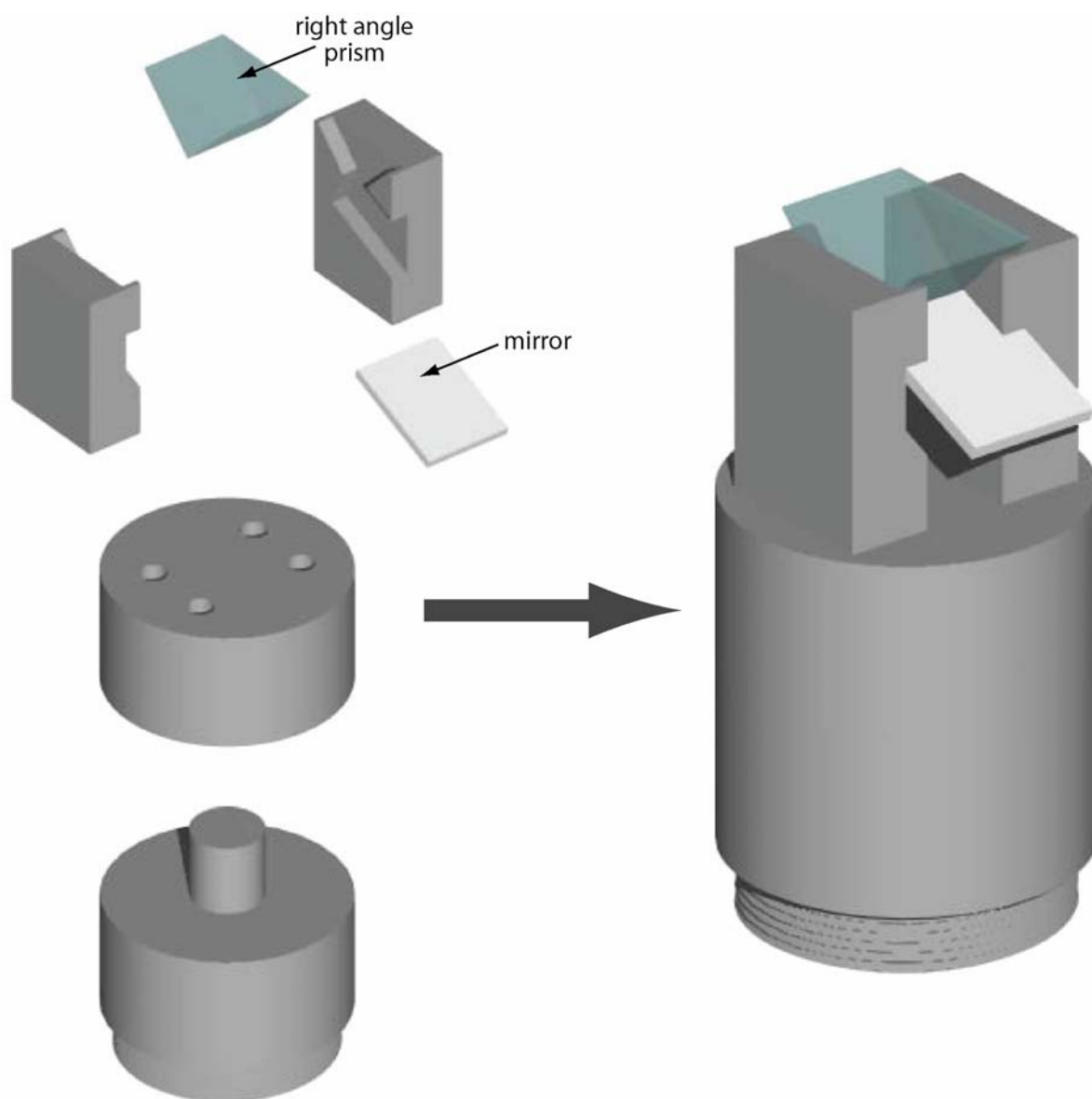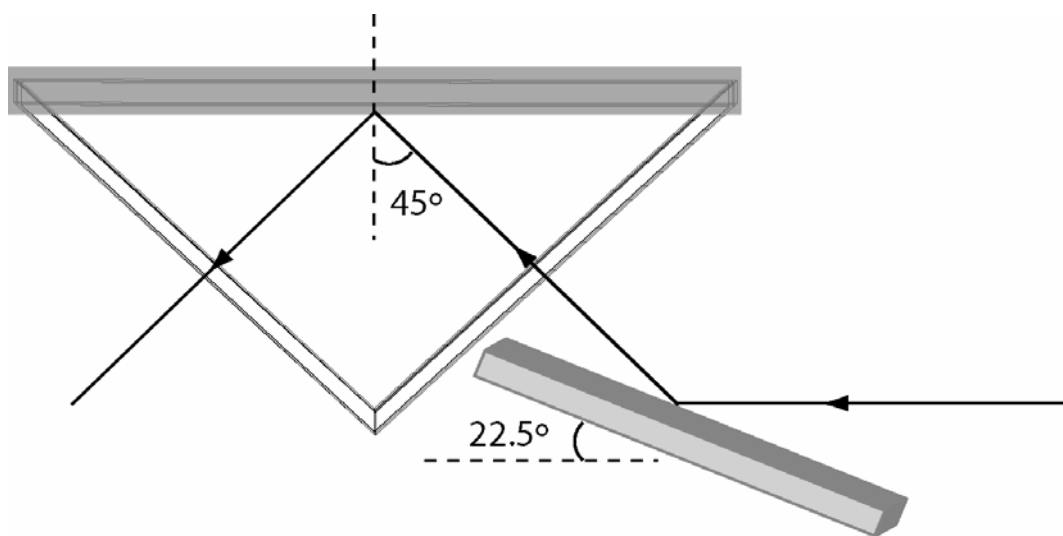
1. Obtain an image (topography and optical) using collection NSOM.

2. When the scan is complete, from the menu bar select:

   Acquire → Point Spectroscopy → F/S

3. Again from the menu bar select:

   Acquire → Advanced Setup

4. In the **Point Spectroscopy (PS)** window enter the following parameters (Figure A2.1):

<u>Example Values</u>

<u>Set Point</u>:   -32 nA   ← This value is automatically set, and corresponds to the set point used during NSOM scan. This value should not be changed.

<u>Start Delay</u>:   100 μs   ← Time delay between probe movement and spectra acquisition. 100 μs is a good starting value.

<u>Z Start</u>:   -250 nm/ 0 nm   ← Initial distance at which you want to start collecting spectra. Negative sign means the probe is away from the surface. When set at negative value the probe will move away from the surface and collect the spectra as it moves closer to the surface.

<u>Z End</u>:   0 nm/ -250 nm   ← If set at 'zero' this value represents the height of the probe from the surface during the scan (i.e. at the set-point).

<u>Points</u>:   100   ← Number of data points you want to acquire within the specified Z range (e.g. 250 nm in the example).

<u>Force Limit</u>:   -30 nA   ← This value should be set 2-3 nA higher than the set point. For example, if the set point was -32 nA, force limit can be set at -30 nA.

<u>Pull Back</u>:   ← The box can be unchecked. If you would like to withdraw the probe away from the surface after PS is performed, check the box and enter a negative value

corresponding to the height to which you want to retract the probe.

5. In the **Additional Parameters Setup** (Figure A2.2) under:

   a. *Data Channels.* Check the boxes next to *Feedback* (for topography) and *Counter 1* (for optical).

   b. *Approaching Speeds.* Good starting values are 1 µm/s.

   c. *Miscellaneous.* Averaging can be set at 50 and ½ cycle to 1. Feedback between cycles can be left unchecked.

   d. *Time Delays.* Longer delays result in smaller hysteresis. Good starting values are:

      1. *Establish Feedback*   250 µs

      2. *Before Sample*   500 µs

      3. *After Pull-back*   500 µs

6. Once these parameters have been set, select a point on the optical image at which you would like to perform SPS. By moving the cursor over the image distance and pixel information can be read out in the **Point Spectroscopy** window under *Cursor Location*. These numbers can then be entered under *Point x-location and y-location* by selecting either distance or pixels radio button, inputting the numbers into the *X:* and *Y:* and clicking the *Add* button.

7. When the point is selected, click on *Measure* and wait for the spectra to appear.

8. The spectra can then be saved as a .txt file, which can be later imported into a graphing program for further analysis.

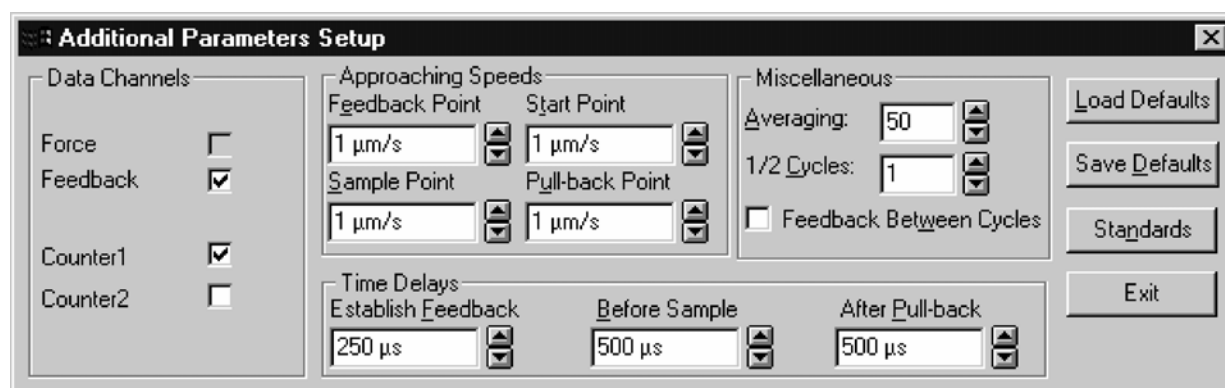**Figure A2.1.** Point Spectroscopy window with sample parameters.

Figure A2.2. Additional Parameters Setup window with sample parameters.

Yelizaveta Babayan

1406 Elmwood Ave. #3E · Evanston, IL 60201· 847-542-9191 · *y-babayan@northwestern.edu*

EDUCATION

Northwestern University, Evanston, IL
Ph.D. Candidate, Chemistry, Anticipated Graduation: December 2007
Dissertation: *Fabrication and Near-field Characterization of Mesoscale Strcutures*

University of Southern California, Los Angeles, CA
B.S., Chemistry, May 2002

HONORS AND AWARDS

- **Industrial Associates Research Poster Award, 1st Place** from Northwestern University (2007)
- **Gelewitz Award Finalist** from Northwestern University (2006)
- **Graduate School Conference Travel Grant** from Northwestern University (2006)
- **Award for Excellence in Undergraduate Research** from University of Southern California (2002)
- **Molecular Approaches to Photochemical Energy Scholarship** from University of Southern California (2002)
- **NSF Summer REU Fellowship** from National Science Foundation (2000)

RESEARCH EXPERIENCE

Northwestern University, Department of Chemistry, Evanston, IL
Graduate Research Assistant, September 2002 – Present
Research Advisor: Teri W. Odom
- Used lithographic techniques to fabricate mesoscale (100-1000 nm) structures for confining and manipulating light on surfaces.
- Assembled instrumentation for optical characterization of nanoscale and mesoscale structures.
- Used near-field scanning optical microscopy (NSOM) to study light confinement within metallic structures and light propagation on dielectric surfaces.
- Helped establish a new laboratory by purchasing equipment and instrumentation.
- Developed undergraduate curriculum through participation with the first National Center for Learning and Teaching of nanoscale science and engineering.
- Organized and lead scientific instrumentation demonstrations for students, teachers and professors.

University of Southern California, Department of Chemistry, Los Angeles, CA
Undergraduate Research Assistant, January 2000 – July 2002
Research Advisor: Mark E. Thompson
- Synthesized organic ligands for color tuning the emission of platinum (II) complexes for use in organic light emitting devices.
- Synthesized and characterized platinum (II) cyclometalated complexes as potential blue phosphorescent emitters.
- Studied substituent effects and excimer formation in organometallic complexes.

University of Southern California, Department of Chemistry, Los Angeles, CA
NSF Summer Research Education for Undergraduate (REU) Fellow, Summer 2000
- Synthesized molecules for enhanced photoinduced charge separation in photovoltaic devices.
- Fabricated photocurrent generation devices.

WORK EXPERIENCE

Avery Research Center, Pasadena, CA
Assistant Research Analyst, March 2001 – July 2001
- Prepared samples by chemical extraction of different organic components from adhesives, epoxies, polymer formulations and inks.
- Conducted spectroscopic analysis of polymers and organic molecules using FTNMR and FTIR.
- Performed particle size analysis using scattering techniques.

University of Southern California, Los Angeles, CA
Administrative Assistant to a Professor of Electrical Engineering, May 1999 – May 2002
- Helped prepare business plan, corporate presentation and financial planning for a start-up company that raised $7 million in the first round of funding.
- Reviewed grant proposal drafts for university funding.
- Gathered research references.
- Created short-course presentations in Power Point and Claris Draw.
- Coordinated laboratory demonstrations for visitors.
- Prepared expense reports and budgets.

TEACHING EXPERIENCE

Northwestern University, School of Continuing Studies, Evanston, IL
Teaching Assistant, Fall 2006, Fall 2007
- Taught laboratory section in general chemistry, wrote solutions to homework assignments, and graded exams.
- Assisted students with time management and problem solving.
- Held review sessions before midterms and final exam.

Northwestern University, Department of Chemistry, Evanston, IL
Teaching Assistant, September 2002 – December 2003
- Taught a year and a half of laboratory section in freshman accelerated inorganic and physical chemistry.
- Taught advanced analytical chemistry laboratory.
- Developed a laboratory experiment on nanoscience, which was incorporated into the general chemistry laboratory curriculum.
- Held weekly review sessions.

International Development Education Association (I.D.E.A.), Los Angeles, CA
Tutor, March 2001– July 2001
- Worked one-on-one with individual students to help them understand and apply complex concepts in science and mathematics.
- Tutored college students in general chemistry, organic chemistry, physics, and mathematics.

Med-Cor at University of Southern California, Los Angeles, CA
Facilitator/Tutor, October 1998 – December 2001
- Developed interactive lesson plans.
- Taught algebra, AP calculus, and physics to a class of 15 eight graders and a class of 10 twelfth graders.
- Performed student assessment.

PUBLICATIONS

"Benchtop Nanoscale Patterning Experiments," **Babayan, Y.**, Meenakshi, V., Odom, T.W.; submitted to ACS symposium series book (2007).

"Benchtop Nanoscale Patterning Using Soft Lithography," Meenakshi, V., **Babayan, Y.**, Odom, T.W.; *J. Chem. Ed, 84 (11), 1795-1798* (2007).

"Patterned MoS_2-Nanostructures over cm^2 – Areas," Stender, C.L.; Greyson, E.C.; **Babayan, Y.,** Odom, T.W.; *Advanced Materials,* 17, 2837-2841 (2005).

"Optical Properties of Surface-Patterned Nanostructures," Odom, T.W.; Henzie, J.; **Babayan, Y.**; Greyson, E.C.; Kwak, E.-S.; *Talanta*, 67, 507-513 (2005).

"Directed Growth of Ordered Arrays of Small Diameter ZnO Nanowires," Greyson, E.C.; **Babayan, Y.**; Odom, T.W.; *Adv. Mat.,* 16 (15), 1348-1352 (2004).

"Templated and Hierarchical Assembly of CdSe/ZnS Quantum Dots," **Babayan, Y.**; Barton, J.E.; Greyson, E.C.; Odom, T.W.; *Adv. Mat.,* 16 (15), 1341-1345 (2004).

"Synthesis and Characterization of Phosphorescent Cyclometalated Platinum Complexes," Brooks, J.; **Babayan, Y**.; Lamansky, S.; Djurovich, P. I.; Tsyba, I.; Bau, R.; Thompson, M. E.; *Inorg. Chem., 41*(12), 3055-3066 (2002).

PRESENTATIONS

Babayan, Y.. *Manipulating Light on Dielectric Surfaces: Confining Standing Waves in Optical Corrals.* Northwestern University Department of Chemistry Physical Chemistry Seminar Presentation (May 2007).

Babayan, Y.; Odom, T.W. *Manipulating Light on Dielectric Surfaces: Confining Standing Waves in Optical Corrals.* Poster Session at the Industrial Associates Meeting at Northwestern University, Evanston, IL (May 2007).

Babayan, Y.; Meenakshi, V.; and Odom, T.W. *Benchtop Nanopatterning Using Soft Lithography*. Oral presentation at the 233rd American Chemical Society National Meeting, Chicago, IL (March 2007).

Babayan, Y. and Odom, T.W. *Exploration of Optical Analog to the Quantum Corral*. Oral presentation at the 233rd American Chemical Society National Meeting, Chicago, IL (March 2007).

Babayan, Y.; Meenakshi, V.; and Odom, T.W. *Benchtop Nanopatterning Using Soft Lithography*. Oral presentation at the 41st Midwest Regional Meeting of the American Chemical Society, Quincy, IL (October 2006).

Babayan, Y. and Odom, T.W. *Optical Corrals*. Oral presentation at the 41st Midwest Regional Meeting of the American Chemical Society, Quincy, IL (October 2006).

Babayan, Y.; Meenakshi, V.; and Odom, T.W. *Benchtop Nanopatterning Using Soft Lithography*. Poster presentation at the annual meeting for Nanoscale Center for Learning and Teaching at Northwestern University, Evanston, IL (May 2006).

Babayan, Y. and Odom, T.W. *Towards Optical Whispering Galleries*. Poster presentation at SERSabration Symposium, Northwestern University, Evanston, IL (October 2005).

Barton, J.E.; **Babayan, Y.**; and Odom, T.W. *Nanoscale Patterning and Assembly of Nanocrystals*. Poster Session at the NSF site visit to the Nanoscale Science and Engineering Center at Northwestern University, Evanston, IL (June 2005).

Babayan, Y. and Odom, T.W. *Toward the Fabrication of an Optical Analog to the Quantum Corral*. Poster Session at the Industrial Associates Meeting at Northwestern University, Evanston, IL (April 2004).

Babayan, Y.; Brooks, J.; and Thompson, M.E. *Platinum (II) Cyclometalated Complexes as Potential Blue Phosphorescent Emitters*. Poster presentation at the 222nd American Chemical Society National Meeting, Chicago, IL (August 2001).

Babayan, Y.; Brooks, J.; and Thompson, M.E. *Substituent Effects and Excimer Formation in Platinum Complexes*. Poster presentation at the 3rd International Conference on Electroluminescence of Molecular Materials and Related Phenomena, Los Angeles, CA (September 2001).

Babayan, Y.; Brooks, J.; and Thompson, M.E. *Platinum (II) Cyclometalated Complexes as Potential Blue Phosphorescent Emitters*. Poster presentation at the Western Regional Meeting of the American Chemical Society National Meeting, Santa Barbara, CA (October 2001).
Babayan, Y.; Thompson, M.E. *Photocurrent Generation Devices: Solar Cells*. Oral presentation at the NSF REU Symposium of Solid State Chemistry, San Diego, CA (August 2000).

OUTREACH ACTIVITIES

- Organized a presentation on nanotechnology for "FIRST LEGO League 2006-2007 NANO" and provided technical and scientific help to the participating students from the Chicago, IL region (October 2006).

- Coordinated and lead instrument demonstrations for a short course offered through NSF Summer Institute on Nano Mechanics and Materials at Northwestern University, Evanston, IL (August 2006).

- Participated in a science outreach program for fourth graders at Steven K. Hayt Elementary School, Chicago, IL. Responsibilities included writing lesson plans, leading a group of graduate student volunteers, teaching science to a group of fourth graders, and organizing an end-of-the-year science demo (January 2006-Present).

- Acted as a mentoring scientist for students of New Trier High School Internship program, Evanston, IL (April-May 2006).

- Acted as a mentoring scientist for students of Evanston Township High School Honors Biology Internship program, Evanston, IL (April 2005 & March 2007).

- Organized, coordinated and lead scientific instrumentation demonstrations for high school students, Northwestern University, Evanston, IL (2004-2007).

- Organized the 3rd annual "Nanoscience Day" for local Boy Scout and Girl Scout troops in 2004. Also, participated in the 2nd, 4th, and 5th annual "Nanoscience Day" events by conducting demonstrations of advanced laboratory instrumentation and helping with hands-on lab experiments demonstrating nanoscience/technology at Northwestern University, Evanston, IL (2003-2006).

- Co-organized and conducted demonstrations for "Youth Science Day" at University of Southern California, Los Angeles, CA (1999).

PROFESSIONAL AFFILIATIONS

- American Chemical Society (ACS)
- American Physical Society (APS)
- Materials Research Society (MRS)
- Phi Lambda Upsilon, Graduate Chemistry Honor Society

SKILLS

- **Microscopy:** Near-field scanning optical microscopy (NSOM), light microscopy (dark field and bright field), scanning electron microscopy (SEM), atomic force microscopy (AFM).
- **Fabrication and Assembly:** Electron-beam lithography, photolithography, phase-shifting photolithography.
- **Thin Film Deposition:** Electron beam deposition, sputtering, Langmuir-Blodgett.
- **Spectroscopy:** Extensive experience with: UV-visible extinction, dark field scattering, single particle spectroscopy, fluorescence spectroscopy. Laboratory experience with: Nuclear magnetic resonance (NMR), infrared absorption (IR), mass spectrometry (MS).
- **Synthesis:** Organometallic, colloidal and solution based nanocrystal synthesis.
- **Separation techniques:** Thin layer chromatography (TLC), liquid chromatography (LC).
- **Electrochemistry:** Cyclic voltammetry (CV).
- **Lasers:** continuous wave (gas, solid state), pulsed, ultrafast (femtosecond Ti:Sapphire and harmonic generation).
- **Computer:** Word, Excel, Adobe Illustrator, Adobe Photoshop, C programming, HTML

LANGUAGES

English (fluent), Armenian (fluent), Russian (fluent), Spanish (learning), Italian (learning)